A novel Fc-engineered cathepsin D-targeting antibody enhances ADCC, triggers tumor-infiltrating NK cell recruitment, and improves treatment with paclitaxel and enzalutamide in triple-negative breast cancer

Pénélope Desroys Du Roure, Laurie Lajoie, Aude Mallavialle, Lindsay Alcaraz, Hanane Mansouri, Lise Fenou, Véronique Garambois, Lucie Rubio, Timothée David, Loïs Coenon, et al.

Journal for ImmunoTherapy of Cancer

A novel Fc-engineered cathepsin D-targeting antibody enhances ADCC, triggers tumor-infiltrating NK cell recruitment, and improves treatment with paclitaxel and enzalutamide in triple-negative breast cancer

Pénélope Desroys du Roure ,[1] Laurie Lajoie ,[2] Aude Mallavialle ,[1] Lindsay B Alcaraz ,[1] Hanane Mansouri,[1,3] Lise Fenou ,[1] Véronique Garambois,[1] Lucie Rubio,[1] Timothée David ,[1] Loïs Coenon ,[4] Florence Boissière-Michot ,[5] Marie-Christine Chateau ,[5] Giang Ngo ,[1] Marta Jarlier ,[6] Martin Villalba ,[4,7] Pierre Martineau ,[1] Valérie Laurent-Matha ,[1] Pascal Roger ,[1,8] Séverine Guiu ,[1,9] Thierry Chardès ,[1,10] Laurent Gros ,[1,10] Emmanuelle Liaudet-Coopman [1]

To cite: Desroys du Roure P, Lajoie L, Mallavialle A, *et al*. A novel Fc-engineered cathepsin D-targeting antibody enhances ADCC, triggers tumor-infiltrating NK cell recruitment, and improves treatment with paclitaxel and enzalutamide in triple-negative breast cancer. *Journal for ImmunoTherapy of Cancer* 2024;**12**:e007135. doi:10.1136/jitc-2023-007135

► Additional supplemental material is published online only. To view, please visit the journal online (http://dx.doi.org/10.1136/jitc-2023-007135).

TC and LG contributed equally.

Accepted 19 December 2023

For numbered affiliations see end of article.

Correspondence to
Dr Emmanuelle Liaudet-Coopman;
emmanuelle.liaudet-coopman@inserm.fr

ABSTRACT

Introduction Triple-negative breast cancer (TNBC) prognosis is poor. Immunotherapies to enhance the antibody-induced natural killer (NK) cell antitumor activity are emerging for TNBC that is frequently immunogenic. The aspartic protease cathepsin D (cath-D), a tumor cell-associated extracellular protein with protumor activity and a poor prognosis marker in TNBC, is a prime target for antibody-based therapy to induce NK cell-mediated antibody-dependent cellular cytotoxicity (ADCC). This study investigated whether Fc-engineered anti-cath-D antibodies trigger ADCC, their impact on antitumor efficacy and tumor-infiltrating NK cells, and their relevance for combinatory therapy in TNBC.

Methods Cath-D expression and localization in TNBC samples were evaluated by western blotting, immunofluorescence, and immunohistochemistry. The binding of human anti-cath-D F1M1 and Fc-engineered antibody variants, which enhance (F1M1-Fc$^+$) or prevent (F1M1-Fc$^-$) affinity for CD16a, to secreted human and murine cath-D was analyzed by ELISA, and to CD16a by surface plasmon resonance and flow cytometry. NK cell activation was investigated by flow cytometry, and ADCC by lactate dehydrogenase release. The antitumor efficacy of F1M1 Fc-variants was investigated using TNBC cell xenografts in nude mice. NK cell recruitment, activation, and cytotoxic activity were analyzed in MDA-MB-231 cell xenografts by immunophenotyping and RT-qPCR. NK cells were depleted using an anti-asialo GM1 antibody. F1M1-Fc$^+$ antitumor effect was assessed in TNBC patient-derived xenografts (PDXs) and TNBC SUM159 cell xenografts, and in combination with paclitaxel or enzalutamide.

Results Cath-D expression on the TNBC cell surface could be exploited to induce ADCC. F1M1 Fc-variants recognized human and mouse cath-D. F1M1-Fc$^+$ activated NK cells in vitro and induced ADCC against TNBC cells and cancer-associated fibroblasts more efficiently than F1M1. F1M1-Fc$^-$ was ineffective. In the MDA-MB-231 cell xenograft model, F1M1-Fc$^+$ displayed higher antitumor activity than F1M1, whereas F1M1-Fc$^-$ was less effective,

WHAT IS ALREADY KNOWN ON THIS TOPIC

⇒ Cathepsin D (cath-D) is a tumor cell-associated extracellular protein with protumor activity, a poor prognosis marker, and a target for antibody-based therapy in triple-negative breast cancer (TNBC).

WHAT THIS STUDY ADDS

⇒ This study first shows that cath-D is a tumor microenvironment antigen eligible for Fc-engineered antibody targeted therapy to trigger antibody-dependent cellular cytotoxicity (ADCC).

⇒ The Fc-optimized F1M1-Fc$^+$ antibody (derived from F1M1 by introducing the S239D, H268F, S324T, and I332E mutations to enhance the affinity for CD16a) promotes ADCC induction, improves antitumor potency, and triggers natural killer (NK) cell recruitment, activation and cytotoxic activity in tumors. NK cell depletion impaired F1M1-Fc$^+$ therapeutic efficacy, proving their key role.

⇒ F1M1-Fc$^+$ improves paclitaxel and enzalutamide therapeutic efficacy in combination, demonstrating its clinical relevance.

HOW THIS STUDY MIGHT AFFECT RESEARCH, PRACTICE OR POLICY

⇒ F1M1-Fc$^+$ is a promising immunotherapy for TNBC that could be combined with conventional regimens, including chemotherapy or antiandrogens.

reflecting the importance of Fc-dependent mechanisms in vivo. F1M1-Fc$^+$ triggered tumor-infiltrating NK cell recruitment, activation and cytotoxic activity in MDA-MB-231 cell xenografts. NK cell depletion impaired F1M1-Fc$^+$ antitumor activity, demonstrating their key role. F1M1-Fc$^+$ inhibited growth of SUM159 cell xenografts and two TNBC PDXs. In combination therapy, F1M1-Fc$^+$ improved paclitaxel and enzalutamide therapeutic efficacy without toxicity.

Conclusions F1M1-Fc$^+$ is a promising immunotherapy for TNBC that could be combined with conventional regimens, including chemotherapy or antiandrogens.

INTRODUCTION

Triple-negative breast cancers (TNBCs; 15% of all breast cancers (BCs)) lack estrogen, progesterone and HER2 receptors and are a clinically aggressive BC subtype (highest metastatic potential and recurrence in the first 5 years after diagnosis).[1] The prognosis of patients with TNBC is poor, mainly due to disease heterogeneity and lack of targeted therapies. Although conventional chemotherapy remains the standard treatment, immunotherapy is changing the paradigm of anticancer treatment and is emerging as an alternative treatment for TNBC, classified as an immunogenic BC subtype.[2 3]

Recent studies and clinical trials highlighted that natural killer (NK) cell-based immunotherapy can awake the innate anticancer response, particularly against tumor metastases,[4–6] and sustain BC dormancy.[7] Hence, different immunotherapeutic strategies are tested to improve the efficacy of antibody-induced NK cell-mediated antitumor activity. Glycoengineering and protein-engineering of the Fc region of tumor-targeting antibodies have been exploited to modulate their interaction with activating or inhibitory members of the FcγR family.[8] Afucosylation and selected amino acid substitutions increase the affinity for FcγRs, thus enhancing NK cell-mediated antibody-dependent cellular cytotoxicity (ADCC),[8] a major mechanism contributing to the therapeutic efficacy of antibodies.[9] Many clinically relevant anticancer antibodies, such as rituximab, cetuximab and trastuzumab, induce NK cell-mediated ADCC in vitro.[6 8] NK cells bind to the Fc of antibody-labeled tumor cells, predominantly through a single activating FcγR (FcγRIIIA, also named CD16a), a low-affinity receptor for IgG.[10] Binding of IgG to CD16a can activate NK cells and stimulate the release of lytic granules that contain molecules, such as perforin and granzymes[11 12] ultimately leading to the target cell lysis. FcγR ligation also affects NK cell survival and proliferation[13] and induces the release of cytokines and chemokines that promote the recruitment and activation of tumor-infiltrating immune cells.[10]

The aspartyl protease cathepsin D (cath-D), a marker of poor prognosis in BC[14] and TNBC,[15 16] is overexpressed and hypersecreted in the tumor microenvironment[17] and exhibits protumor activity.[18–26] In TNBC, cath-D is a tumor cell-associated extracellular biomarker and a target for antibody-based therapy.[27] We previously showed that F1, a fully human anti-cath-D IgG1 originally isolated by phage display, inhibits growth of TNBC cell xenografts and TNBC patient-derived xenografts (PDX), activates NK cells, and prevents the tumor recruitment of M2-polarized tumor-associated macrophages and myeloid-derived immunosuppressive populations in nude mice.[27] We found that an Fc-aglycosylated F1 anti-cath-D antibody, in which the N297A mutation prevents Fcγ receptor (FcγR) binding, no longer induces NK cell activation. This was associated with reduced tumor growth inhibition.[27] This demonstrated the essential role of the Fc part of the F1 antibody for anti-cath-D antibody-based therapy through NK cell activation. Therefore, cath-D is a prime target for monoclonal antibody-based therapies to induce NK cell-mediated ADCC.

Here, we showed that cath-D expression on the TNBC cell surface can be exploited to induce ADCC. We applied Fc-engineering to F1M1, a novel fully human anti-cath-D IgG1 antibody in which the variable regions were derived from F1,[27] to generate three antibody variants that harbor the wild-type (F1M1) or mutated Fc region to enhance (F1M1-Fc$^+$) or prevent (F1M1-Fc$^-$) binding to CD16a on NK cells. This study explored whether targeted therapy with Fc-engineered anti-cath-D antibodies triggers ADCC, its impact on antitumor efficacy and tumor-infiltrating NK cells, and the relevance of combination therapies with anti-cath-D antibodies in TNBC.

MATERIALS AND METHODS

The materials used, cell lines, conditioned medium, western blotting, ELISA, immunoprecipitation, fluorescence microscopy, immunohistochemistry (IHC), surface plasmon resonance, quantitative RT-qPCR as well as in vivo experiments and study approvals are described in online supplemental file 1.

Binding of human Fc-engineered anti-cath-D antibodies to human CD16a (hCD16a)

To analyze the anti-cath-D antibody binding to human FcγRIIIA (hCD16a), hCD16a 158V or 158F-transduced NK92 cells (2×10^4) were incubated in the absence or in the presence of increasing concentrations of the F1M1-Fc$^-$, F1M1, or F1M1-Fc$^+$ antibodies (4°C, 30 min). Then, cells were incubated with APC-conjugated 3G8 (anti-hCD16a antibody; 1:100) (4°C, 30 min), washed twice in phosphate-buffered saline (PBS) at 4°C, and analyzed by flow cytometry. Fluorescence was acquired with a MACSQuant cytometer (Miltenyi) and analyzed with the Kaluza software V.2.1 (Beckman Coulter). Results were expressed as percentage of fluorescent 3G8 binding inhibition: (MFI without anti-cath-D antibody - MFI with anti-cath-D antibody)×100/(MFI without anti-cath-D antibody). This allowed the standardization and comparison between hCD16a 158V- and 158F-transduced NK92 cells.

In vitro stimulation and functional responses of hCD16a-transduced NK92 cells

For in vitro stimulation and functional responses of hCD16a-transduced NK92 cells, NUNC Maxisorp 96-well

plates were directly sensitized with F1M1-Fc$^-$, F1M1, F1M1-Fc$^+$, or 3G8 (5 µg/mL) at 4°C for 12 hours or precoated with the M2E8 anti-cath-D antibody in PBS (2500 ng/well), then incubated or not with increasing concentrations of cath-D (3–50 nM), and finally incubated with F1M1-Fc$^+$ (5 µg/mL). After three washes with PBS/Tween-20 solution (PBS-T; 45 µL Tween-20 in 100 mL PBS), plates were saturated with 1% bovine serum albumin for 1 hour, then washed three times with PBS-T. NK92 hCD16a 158V or 158 F cells (1×10^5) in 100 µL RPMI were then incubated on non-sensitized or sensitized plates in the presence of the anti-CD107a-PC5 antibody (1:20) and 0.1 µg/mL BD GolgiPlug containing brefeldin A (BD Biosciences) at 37°C in 5% CO_2 humidified air for 4 hours. Cells were then fixed and permeabilized using the BD Cytofix/Cytoperm Plus Kit (BD Biosciences) and stained with an anti-IFNγ-PE antibody (1:20) at 4°C for 30 min to detect intracellular IFNγ. The proportions of responding (degranulating (CD107a$^+$), IFNγ-producing (IFNγ$^+$) NK cells and cells with both responses (CD107a$^+$ IFNγ$^+$) were analyzed by flow cytometry with a Cytoflex S cytometer and the Kaluza V.2.1 software (Beckman Coulter).

NK cell-mediated ADCC toward TNBC cells and cancer-associated fibroblasts

MDA-MB-231 cells (1×10^4 target; T) or human breast cancer-associated fibroblasts (hCAF1) cells (2×10^4 target; T) were plated in 96-well plates. After 24 hours, they were first incubated with F1M1-Fc$^+$, F1M1, F1M1-Fc$^-$ or cetuximab (positive control) at 37°C for 30 min. Then, cells were incubated with NK92 hCD16a 158V or 158F at an effector:target (E:T) ratio of 10:1, or human primary expanded NK cells (effector; E) at an E:T ratio of 3:1 at 37°C for 24 hours. MDA-MB-231 cell lysis (ADCC) or hCAF1 cell lysis was evaluated by measuring lactate dehydrogenase (LDH) release with the Cytotox 96 Non-radioactive Cytotoxicity Assay (Promega). The percentage of specific lysis in each sample was determined using the following formula: percentage of specific lysis=(sample LDH release–[E cell+T cell] spontaneous LDH release)/(T cell maximum LDH release -T cell spontaneous LDH release)×100. For ADCC in cell spheroids, target MDA-MB-231 cells (5×10^3) were seeded on Ultra-Low Attachment 96-well plates (#7007, Corning). After 72 hours, MDA-MB-231 cell spheroids were first incubated with F1M1-Fc$^+$, F1M1-Fc$^-$, or cetuximab at 37°C for 30 min, and then with effector NK92 hCD16a$^+$ 158V cells (E:T ratio of 20:1) for 24 hours. ADCC was assessed using the Cytotox 96 Non-radioactive Cytotoxicity Assay (Promega). The percentage of specific lysis in each sample was determined as described above.

In vivo isolation and immunophenotyping of tumor-infiltrating NK cells

Tumors were shredded and digested with a mixture of collagenase IV (1 mg/mL) and DNase I (200 U/mL) in RPMI at 37°C. The mixture was transferred into a gentleMACS C tube for enzymatic and mechanical digestion using a gentleMACS Octo Dissociator (Miltenyi Biotec) at 37°C. After digestion, tumor suspensions were passed through a 70 µm nylon cell strainer (#22-363-548, Thermo Fisher Scientific), centrifuged and resuspended in FACS Buffer (PBS pH 7.2, 1% decomplemented fetal calf serum, 2 mM EDTA, and 0.02% sodium azide). Cells were blocked with FACS Buffer containing 1% (v/v) of mouse Fc block for 30 min and stained with fluorescent-conjugated antibodies against the cell surface markers CD45, CD3, CD19, CD11c, F4/80, NKp46, CD27, CD11b, and CD107a for 45 min. Then, cells were fixed, permeabilized and stained with fluorescent-conjugated antibodies against the intracellular marker granzyme B overnight. After fixation with 1% paraformaldehyde in PBS, cell samples were analyzed by flow cytometry using a Beckman and Coulter Cytoflex flow cytometer and FlowJo V.10.8.1. Living immune cells were defined as Viakrome IR808$^-$ CD45$^+$. NK cells were defined as NKp46$^+$ cells within the gate excluding CD3$^+$ T and NKT cells, CD19$^+$ B cells, F4/80$^+$ macrophages, and CD11c$^+$ dendritic cells. NK cell maturation stage was analyzed with the CD27 and CD11b cell surface markers. Functional markers (CD107a, granzyme B) were studied in the NK cell subpopulations.

Statistical analysis

A linear mixed regression model was used to determine the relationship between tumor growth and number of days postxenograft. The variables included in the fixed part of the model were: number of days postxenograft and treatment groups. Their interaction also was evaluated. Random intercepts and random slopes were included to take into account the time effect. The model coefficients were estimated by maximum likelihood. Survival rates were estimated using the Kaplan-Meier method and compared with the log-rank test. Comparisons of more than two groups were done using the non-parametric Kruskal-Wallis test; the Mann-Whitney test was used for pairwise comparisons. Statistical significance was set at the 0.05 level. All statistical analyses were done with STATA V.16.0.

RESULTS

In TNBC, cath-D is a tumor microenvironment antigen eligible for Fc-engineered antibody targeted therapy to trigger ADCC

ADCC initiation requires the presence of antibody-antigen complexes at the cell surface. Cath-D localizes at the cell surface through its binding to the M6P/IGF2 receptor via its mannose-6-phosphate (M6P) motif (BC cells and stromal fibroblasts)[28 29] and to LRP1 (fibroblasts).[23] We first examined the expression of cath-D, M6P/IGF2 receptor and LRP1 in a panel of TNBC cell lines (MDA-MB-231, SUM-159, MDA-MB-436, MDA-MB-453, BT-549) and hCAF1 cells (figure 1A). We detected the fully mature cellular lysosomal protease cath-D (34 kDa heavy chain) and the IGF2/M6P receptor in all TNBC cell lines and hCAF1s. We could not detect cath-D only

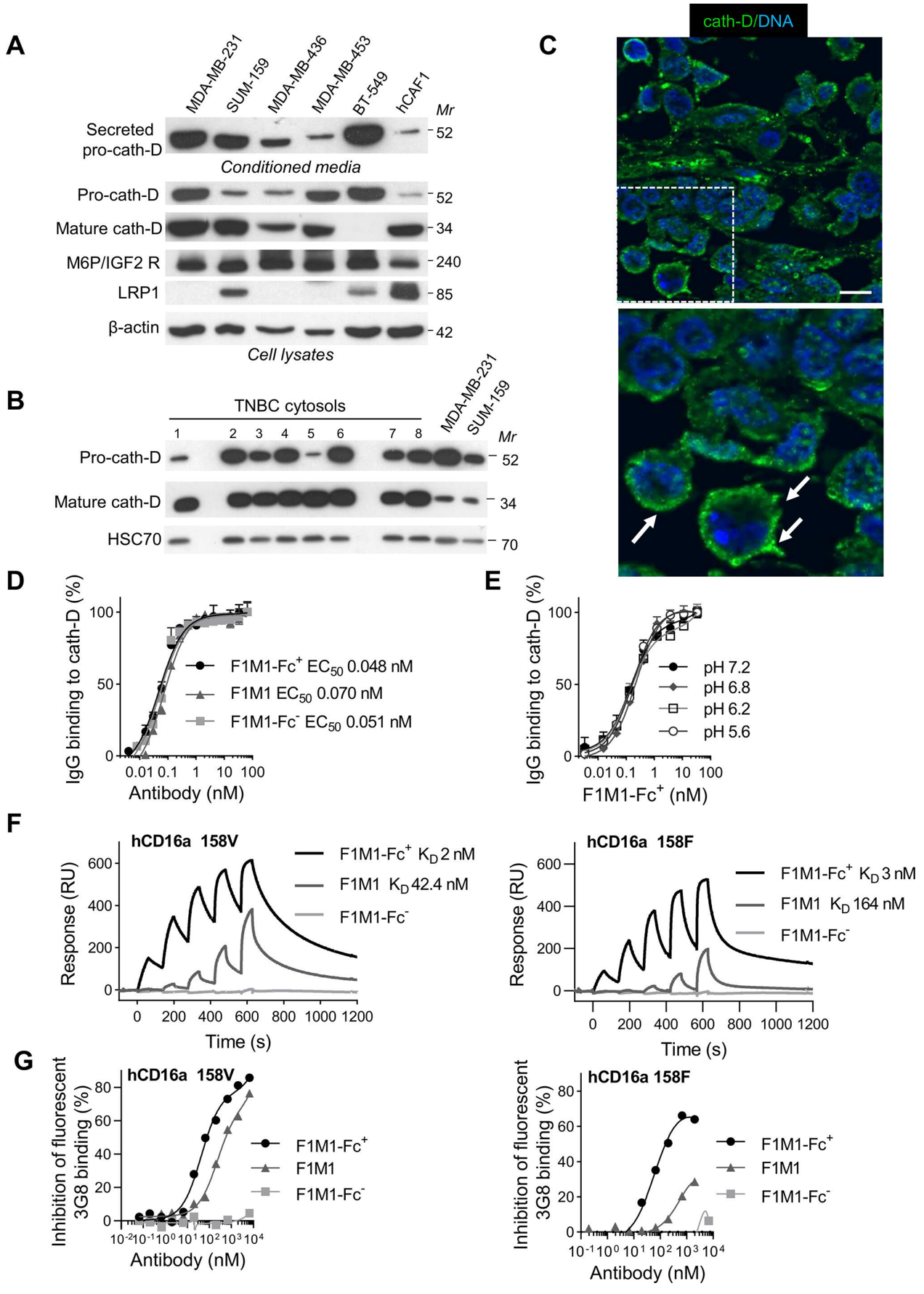

Figure 1 (Continued)

Figure 1 Cath-D is a tumor microenvironment antigen eligible to trigger ADCC and relevant for Fc-engineered antibody-based targeted therapy in TNBC. (A) Cath-D expression and secretion, and M6P/IGF2 and LRP1 receptor expression in TNBC cell lines and breast hCAFs. Whole cell extracts (cell lysates, 20 µg proteins) and 24 hours conditioned media in the absence of serum (40 µL) were separated on 13.5% SDS-PAGE and analyzed by immunoblotting with the anti-cath-D mouse monoclonal antibody (#610801) (to detect mature cath-D), and anti-cath-D rabbit polyclonal antibody (E-7) (to detect pro-cath-D). Whole cell extracts were also immunoblotted with the 11H4 hybridoma against the LRP1 receptor, and with a mouse monoclonal antibody (clone MEM-238) against the M6P/IGF2 receptor (M6P/IGF2R). β-actin (#A2066) was used as loading control. *Mr*, relative molecular mass (kDa). (B) Cath-D expression in TNBC cytosols. Cath-D expression was determined in eight cytosols from primary TNBC samples. Whole cytosols (5 µg proteins) were immunoblotted with the mouse monoclonal (#610801) (to detect mature cath-D), and rabbit polyclonal (E-7) (to detect pro-cath-D) anti-cath-D antibodies. HSC70 (clone B-6) was used as loading control. MDA-MB-231 and SUM-159 TNBC cell xenografts were used as positive controls for cath-D expression. *Mr*, relative molecular mass (kDa). (C) Cath-D expression and localization in MDA-MB-231 cell xenografts. Representative image of MDA-MB-231 cell xenograft sections incubated with a monoclonal anti-human cath-D antibody (clone C-5) (green). Nuclei were stained with Hoechst 33 342 (blue). Scale bar, 10 µm (upper panel). Higher magnification of the boxed region showing cell-surface associated cath-D (lower panel). Arrows show the localization of cath-D at the cancer cell surface. (D) Binding of F1M1, F1M1-Fc$^-$, and F1M1-Fc$^+$ to human pro-cath-D secreted from MDA-MB-231 cells. Sandwich ELISA in which pro-cath-D from conditioned medium of MDA-MB-231 cells was added to wells precoated with the anti-human pro-cath-D M2E8 monoclonal antibody in the presence of increasing concentrations of F1M1, F1M1-Fc$^-$, or F1M1-Fc$^+$. Binding of F1M1, F1M1-Fc$^-$ and F1M1-Fc$^+$ to pro-cath-D was revealed with an anti-human Fc HRP-conjugated antibody. The EC_{50} values are shown. (E) Binding of F1M1-Fc$^+$ to human pro-cath-D secreted from MDA-MB-231 cells at acidic pH. Sandwich ELISA was performed as in (D), but at different pH values (7.2, 6.8, 6.2 and 5.6). (F) Binding of F1M1, F1M1-Fc$^-$, and F1M1-Fc$^+$ to human CD16a 158V and CD16a 158F by surface plasmon resonance. Increasing concentrations of F1M1, F1M1-Fc$^-$, and F1M1-Fc$^+$ (3.7, 11, 33, 100, 300 nM) were injected into the sensor chip on which hCD16a 158V (left panel) or hCD16a 158F (right panel) had been captured. The K_D values are shown. (G) Binding of F1M1, F1M1-Fc$^-$, and F1M1-Fc$^+$ to human CD16a 158V and CD16a 158F by flow cytometry. NK92 cells transduced to express hCD16a 158V (left panel) or hCD16a 158F (right panel) were incubated with increasing concentrations (0.6 to 6666 nM) of F1M1-Fc$^-$, F1M1 or F1M1-Fc$^+$ at 4°C for 30 min, followed by incubation with the APC-AF750 conjugated anti-CD16 3G8 antibody (positive control of human CD16 engagement) at 4°C for 30 min. Results were expressed as percentage of fluorescent 3G8 binding: (MFI without anti-cath-D antibody–MFI with anti-cath-D antibody) ×100/(MFI without anti-cath-D antibody). This allowed the standardization and comparison of results between NK92 hCD16a 158F and NK92 hCD16a 158V. ADCC, antibody-dependent cellular cytotoxicity; hCAFs, human breast cancer-associated fibroblasts; MFI, mean fluorescence intensity; TNBC, triple-negative breast cancer,

in BT549 cells. Similarly, we did not detect LRP1 expression in TNBC cells, except for SUM159 and BT549 cells. Conversely, it was strongly expressed in hCAF1 cells. The 52-kDa cath-D precursor (pro-cath-D) was secreted in the culture medium of all TNBC cell lines and of hCAFs and was detectable in cell lysates, in agreement with its cell surface association after secretion (figure 1A). Moreover, we detected the 52-kDa cath-D precursor and IGF2/M6P receptor in the cytosol (ie, whole tumor lysate) of eight primary TNBC samples and in MDA-MB-231 and SUM-159 cell xenografts (figure 1B). Immunofluorescence analysis of cath-D in MDA-MB-231 cell xenografts showed intense, punctate staining at the tumor periphery and in cell membrane protrusions, potentially in areas of exocytosis (figure 1C), reflecting cath-D expression profile in TNBC biopsy samples (online supplemental figure 1). This is in agreement with recent IHC results showing membrane-associated cath-D expression in 85.7% of TNBC samples in a tissue microarray.[27] These observations strongly suggest that cath-D is a tumor microenvironment antigen eligible for Fc-engineered antibody targeted therapy to trigger ADCC.

Generation of anti-cath-D F1M1 Fc-variant antibodies with different CD16a binding properties

We next evaluated whether manipulation of the Fc portion of F1, our lead anti-cath-D antibody, by protein-engineering to increase ADCC could potentiate its anti-tumor effectiveness in TNBC. We first improved F1 format by introducing two-point mutations (one in VL CDR3 and one in VH FR3) to abrogate N-glycosylation at these two sites (F1M1 antibody) that may lead to the production of glycoforms associated with the risk of immunogenic responses in patients, as described for cetuximab.[30] The migration profiles of F1 and F1M1 in the IgG1 format showed that the light and heavy chains molecular weights were lower in F1M1 than F1, as expected due to reduced glycosylation (online supplemental figure 2A). Sandwich ELISA using human cath-D secreted from MDA-MB-231 cells showed that F1M1 (online supplemental figure 2B) had good binding capacities (0.04 nM), as previously shown for F1 (0.2 nM).[27] Sandwich ELISA using cath-D secreted from mouse E0771 TNBC cells showed that F1M1 and F1 (online supplemental figure 2C) retained good binding capacities also toward mouse cath-D (EC_{50}=0.9 nM and 26.3 nM, respectively). The lower EC_{50} of F1M1 indicated that the two-point mutations leading to Fab aglycosylation enhanced F1M1 capacity to recognize human and mouse cath-D, presumably because the VL-CDR3 glycosylation decreased F1 affinity due to steric hindrance. To compare the antitumor efficacy of F1M1 and F1, we xenografted athymic Foxn1^{nu} nude mice with MDA-MB-231 cells. When tumor volume reached 50 mm^3, we treated mice with F1M1, F1, or negative isotype control (rituximab) (15 mg/kg) by ip three times per week for 35 days (days 21–56 postgraft), and then sacrificed all mice at treatment end. Both F1M1 and F1 significantly delayed

tumor growth compared with negative control (online supplemental figure 2D; p=0.003 for F1M1, p<0.001 for F1). Thus, the VH and VL aglycosylated F1M1 antibody appears to be a suitable candidate for future clinical development.

We then designed an Fc-optimized F1M1 (F1M1-Fc$^+$), in which the S239D, H268F, S324T, I332E mutations should increase the binding affinity to CD16a (FcγRIIIA) to enhance NK cell activation, and a F1M1 Fc-silent (F1M1-Fc$^-$) in which the L234A, L235A and P329G mutations prevented binding to FcγRs[8] and ADCC induction. F1M1-Fc$^-$ activities should rely exclusively on Fab-mediated effector functions. Antibody preparations were highly pure, and after SDS-PAGE in reducing conditions, the heavy and light chains were of the expected molecular mass (50 and 25 kDa respectively) (online supplemental figure 3A). The three F1M1 antibody variants showed almost identical, concentration-dependent binding to secreted cath-D with EC_{50} values in the low nanomolar range (EC_{50}=0.07 nM, 0.051 nM, and 0.048 nM for F1M1, F1M1-Fc$^-$ and F1M1-Fc$^+$, respectively) (figure 1D). Moreover, F1M1-Fc$^+$ binding to pro-cath-D was comparable at pH values from 7.2 to 5.6 (figure 1E). All F1M1 variant antibodies immunoprecipitated secreted cath-D at pH values from 7.5 to 5.5 (online supplemental filgure 3B), suggesting that the highly acidic tumor microenvironment does not inhibit cath-D recognition and binding by antibodies. Then, we investigated by surface plasmon resonance F1M1-Fc$^+$, F1M1 and F1M1-Fc$^-$ binding to hCD16a (158V or 158F allotype). F1M1 binding to hCD16a 158V was 3.9-fold higher than to hCD16a 158F (K_D=42 nM and K_D 164 nM, respectively) (figure 1F). Compared with F1M1, F1M1-Fc$^+$ binding to hCD16a 158V was increased by 21.2-fold (K_D=2 nM for F1M1-Fc$^+$ and 42.4 nM for F1M1), and even more to hCD16a 158F (by 54.6-fold) (K_D=3 nM for F1M1-Fc$^+$, and 164 nM F1M1). As F1M1-Fc$^-$ showed no detectable binding to both hCD16a allotypes, we used it as control devoid of effector function. Finally, we investigated by flow cytometry F1M1-Fc$^+$, F1M1 and F1M1-Fc$^-$ binding to hCD16a (158V or 158F allotype) expressed on the surface of human NK92 cells. It has been shown that the hCD16a 158V/F polymorphism in NK cells influences its binding to human IgG1.[31] Specifically, hCD16a V158 displays increased affinity for human IgG1, resulting in increased NK cell activation. F1M1 binding to hCD16a 158V was approximately fivefold higher than to hCD16a 158F at all tested concentrations (figure 1G). Compared with F1M1, F1M1-Fc$^+$ binding to hCD16a 158V was increased (2–3 fold), and even more to hCD16a 158F (7–20 fold).

F1M1-Fc$^+$ increases NK cell activation in vitro, and ADCC of TNBC cells and CAFs

We next compared F1M1-Fc$^+$, F1M1 and F1M1-Fc$^-$ in vitro capacity to activate NK cells by analyzing cell surface CD107a expression, as a functional marker of NK cell degranulation, and intracellular IFNγ, a cytokine secreted following NK cell activation,[32] in hCD16a-transduced human NK92 cell line. The percentages of CD107a$^+$ NK, IFNγ$^+$ NK and CD107a$^+$ IFNγ$^+$ NK subsets were increased similarly by 2–3 fold following incubation with F1M1-Fc$^+$, compared with F1M1, in hCD16a 158V-expressing or 158F-expressing NK cells (figure 2A). Conversely, F1M1-Fc$^-$ did not activate NK effector functions. Moreover, the percentages of CD107a$^+$ NK, IFNγ$^+$ NK and CD107a$^+$ IFNγ$^+$ NK cells were increased in a dose-dependent manner in the presence of increasing concentrations of cath-D bound to F1M1-Fc$^+$ (figure 2B). Overall, F1M1-Fc$^+$ was the most potent antibody to activate NK cell response. Next, we determined whether the F1M1-Fc$^+$-enhanced binding to hCD16a-expressing NK cells translated into increased cytotoxic activity. First, incubation of MDA-MB-231 cells with F1M1-Fc$^+$ significantly increased ADCC by 5-fold (p<0.0001) and 18-fold (p=0.0002), compared with F1M1, in the presence of NK92-hCD16a 158V cells and NK92-hCD16a 158F cells, respectively (figure 2C). F1M1-Fc$^-$ did not induce ADCC. Moreover, F1M1-Fc$^+$ triggered ADCC in a dose-dependent manner in the presence of NK92-hCD16a 158V cells (figure 2D). F1M1-Fc$^+$-induced ADCC was exclusively dependent on Fc binding to the hCD16 receptor on NK92-hCD16a 158V cells, because addition of a Fc block completely inhibited ADCC, to a level similar to that observed with F1M1-Fc$^-$ (figure 2E). We then evaluated ADCC against MDA-MB-231 cells using primary human NK cells (158V/F allotype) (online supplemental figure 4A). ADCC was significantly increased by 3.5-fold on incubation with F1M1-Fc$^+$, compared with F1M1 (p<0.0001) (online supplemental figure 4B).

As cath-D localizes at the surface of BC cells and stromal fibroblasts by binding to the M6P/IGF2 receptor,[28] we assessed whether M6P/IGF2 receptor-bound cath-D was involved in ADCC induction by F1M1-Fc$^+$. Thus, we evaluated ADCC against MDA-MB-231 cells in the presence of NK92-hCD16a 158V cells and of excess M6P to compete with cath-D binding to the M6P/IGF2 receptor (figure 2F). Addition of M6P, but not glucose-6-phosphate (negative control for M6P), significantly inhibited ADCC induction by F1M1-Fc$^+$ by 51% (p<0.0001), indicating that cath-D bound to its M6P/IGF2 receptor at the cell surface was involved in ADCC. Similarly, using primary human NK cells (158V/V allotype) (online supplemental figure 4C), ADCC of MDA-MB-231 cells was inhibited by 70% (p<0.0001) in the presence of M6P (online supplemental figure 4D). Moreover, F1M1-Fc$^+$ efficiently triggered ADCC against hCAF1 cells in the presence of NK92-hCD16a 158V cells, and excess M6P significantly inhibited ADCC by 62% (p<0.0001) (figure 2G). Lastly, to better recapitulate the in vivo cancer cell environment, we prepared spheroids of MDA-MB-231 cells co-cultured with NK92 hCD16a 158V cells. F1M1-Fc$^+$ also induced ADCC of MDA-MB-231 cell spheroids (figure 2H). Live imaging of ADCC in calcein-labeled MDA-MB-231 cell spheroids showed their time-dependent lysis in response to F1M1-Fc$^+$ exposure (online supplemental figure 5A,B). At 24 hours, the fluorescence signal of calcein-labeled

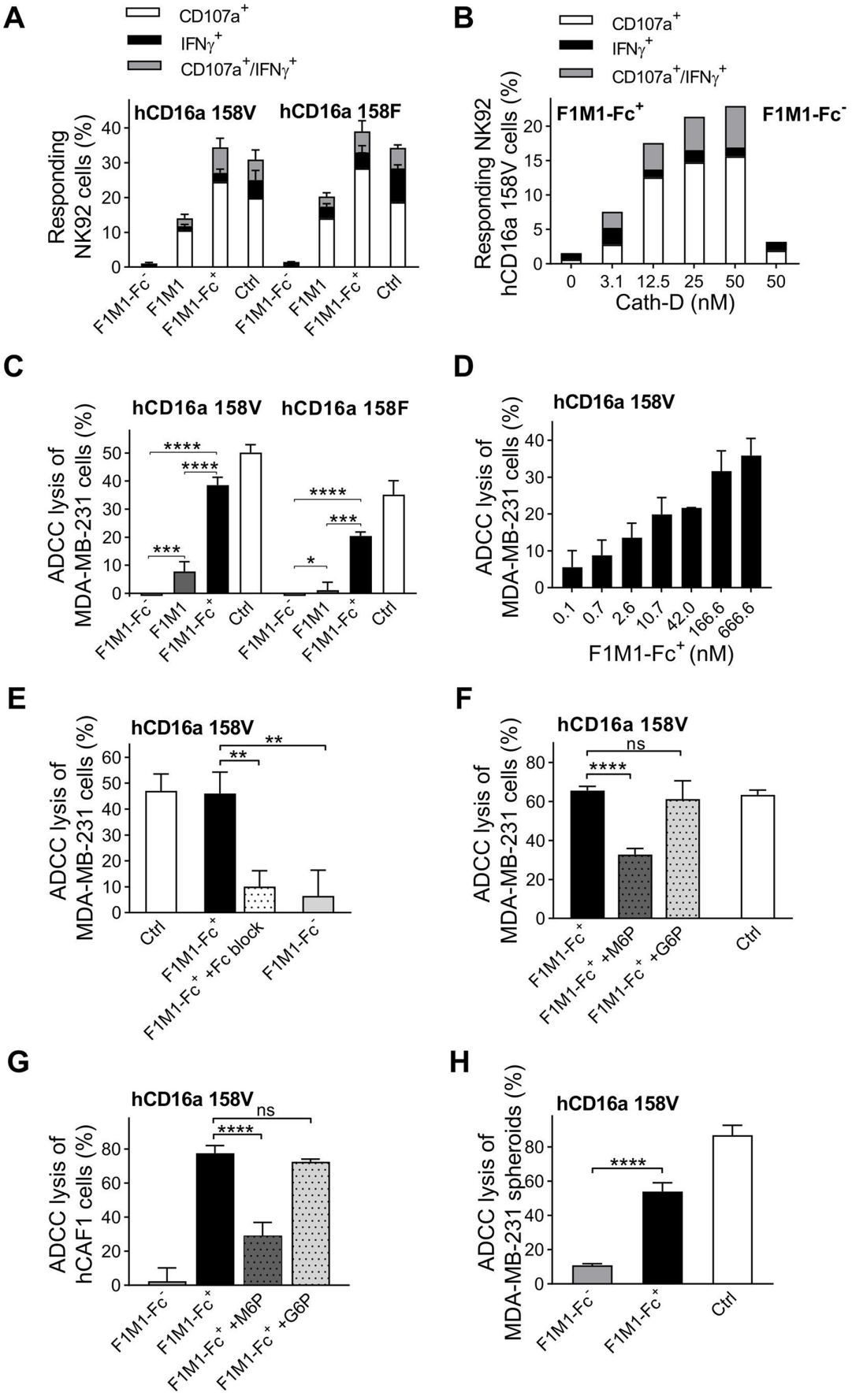

Figure 2 (Continued)

Figure 2 Fc-engineered F1M1-Fc$^+$ increases NK cell activation in vitro, and ADCC in TNBC cells and CAFs. (A) Functional responses of NK92 hCD16a 158V and NK92 hCD16a 158F cells induced by F1M1-Fc$^-$, F1M1, and F1M1-Fc$^+$. For in vitro stimulation and functional responses of hCD16a-transduced NK92 cells, 96-well plates were sensitized with a saturating concentration (5 µg/mL; 33.3 nM) of F1M1-Fc$^-$, F1M1, F1M1-Fc$^+$, or anti-hCD16a (3G8) monoclonal antibodies at 4°C for 12 hours. NK92 hCD16a 158V and NK92 hCD16a 158F cells were incubated on non-sensitized or sensitized plates with/without the anti-CD107a-PC5 antibody (1:20) and 0.1 µg/mL BD GolgiPlug containing brefeldin A at 37°C for 4 hours. Cells were then fixed and permeabilized and stained with an anti-IFNγ-PE antibody (1:20) at 4°C for 30 min to detect intracellular IFNγ. The percentages of degranulating NK92 cells (CD107a$^+$IFNγ$^-$; white bars), IFNγ-producing NK92 cells (CD107a$^-$IFNγ$^+$; black bars), and NK92 cells exhibiting both responses (CD107a$^+$IFNγ$^+$; gray bars) were quantified by flow cytometry after 4 hours of stimulation. Mean (%) ±SD (n=3). 3G8 (anti-hCD16a antibody) was used as positive control of CD16 engagement (Ctrl). (B) Functional responses of NK92-hCD16a 158V cells induced by F1M1-Fc$^+$ in the presence of increasing concentrations of cath-D. 96-well plates were coated with the M2E8 anti-cath-D antibody (2500 ng/well) at 4°C overnight, incubated or not with increasing concentrations of cath-D (3-50 nM) and then sensitized with F1M1-Fc$^+$ (5 µg/mL). The percentage of degranulating (CD107a$^+$IFNγ-; white bars), IFNγ-producing (CD107a$^-$IFNγ$^+$; black bars), and NK92-hCD16a 158V cells exhibiting both responses (CD107a$^+$IFNγ$^+$; gray bars) was evaluated as in (A) after 4 hours of stimulation. (C) ADCC activity against MDA-MB-231 cells in the presence of NK92-hCD16a cells in response to F1M1-Fc$^-$, F1M1 or F1M1-Fc$^+$. MDA-MB-231 cells (target) were preincubated with F1M1-Fc$^-$, F1M1, F1M1-Fc$^+$, or with cetuximab at 100 µg/mL (666 nM) at 37°C for 30 min, followed by incubation with NK92-hCD16a 158V (left) or NK92-hCD16a 158F (right) cells (effector) at an effector:target ratio of 10:1 for 24 hours. MDA-MB-231 cell lysis was evaluated by measuring LDH release. Cetuximab (anti-EGFR antibody) was used as positive control (Ctrl). For hCD16a 158V cells (left): ****p<0.0001 for F1M1-Fc$^+$ vs F1M1, ****p<0.0001 for F1M1-Fc$^+$ vs F1M1-Fc$^-$, ***p=0.0003 for F1M1 vs F1M1-Fc$^-$ (one-way ANOVA). For hCD16a 158F cells (right): ***p=0.0002 for F1M1-Fc$^+$ vs F1M1, ****p<0.0001 for F1M1-Fc$^+$ vs F1M1-Fc$^-$, *p=0.015 for F1M1 vs F1M1-Fc$^-$ (one-way ANOVA). (D) Dose-dependent induction of ADCC against MDA-MB-231 cells in the presence of hCD16a 158V-expressing NK92 cells in response to F1M1-Fc$^+$. ADCC was evaluated in MDA-MB-231 cells incubated with hCD16a 158V-expressing NK92 cells at an effector:target ratio of 10:1, as described in (C), after incubation with increasing concentrations of F1M1-Fc$^+$, from 0.1 to 666 nM (0.015–100 µg/mL). (E) Effect of blocking Fc binding sites in NK92-hCD16a 158V cells on F1M1-Fc$^+$-induced ADCC in MDA-MB-231 cells. NK92-hCD16a 158V cells were preincubated or not with Fc block (to saturate the Fc binding sites in NK92-hCD16a 158V cells) for 30 min. MDA-MB-231 cells, preincubated with F1M1-Fc$^+$ at 100 µg/mL (666 nM) for 30 min, were incubated with NK92-hCD16a 158V cells preincubated or not with Fc block. ADCC was analyzed as described in (C). Cetuximab (100 µg/mL), positive control (Ctrl); F1M1-Fc$^-$, negative control (100 µg/mL). **p=0.0023 for F1M1-Fc$^+$ vs F1M1-Fc$^+$+Fc block, **p=0.0012 for F1M1-Fc$^+$ vs F1M1-Fc$^-$ (one-way ANOVA). (F) Blocking cath-D binding to M6P receptors in MDA-MB-231 cells affects F1M1-Fc$^+$-induced ADCC in the presence of NK92-hCD16a 158V cells. MDA-MB-231 cells (target) were preincubated with M6P (10 mM) or G6P (10 mM) for 24 hours. Then, ADCC was assessed in these cells with NK92-hCD16a 158V cells (effector) at an effector:target ratio of 10:1, as described in C, after incubation with F1M1-Fc$^+$ at 100 µg/mL (666 nM) in the presence of M6P (10 mM) or G6P (10 mM). M6P, mannose-6-phosphate; G6P, glucose-6-phosphate (negative control for M6P). Cetuximab (100 µg/mL), positive control (Ctrl). ****p<0.0001 for F1M1-Fc$^+$ vs F1M1-Fc$^+$+M6P, ***p=0.0002 for F1M1-Fc$^+$+G6P vs F1M1-Fc$^+$+M6P (one-way ANOVA). (G) Blocking cath-D binding to M6P receptors in hCAFs affects F1M1-Fc$^+$-induced ADCC in the presence of NK92-hCD16a 158V cells. Breast hCAF1 cells (target) were pre-incubated with M6P (10 mM) or G6P (10 mM) for 24 hours. ADCC was assessed in these hCAF1 cells in the presence of NK92-hCD16a 158V cells (effector) at an effector:target ratio of 10:1, as described in F, after incubation with F1M1-Fc$^+$ at 100 µg/mL (666 nM) and M6P (10 mM) or G6P (10 mM). Cetuximab (100 µg/mL), positive control (Ctrl); F1M1-Fc$^-$, negative control (100 µg/mL). ****p<0.0001 for F1M1-Fc$^+$ vs F1M1-Fc$^+$+M6P, ****p<0.0001 for F1M1-Fc$^+$+G6P vs F1M1-Fc$^+$+M6P (one-way ANOVA). (H) ADCC against MDA-MB-231 cell spheroids in the presence of NK92-hCD16a 158V cells in response to F1M1-Fc$^+$. MDA-MB-231 cell spheroids (target) were first incubated with F1M1-Fc$^+$, F1M1-Fc$^-$, or cetuximab (100 µg/mL) positive control (Ctrl) at 37°C for 30 min. Then, spheroids were incubated with NK92-hCD16a 158V cells (effector) at an effector:target ratio of 20:1 for 24 hours, and ADCC was assessed as described in (C). ****p<0.0001 for F1M1-Fc$^+$ vs F1M1-Fc$^-$ (one-way ANOVA). ADCC, antibody-dependent cellular cytotoxicity; ANOVA, analysis of variance; CAF, cancer-associated fibroblasts; LDH, lactate dehydrogenase; TNBC, triple-negative breast cancer.

MDA-MB-231 spheroids was significantly decreased by 29.5% in response to F1M1-Fc$^+$ compared with F1M1-Fc$^-$ (p=0.005) (online supplemental figure 5C). Overall, our results demonstrated that F1M1-Fc$^+$ is the most potent anti-cath-D antibody to trigger ADCC in TNBC cells and CAFs.

F1M1-Fc$^+$ is the best candidate to reduce MDA-MB-231 cell xenograft growth and improve mouse survival

To compare the in vivo antitumor efficacy of F1M1-Fc$^+$, F1M1, and F1M1-Fc$^-$, we used athymic Foxn1^{nu} nude mice subcutaneously xenografted with MDA-MB-231 cells. When MDA-MB-231 tumors reached 50 mm^3, we treated mice with F1M1-Fc$^+$, F1M1, F1M1-Fc$^-$, or the anti-human CD20 IgG1 rituximab, as negative isotype control (Ctrl) (15 mg/kg) by ip three times per week for 35 days (days 13–48 postgraft), and sacrificed mice when tumor volume reached 2000 mm^3. Both F1M1-Fc$^+$ and F1M1 significantly delayed tumor growth compared with negative control (p=0.001 for F1M1-Fc$^+$, p=0.011 for F1M1). F1M1-Fc$^-$ slightly delayed tumor growth (p=0.057) (figure 3A). F1M1-Fc$^+$ tended to be more effective than F1M1-Fc$^-$ (p=0.055). At day 48 (treatment end), tumor volume was significantly reduced by 77% (p=0.0002) in the F1M1-Fc$^+$ group, by 60% (p=0.0007) in the F1M1 group, and by 40.5% (p=0.0289) in the F1M1-Fc$^-$ group compared with control (figure 3B). Tumor volume was significantly

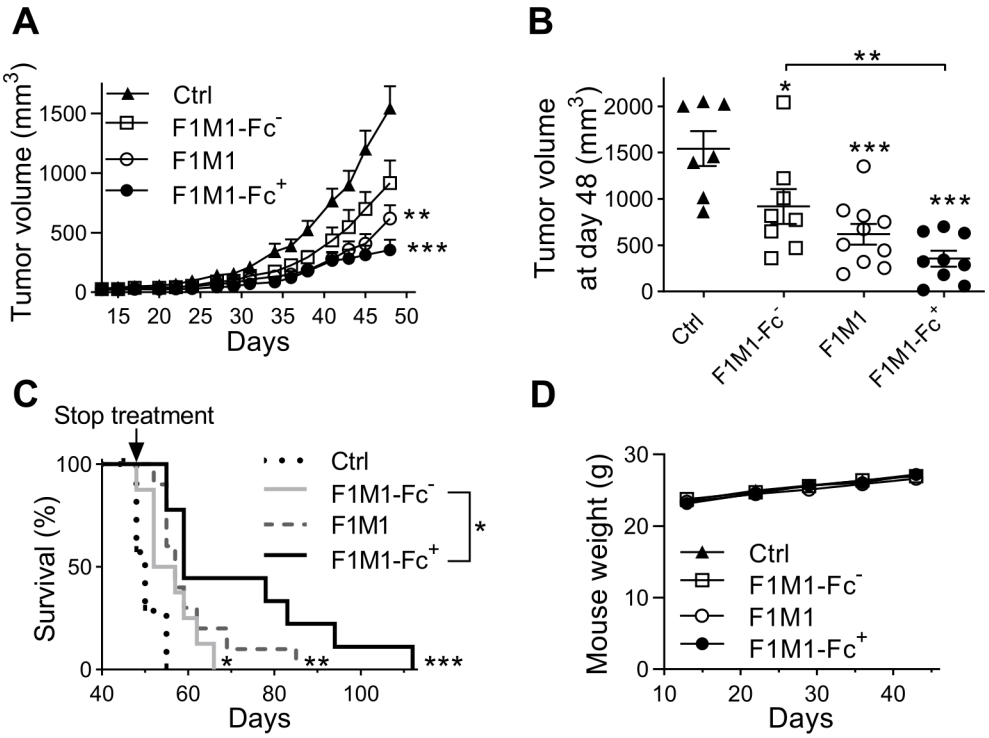

Figure 3 F1M1-Fc$^+$ is the best candidate to reduce growth of MDA-MB-231 cell xenografts and improve mouse survival. (A) Tumor growth. MDA-MB-231 cells were subcutaneously injected in nude mice. When tumor volume reached 50 mm^3, mice were treated with F1M1 (n=10), F1M1-Fc$^-$ (n=8), F1M1-Fc$^+$ (n=9) (15 mg/kg), or rituximab (Ctrl; n=7) (15 mg/kg), three times per week for 35 days. Mice were sacrificed when tumor volume reached 2000 mm^3. Tumor volume (in mm^3) is shown as the mean±SEM. p=0.057 for F1M1-Fc$^-$ vs Ctrl, **p=0.011 for F1M1 vs Ctrl, ***p=0.001 for F1M1-Fc$^+$ vs Ctrl, p=0.055 for F1M1-Fc$^+$ vs F1M1-Fc$^-$, p=0.416 for F1M1-Fc$^+$ vs F1M1, p=0.066 for F1M1 vs F1M1-Fc$^-$ (mixed-effects multiple linear regression test). (B) Mean tumor volume at day 48. n=7 for Ctrl (rituximab); n=10 for F1M1; n=8 for F1M1-Fc$^-$; n=9 for F1M1-Fc$^+$. ***p=0.0003 for all groups (Kruskal-Wallis). *p=0.0289 for F1M1-Fc$^-$ vs Ctrl, ***p=0.0007 for F1M1 vs Ctrl, ***p=0.0002 for F1M1-Fc$^+$ vs Ctrl, **p=0.0041 for F1M1-Fc$^+$ vs F1M1-Fc$^-$, p=0.0947 for F1M1-Fc$^+$ vs F1M1, p=0.2114 for F1M1 vs F1M1-Fc$^-$ (Mann-Whitney t-test). Data are the mean±SEM. (C) Kaplan-Meier survival analysis. n=7 for Ctrl (rituximab); n=10 for F1M1; n=8 for F1M1-Fc$^-$; n=9 for F1M1-Fc$^+$. *p=0.0275 for F1M1-Fc$^-$ vs Ctrl, **p=0.0011 for F1M1 vs Ctrl, ***p=0.0003 for F1M1-Fc$^+$ vs Ctrl, *p=0.0253 for F1M1-Fc$^+$ vs F1M1-Fc$^-$, p=0.3093 for F1M1 vs F1M1-Fc$^-$, p=0.0953 for F1M1-Fc$^+$ vs F1M1 (log-rank Mantel-Cox test). (D) Mouse weight monitoring. n=7 for Ctrl (rituximab); n=10 for F1M1; n=8 for F1M1-Fc$^-$; n=9 for F1M1-Fc$^+$. Data are the mean±SEM.

smaller in the F1M1-Fc$^+$ group than in the F1M1-Fc$^-$ group (p=0.0041). The overall survival rate, reflected by a tumor volume <2000 mm^3, was significantly longer in the F1M1-Fc$^+$, F1M1, and F1M1-Fc$^-$ groups than in controls. The median survival was 59, 57, 54.5, and 50 days in the F1M1-Fc$^+$, F1M1, F1M1-Fc$^-$, and control groups, respectively (figure 3C; Kaplan-Meier survival analysis, p=0.0003 for F1M1-Fc$^+$, p=0.0011 for F1M1, p=0.0275 for F1M1-Fc$^-$ compared with control). The overall survival rate was significantly longer in mice treated with F1M1-Fc$^+$ than with F1M1-Fc$^-$ (p=0.0253). Moreover, all treated mice gained weight (figure 3D) and displayed normal activities, suggesting no apparent toxicity. Overall, the results suggest that F1M1-Fc$^+$ is the anti-cath-D antibody with the best antitumor activity.

F1M1-Fc$^+$ triggers in vivo recruitment, activation, and cytotoxic activity of NK cells to induce ADCC in MDA-MB-231 TNBC cell xenografts

To investigate the in vivo mechanisms underlying the antitumor effect of F1M1-Fc$^+$, F1M1, and F1M1-Fc$^-$, we treated nude mice xenografted with MDA-MB-231 cells with F1M1-Fc$^+$, F1M1, F1M1-Fc$^-$, or rituximab as negative isotype control (same schedule as before), and then sacrificed all mice at treatment end (day 48). F1M1-Fc$^+$, F1M1, and F1M1-Fc$^-$ inhibited tumor growth compared with rituximab, but only F1M1-Fc$^+$ resulted in significant tumor growth inhibition compared with rituximab (p=0.003) (figure 4A). At day 48, tumor volume was significantly reduced by 60.3% (p=0.0005) in the F1M1-Fc$^+$ group, by 42.9% (p=0.02) in the F1M1 group, and by 36.6% (p=0.0368) in the F1M1-Fc$^-$ group compared with control group (figure 4B,C). Tumor volume was significantly more reduced in the F1M1-Fc$^+$ group than in the F1M1-Fc$^-$ group (p=0.0368). Human cath-D expression level in tumors was not affected by F1M1-Fc$^+$, F1M1, or F1M1-Fc$^-$ treatment, as shown by IHC and western blot analyses (online supplemental figure 6A–C). To study the impact of the Fc part of F1M1 on NK cell recruitment and activation, we identified and quantified by flow cytometry tumor-infiltrating NK cells in MDA-MB-231 xenografts

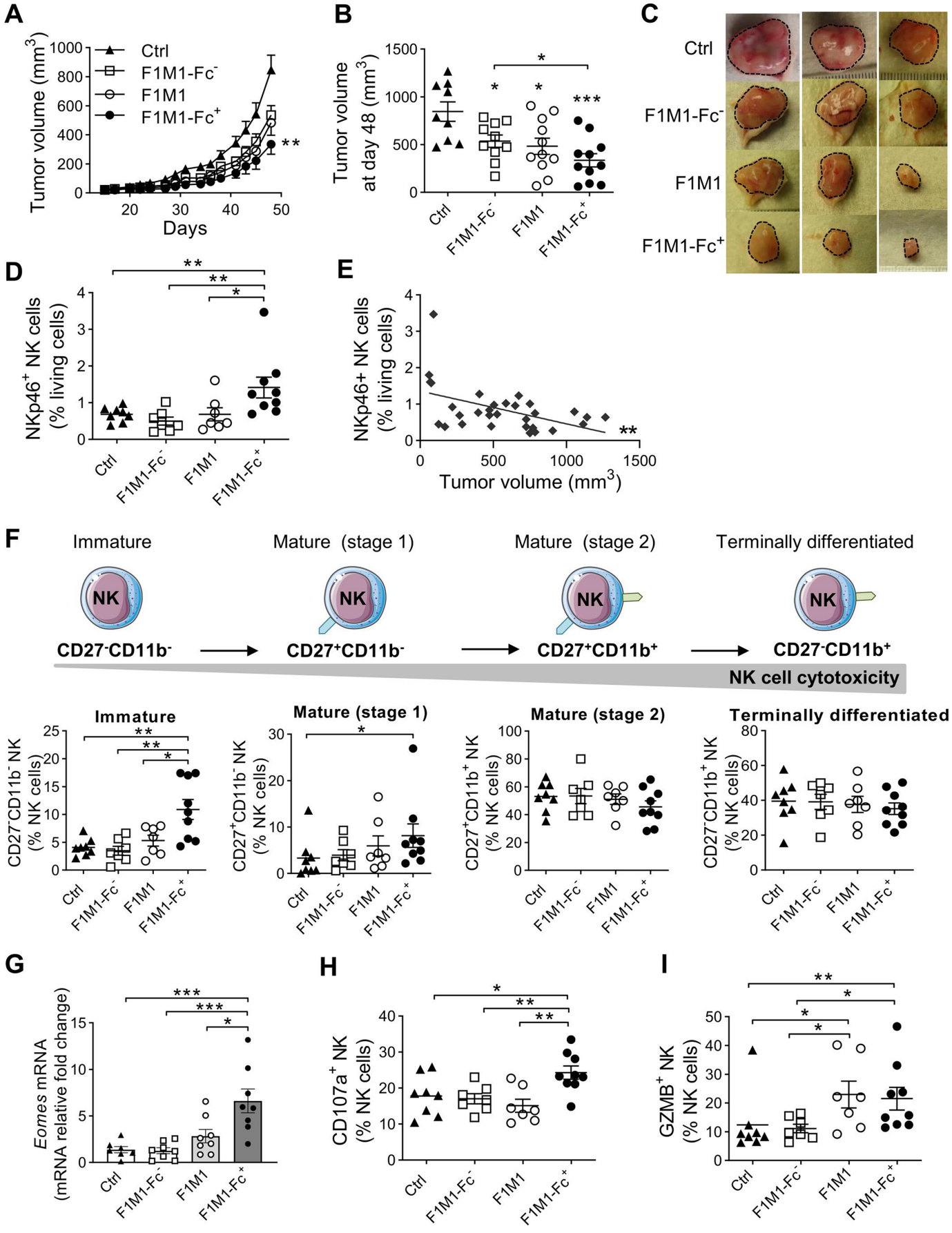

Figure 4 (Continued)

Figure 4 F1M1-Fc$^+$ triggers recruitment and activation of NK cells to induce ADCC in MDA-MB-231 cell xenografts. (A) Tumor growth. MDA-MB-231 cells were subcutaneously injected in nude mice. When tumor volume reached 50 mm^3, mice were treated with F1M1 (n=11), F1M1-Fc$^-$ (n=10), F1M1-Fc$^+$ (n=11), or rituximab (15 mg/kg) (Ctrl; n=9), three times per week for 30 days. At day 48, mice were sacrificed. Tumor volume (in mm^3) is shown as the mean±SEM. **p=0.003 for F1M1-Fc$^+$ vs Ctrl, p=0.066 for F1M1 vs Ctrl, p=0.353 for F1M1-Fc$^-$ vs Ctrl, p=0.061 for F1M1-Fc$^+$ vs F1M1-Fc$^-$, p=0.413 for F1M1 vs F1M1-Fc$^-$, p=0.995 for F1M1-Fc$^+$ vs F1M1 (mixed-effects multiple linear regression test). (B) Mean tumor volume at day 48. n=9 for Ctrl (rituximab); n=11 for F1M1; n=10 for F1M1-Fc$^-$; n=11 for F1M1-Fc$^+$. **p=0.0044 for all groups (Kruskal-Wallis), *p=0.0368 for F1M1-Fc$^-$ vs Ctrl, *p=0.020 for F1M1 vs Ctrl, ***p=0.0005 for F1M1-Fc$^+$ vs Ctrl, *p=0.0368 for F1M1-Fc$^+$ vs F1M1-Fc$^-$, p=0.6047 for F1M1 vs F1M1-Fc$^-$, p=0.2234 for F1M1 vs F1M1-Fc$^+$ (Mann-Whitney t-test). Mean±SEM. (C) Representative images of three tumors per treatment group. (D) NK cell recruitment at day 48. The percentage of NKp46$^+$ NK cells was quantified by FACS and expressed relative to all living cells (n=7 for F1M1-Fc$^-$; n=7 for F1M1; n=9 for F1M1-Fc$^+$; n=8 for Ctrl). **p=0.0075 for all groups (Kruskal-Wallis), **p=0.0053 for F1M1-Fc$^+$ vs Ctrl, **p=0.0033 for F1M1-Fc$^+$ vs F1M1-Fc$^-$, *p=0.0295 for F1M1-Fc$^+$ vs F1M1, p=0.4359 for F1M1-Fc$^-$ vs F1M1 (Mann-Whitney t-test). (E) Linear regression analysis of NK cells and tumor volumes at day 48. R^2 =0.2139; **p=0.0062; n=31 mice (all treatment groups). (F) NK cell maturation at day 48. NK cell maturation is divided into four stages [immature, mature (stage 1), mature (stage 2) and terminally differentiated] based on the expression of the CD27 and CD11b cell surface maturation markers, and is associated with NK cell-mediated cytotoxicity (upper panels). In the lower panels, the percentage of NKp46$^+$ NK cells at the different maturation stages was quantified by FACS and expressed relative to all NKp46$^+$ NK cells: immature CD27$^-$CD11b$^-$ NKp46$^+$ NK cells [(n=7 for F1M1-Fc$^-$; n=7 for F1M1; n=9 for F1M1-Fc$^+$; n=8 for Ctrl). **p=0.0049 for all groups (Kruskal-Wallis); **p=0.0016 for F1M1-Fc$^+$ vs Ctrl; **p=0.0033 for F1M1-Fc$^+$ vs F1M1-Fc$^-$; *p=0.0404 for F1M1-Fc$^+$ vs F1M1; p=0.2086 for F1M1 vs F1M1-Fc$^-$ (Mann-Whitney t-test)], mature (stage 1) CD27$^+$CD11b$^-$ NKp46$^+$ NK cells [(n=7 for F1M1-Fc$^-$; n=7 for F1M1; n=9 for F1M1-Fc$^+$, n=8 for Ctrl). p=0.1248 for all groups (Kruskal-Wallis); *p=0.0360 for F1M1-Fc$^+$ vs Ctrl; p=0.1142 for F1M1-Fc$^+$ vs F1M1-Fc$^-$; p=0.3510 for F1M1-Fc$^+$ vs F1M1; p=0.62 for F1M1 vs F1M1-Fc$^-$ (Mann-Whitney t-test)], mature (stage 2) CD27$^+$CD11b$^+$ NKp46$^+$ NK cells [(n=7 for F1M1-Fc$^-$; n=7 for F1M1; n=9 for F1M1-Fc$^+$; n=8 for Ctrl). p=0.5473 for all groups (Kruskal-Wallis), p=0.2086 for F1M1-Fc$^+$ vs Ctrl; p=0.4698 for F1M1-Fc$^+$ vs F1M1-Fc$^-$; p=0.3120 for F1M1-Fc$^+$ vs F1M1; p>0.9999 for F1M1 vs F1M1-Fc$^-$ (Mann-Whitney t-test)], and terminally differentiated CD27$^-$CD11b$^+$ NKp46$^+$ NK cells [(n=7 for F1M1-Fc$^-$; n=7 for F1M1; n=9 for F1M1-Fc$^+$; n=8 for Ctrl). p=0.8272 for all groups (Kruskal-Wallis); p=0.4234 for F1M1-Fc$^+$ vs Ctrl; p=0.4698 for F1M1-Fc$^+$ vs F1M1-Fc$^-$; p=0.8371 for F1M1-Fc$^+$ vs F1M1; p=0.8048 for F1M1 vs F1M1-Fc$^-$ (Mann-Whitney t-test)]. (G) Quantification of *Eomes* mRNA expression at day 48. Total RNA was extracted from MDA-MB-231 tumor cell xenografts at treatment end, and *Eomes* expression level was analyzed by RT-qPCR. Relative fold change was normalized to *Rps9* expression and expressed as fold change relative to control. Data are the mean±SEM (n=8 for F1M1-Fc$^-$; n=8 for F1M1; n=8 for F1M1-Fc$^+$; n=7 for Ctrl). **p=0.0016 for all groups (Kruskal-Wallis). ***p=0.0006 for F1M1-Fc$^+$ vs Ctrl, ***p=0.0006 for F1M1-Fc$^+$ vs F1M1-Fc$^-$, *p=0.0281 for F1M1 vs F1M1-Fc$^+$, p=0.0650 for F1M1 vs F1M1-Fc$^-$ (Mann-Whitney t-test). (H) NK cell degranulation at day 48. The percentage of CD107a$^+$ degranulating NK cells was quantified by FACS and expressed relative to all NKp46$^+$ NK cells (n=7 for F1M1-Fc$^-$; n=7 for F1M1; n=9 for F1M1-Fc$^+$; n=8 for Ctrl). *p=0.0107 for all groups (Kruskal-Wallis), *p=0.0464 for F1M1-Fc$^+$ vs Ctrl, **p=0.0079 for F1M1-Fc$^+$ vs F1M1-Fc$^-$, **p=0.0021 for F1M1-Fc$^+$ vs F1M1, p=0.3176 for F1M1 vs F1M1-Fc$^-$ (Mann-Whitney t-test). (I) Granzyme B$^+$ NK cells at day 48. The percentage of granzyme-positive (GZMB$^+$) activated NK cells was quantified by FACS and expressed relative to all NKp46$^+$ NK cells (n=7 for F1M1-Fc$^-$; n=7 for F1M1; n=9 for F1M1-Fc$^+$; n=8 for Ctrl). *p=0.0119 for all groups (Kruskal-Wallis), **p=0.0079 for F1M1-Fc$^+$ vs Ctrl, *p=0.0289 for F1M1 vs Ctrl, *p=0.0418 for F1M1-Fc$^+$ vs F1M1-Fc$^-$, *p=0.0262 F1M1 vs F1M1-Fc$^-$, p>0.9999 for F1M1-Fc$^+$ vs F1M1 (Mann-Whitney t-test). ADCC, antibody-dependent cellular cytotoxicity; NK, natural killer.

after treatment end (day 48). The overall percentage of living cells was not different between untreated (control) and treated groups (online supplemental figure 7). The percentage of NK (CD45$^+$ F4/80$^-$ CD3$^-$ CD19$^-$ CD11c$^-$ NKp46$^+$) cells within the living immune CD45$^+$ cell population was significantly increased by 207.2% in the F1M1-Fc$^+$ group compared with control (p=0.0053), but not in the F1M1 and F1M1-Fc$^-$ groups (figure 4D). Linear regression analysis showed that the NK cell percentage was inversely correlated with tumor volume in all animals (four treatment groups together) (R^2=0.2139, p=0.0062) (figure 4E). This suggested that in the F1M1-Fc$^+$ group, NK cell recruitment in the tumor contributed to the anti-tumor response.

We also determined the NK cell phenotype based on the expression of the NK cell surface maturation markers CD11b and CD27.[33] The immature CD27$^-$CD11b$^-$ NK cell population was significantly increased by 268% in F1M1-Fc$^+$-treated animals (p=0.0016 compared with the control group), but not in the F1M1-treated and F1M1-Fc$^-$-treated groups (figure 4F). The CD27$^+$CD11b$^-$ NK cell population (mature stage 1) also was increased in the F1M1-Fc$^+$ group by 206.9% (p=0.0360 compared with the control group) (figure 4F). This suggests that F1M1-Fc$^+$ treatment promoted the recruitment of immature NK cells and at an early stage of the maturation process. NK cell development and maturation is orchestrated by a network of transcription factors, including *Eomes*.[34] *Eomes* is mainly expressed in immature NK cells, promotes survival of maturing NK cells, and plays a major role in the induction of genes associated with NK cell cytotoxicity, such as *Prf1*.[35] RT-qPCR analysis of tumor samples showed that *Eomes* expression was significantly upregulated by 479.3% in the F1M1-Fc$^+$ group (p=0.0006 compared with control), but not in the F1M1 and F1M1-Fc$^-$ groups (figure 4G). This strongly suggested that F1M1-Fc$^+$-based therapy triggers the recruitment of immature NK cells that might become cytotoxic in the MDA-MB-231 TNBC model.

Next, we analyzed cell surface expression of CD107a, as a functional marker of NK cell degranulation, by flow

cytometry in tumor-infiltrating NKp46$^+$ cells in MDA-MB-231 cell xenografts at day 48. The percentage of CD107a$^+$ NK cells within the NK cell population was significantly increased by 142% in F1M1-Fc$^+$-treated animals (p=0.0464 compared with control), but not in the F1M1 and F1M1-Fc$^-$ groups (figure 4H). The percentage of CD107a$^+$ NK cells was higher (by 142.6%) in the F1M1-Fc$^+$ group compared with the F1M1-Fc$^-$ group (p=0.0079). Linear regression analysis showed that the percentage of CD107a$^+$ NK cells was inversely correlated with tumor volume in all animals (four treatment groups together) (R^2=0.1703, p=0.0211) (online supplemental figure 8A). This suggested that in the F1M1-Fc$^+$ group, in vivo tumor infiltration by activated CD107a$^+$ NK cells may contribute to the antitumor response.

Lastly, we analyzed intracellular granzyme B (GZMB) expression as a marker of NK cell cytotoxic activity by flow cytometry in tumor-infiltrating NKp46$^+$ cells in MDA-MB-231 cell xenografts at day 48. The percentage of GZMB$^+$ NK cells was significantly increased by 173.8% (p=0.0079) and by 185.4% (p=0.0289) in the F1M1-Fc$^+$ and F1M1 groups, respectively, compared with control, but not in the F1M1-Fc$^-$ group (figure 4I). It also was higher (by 193%) in the F1M1-Fc$^+$ group than in the F1M1-Fc$^-$ group (p=0.0418). Linear regression analysis showed that the percentage of GZMB$^+$ NK cells was inversely correlated with tumor volume in all animals (four treatment groups together) (R^2=0.3085, p=0.0012) (online supplemental figure 8B). This suggested that in the F1M1-Fc$^+$ and F1M1 groups, tumor infiltration by NK cells with cytotoxic activity contributed to the antitumor response.

In agreement, granzyme B (*Gzmb*) and perforin (*Prf1*) mRNA levels, as a read-out of NK cell cytotoxic activity, were upregulated (up to 166.3% and 173.8%, respectively) in the F1M1-Fc$^+$ group compared with control group (p=0.3969 and p=0.2319), and also compared with the F1M1-Fc$^-$ group (up to 256.3% and 243.4%; p=0.0207 and p=0.0379, respectively) (online supplemental figure 9A,B). The antitumor cytokine *Tnf*, secreted by activated NK cells, was also upregulated by 171.5% (p=0.0059) in the F1M1-Fc$^+$ group and by 160.3% (p=0.0541) in the F1M1 group compared with control (online supplemental figure 9C). *Tnf* was upregulated (by 266.8%) (p=0.003) in the F1M1-Fc$^+$ group compared with the F1M1-Fc$^-$ group. Altogether, these results demonstrated that F1M1-Fc$^+$ triggers NK cell recruitment, activation and cytotoxic activity in MDA-MB-231 cell xenografts, and strongly suggest the key role of the Fc part of this anti-cath-D antibody in its antitumor activity via NK cells.

NK cell depletion impairs F1M1-Fc$^+$ therapeutic efficacy in MDA-MB-231 cell xenografts

The significant antitumor effects of F1M1-Fc$^+$ and the F1M1-Fc$^+$-mediated induction of NK cell recruitment, activation and cytotoxic activity strongly suggested that NK cells are crucial for F1M1-Fc$^+$-antitumor activity. To confirm this hypothesis, we depleted NK cells in MDA-MB-231-bearing nude mice by intraperitoneal injection of an anti-asialo-GM1 antibody (αGM1). First, to determine the efficiency of NK cell depletion, we treated non-grafted nude mice with control (saline solution) or αGM1 at day 0 and day 3 (online supplemental figure 10A). Analysis of blood samples at day 4 and day 7 confirmed the efficacy of NK cell depletion, even 4 days (ie, day 7) after the last αGM1 injection (online supplemental figure 10B,C). Other immune cells (B cells, neutrophils, dendritic cells and macrophages) were not affected by αGM1 treatment, as indicated by their quantification in blood and spleen (online supplemental figure 10D,E).

Then, to investigate NK cell role in the antitumor effect of F1M1-Fc$^+$, we treated nude mice harboring MDA-MB-231 cell xenografts with F1M1-Fc$^+$ or rituximab (negative isotype control) in the presence or absence of αGM1, and then sacrificed all mice at treatment end (day 48), according to the schedule described in figure 5A. As previously observed, F1M1-Fc$^+$ significantly inhibited tumor growth compared with control (p<0.001) (figure 5B). In the presence of αGM1, F1M1-Fc$^+$ antitumor activity (tumor growth reduction) was decreased (p=0.021 vs control, and p=0.015 vs F1M1-Fc$^+$ alone), revealing the crucial role of NK cells (figure 5B). At day 48, compared with the control group, tumor volume was significantly reduced by 63.3% (p=0.0003) in the F1M1-Fc$^+$ group, but only by 30.7% (p=0.0881) in the F1M1-Fc$^+$+αGM1 group (figure 5C). Moreover, tumor volume was significantly smaller in the F1M1-Fc$^+$ group than in the F1M1-Fc$^+$+αGM1 group (p=0.0281) (figure 5C). The number of tumor-infiltrating NK cells (CD45$^+$ CD3$^-$ CD19$^-$ Ly6G$^-$ NKp46$^+$) within the living immune CD45$^+$ cell population in tumors was significantly increased by 248.7% in the F1M1-Fc$^+$ group compared with control (p=0.0312). Conversely, very few NK cells were detected in the F1M1-Fc$^+$+αGM1 group (figure 5D). Analysis of blood samples at day 45 and of the spleens at day 48 validated NK cell depletion in the F1M1-Fc$^+$+αGM1 group (online supplemental figure 11). This demonstrated the key role of NK cells in F1M1-Fc$^+$ therapeutic efficiency.

Drug-induced neutropenia is a potentially serious and life-threatening adverse event that may occur after therapy with various agents, including antibodies (eg, immune checkpoint inhibitors). Analysis by flow cytometry of blood from mice from the control and F1M1-Fc$^+$ treated groups (from figure 5) showed that neutrophil count at day 45 was not affected, indicating the absence of neutropenia (online supplemental figure 12A). Similarly, no sign of leukopenia, thrombopenia, and anemia was observed after F1M1-Fc$^+$ treatment, suggesting the absence of toxicity (online supplemental figure 12B).

F1M1-Fc$^+$ inhibits tumor growth of patient-derived TNBC xenografts and improves mouse survival

Next, we tested F1M1-Fc$^+$ therapeutic effect in mice harboring TNBC-PDXs (B1995 and B3977).[36] First, we analyzed the expression of cath-D and the M6P/IGF2 receptor in PDX B1995 and B3977 xenografts (the two fastest growing PDXs in nude mice among a PDX

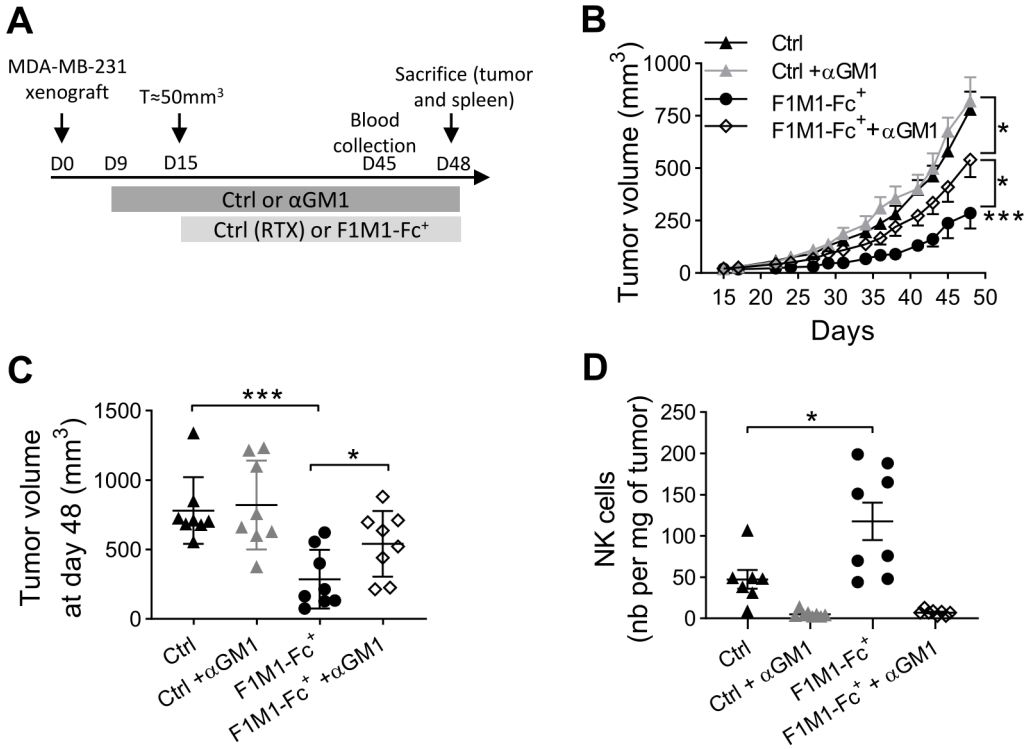

Figure 5 NK cell depletion impairs F1M1-Fc$^+$ therapeutic efficacy in MDA-MB-231 cell xenografts. (A) Treatment schedule for NK cell depletion. MDA-MB-231 cells were subcutaneously injected in nude mice. At day 9 after MDA-MB-231 injection, half of the mice started the treatment with anti-asialo GM1 antibodies (αGM1, 50 µL by ip injection twice per week) to deplete NK cells. When tumor volume reached 50 mm^3 (day 15), mice were treated with F1M1-Fc$^+$ (n=8), or control rituximab (Ctrl; n=8) (15 mg/kg), three times per week for 30 days, in the absence or presence of αGM1. At day 48, mice were sacrificed. (B) Tumor growth. Tumor growth (in mm^3) is shown as the mean±SEM. (n=8 for F1M1-Fc$^+$; n=8 for F1M-Fc$^+$+ αGM1; n=8 for Ctrl; n=8 for Ctrl+αGM1). p=0.449 for Ctrl+αGM1 vs Ctrl, ***p<0.001 for F1M1-Fc$^+$ vs Ctrl, ***p<0.001 for F1M1-Fc$^+$ vs Ctrl+αGM1, *p=0.015 for F1M1-Fc$^+$+αGM1 vs F1M1-Fc$^+$, *p=0.021 for F1M1-Fc$^+$+ αGM1 vs Ctrl + αGM1, p=0.127 for F1M1-Fc$^+$+ αGM1 vs Ctrl (mixed-effects multiple linear regression test). (C) Mean tumor volume at day 48. Mean±SEM. (n=8 for F1M1-Fc$^+$; n=8 for F1M-Fc$^+$+αGM1; n=8 for Ctrl; n=8 for Ctrl + αGM1). **p=0.0018 for all groups (Kruskal-Wallis), ***p=0.0003 for F1M1-Fc$^+$ vs Ctrl, p=0.8785 for Ctrl + αGM1 vs Ctrl, **p=0.0019 for F1M1-Fc$^+$ vs Ctrl + αGM1, *p=0.0281 for F1M1-Fc$^+$+ αGM1 vs F1M1-Fc$^+$, p=0.0881 for F1M1-Fc$^+$+ αGM1 vs Ctrl, p=0.1605 for F1M1-Fc$^+$+ αGM1 vs Ctrl + αGM1 (Mann-Whitney t-test). (D) NK cell recruitment at day 48. The number of NKp46$^+$ NK cells in tumors was quantified by FACS and normalized per mg of tumor with precision count beads (n=8 for F1M1-Fc$^+$; n=8 for F1M-Fc$^+$+ αGM1; n=7 for Ctrl; n=8 for Ctrl + αGM1). ****p<0.0001 for all groups (Kruskal-Wallis), *p=0.0312 for F1M1-Fc$^+$ vs Ctrl, ***p=0.0006 for Ctrl + αGM1 vs Ctrl, ***p=0.0002 for F1M1-Fc$^+$ vs Ctrl + αGM1, ***p=0.0002 for F1M1-Fc$^+$ + αGM1 vs F1M1-Fc$^+$, ***p=0.0008 for F1M1-Fc$^+$+ αGM1 vs Ctrl, p=0.1621 for F1M1-Fc$^+$+ αGM1 vs Ctrl + αGM1 (Mann-Whitney t-test). NK, natural killer.

collection),[36] and in MDA-MB-231 and SUM-159 cell xenografts by western blot analysis. Cath-D and the M6P/IGF2 receptor were similarly expressed in all samples (figure 6A). Immunostaining of the PDX B1995 and B3977 confirmed that cath-D was expressed in tumor cells and in the microenvironment (figure 6B), as previously observed in TNBC biopsy samples (online supplemental figure 1). These results indicated these PDXs are representative of the disease, at least concerning cath-D expression. We then xenografted Swiss nude mice with the PDX B1995 or B3977. Tumor growth was significantly reduced by F1M1-Fc$^+$ (15 mg/kg by ip three times per week) compared with control (rituximab) in both models (p<0.001) (figure 6C,D, left panel). At treatment end (day 48 for the PDX B1995 and day 42 for the PDX B3977), tumor volume was significantly reduced by 61.8% (p=0.0002) and by 44.6% (p=0.0018), respectively, in the F1M1-Fc$^+$ group compared with the control group (figure 6C,D, middle panels). The overall survival rate, reflected by a tumor volume <1500 mm^3, was significantly longer in mice treated with F1M1-Fc$^+$ than in control group (median survival of 64 and 49 days for the F1M1-Fc$^+$ group and for control animals in mice xenografted with PDX B1995, and of 57 and 46 days for the F1M1-Fc$^+$ group and for control animals in mice xenografted with PDX B3977) (figure 6C,D, right panel; Kaplan-Meier survival analysis, p=0.0002 and p=0.0024, respectively). These results showed that F1M1-Fc$^+$ monotherapy very efficiently delayed tumor growth in nude mice xenografted with TNBC PDXs.

F1M1-Fc$^+$ improves paclitaxel therapeutic efficacy

Next, we investigated the therapeutic benefit of combining F1M1-Fc$^+$ with paclitaxel. First, we confirmed paclitaxel cytotoxicity in MDA-MB-231 cells in vitro (IC_{50}=53.4 nM) (online supplemental figure 13A). Then, we showed that

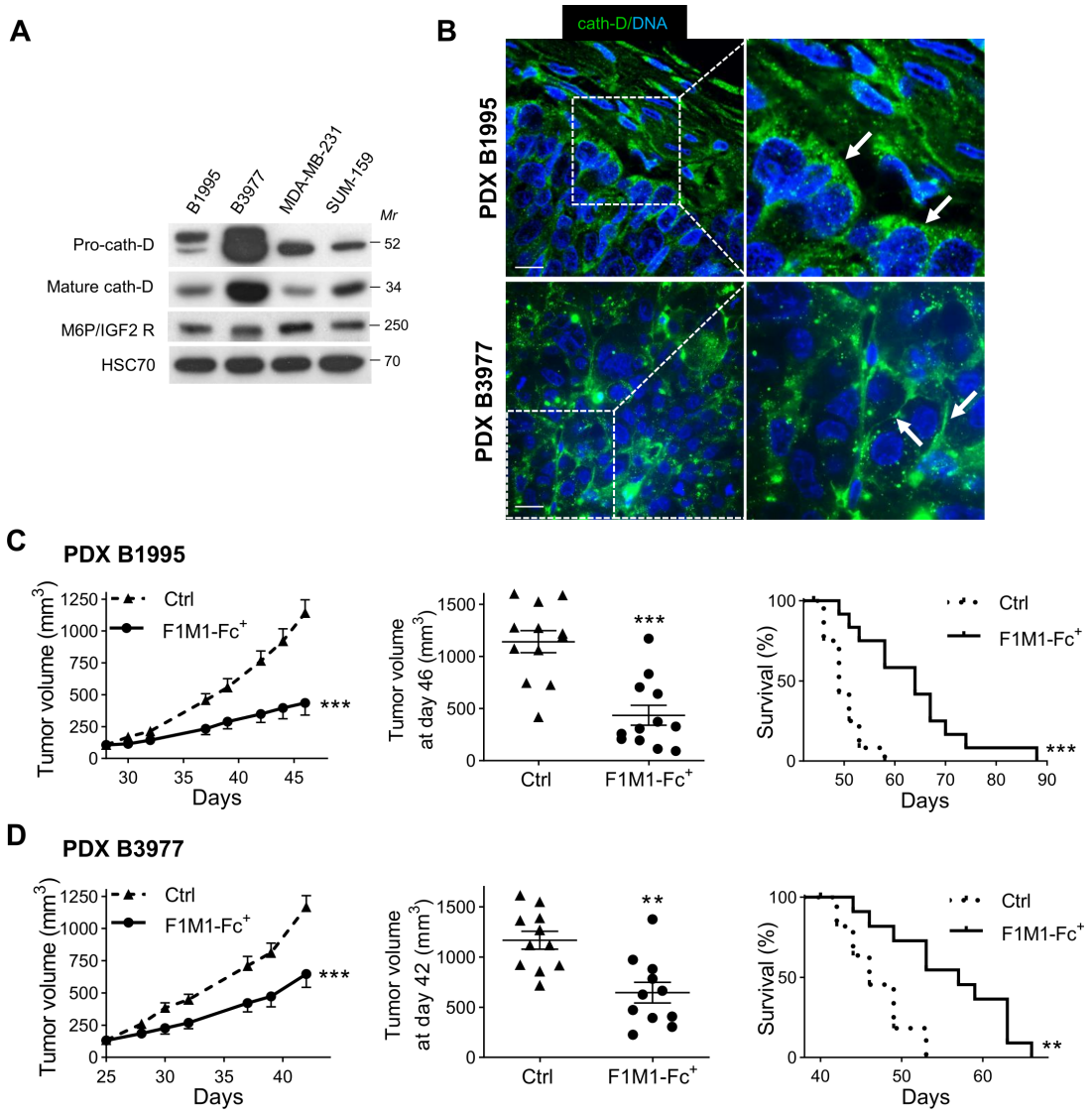

Figure 6 The lead F1M1-Fc$^+$ anti-cath-D antibody inhibits growth of TNBC-PDXs and improves mouse survival. (A) Cath-D expression and secretion, and expression of the M6P/IGF2 in TNBC-PDX tumors. Whole tumor cytosols (5 µg proteins) from PDX B1995 and PDX B3977 tumor xenografts, and from SUM159 and MDA-MB-231 cell xenografts were separated on 13.5% SDS-PAGE and analyzed by immunoblotting with the anti-cath-D mouse monoclonal antibody (#610801) (to detect mature cath-D) and anti-cath-D rabbit polyclonal antibody (E-7) (to detect pro-cath-D). Whole tumor cytosols were also immunoblotted with a mouse monoclonal antibody (clone MEM-238) against the M6P/IGF2 receptor (M6P/IGF2R). HSC70 was used as loading control. *Mr*, relative molecular mass (kDa). (B) Cath-D expression and localization in TNBC-PDX tumors. PDX B1995 (upper panels) and PDX B3977 (lower panels) tumor sections were incubated with a monoclonal anti-human cath-D antibody (clone C-5) (green). Nuclei were stained with Hoechst 33342 (blue). Scale bar, 10 µm (left panels). Higher magnification of the boxed region shows cell surface-associated cath-D (right panels). Arrows show the localization of cath-D at the cancer cell surface. (C) Therapeutic effects of F1M1-Fc$^+$ in mice xenografted with PDX B1995. Mice were xenografted with PDX B1995 and when tumor volume reached 100 mm^3 (day 28), mice were treated with F1M1-Fc$^+$ (15 mg/kg) or rituximab (Ctrl) (15 mg/kg) three times per week. Mice were sacrificed when tumor volume reached 1500 mm^3, and the corresponding tumor growth curves were stopped (left panel). Tumor volume (in mm^3) is shown as the mean±SEM; n=12 for Ctrl (rituximab); n=12 for F1M1-Fc$^+$. ***p<0.001 for F1M1-Fc$^+$ (mixed-effects multiple linear regression test). Mean tumor volume at day 48 (middle panel). Mean±SEM; n=12 for Ctrl (rituximab); n=12 for F1M1-Fc$^+$. ***p=0.0001 for F1M1-Fc$^+$ vs Ctrl (Mann-Whitney t-test). Kaplan-Meier survival analysis (right panel). n=12 for Ctrl (rituximab); n=12 for F1M1-Fc$^+$. ***p=0.0002 for F1M1-Fc$^+$ vs Ctrl (Log-rank Mantel-Cox test). (D) Therapeutic effects of F1M1-Fc$^+$ in mice xenografted with PDX B3977. Mice were xenografted with PDX B3977 and when tumor volumes reached 100 mm^3 (day 25), mice were treated with F1M1-Fc$^+$ (15 mg/kg) or rituximab (Ctrl) (15 mg/kg) three times per week. Mice were sacrificed when tumor volume reached 1500 mm^3, and the corresponding tumor growth curves were stopped (left panel). Tumor volume (in mm^3) is shown as the mean±SEM; n=11 for Ctrl (rituximab); n=11 for F1M1-Fc$^+$. ***p<0.001 for F1M1-Fc$^+$ (mixed-effects multiple linear regression test). Mean tumor volume at day 42 (middle panel). Mean±SEM; n=11 for Ctrl (rituximab); n=11 for F1M1-Fc$^+$. **p=0.0018 for F1M1-Fc$^+$ vs Ctrl (Mann-Whitney t-test). Kaplan-Meier survival analysis (right panel). n=11 for Ctrl (rituximab); n=11 for F1M1-Fc$^+$. **p=0.0024 for F1M1-Fc$^+$ vs Ctrl (log-rank Mantel-Cox test). PDXs, patient-derived xenografts; TNBC, triple-negative breast cancer.

incubation of MDA-MB-231 cells with 5 nM paclitaxel for 48 hours (dose equivalent to the IC_{20}; online supplemental figure 13A) did not affect cath-D expression (cell lysates) and secretion (conditioned media) (online supplemental figure 13B). As paclitaxel is frequently administered to patients with a weekly schedule, we treated nude mice bearing MDA-MB-231 cell xenografts with 1 mg/kg, 4 mg/kg, or 7 mg/kg paclitaxel (PTX) weekly. Higher PTX doses resulted in excessive toxicity (data not shown). PTX induced tumor growth inhibition in a dose-dependent manner (online supplemental figure 13C) that was significant at 4 mg/kg (p=0.007) and 7 mg/kg (p<0.001) compared with control (NaCl).

We then tested the combination therapy (paclitaxel and F1M1-Fc$^+$) in nude mice bearing MDA-MB-231 cell xenografts using a low dose (PTX LD, 1 mg/kg) and a medium dose of paclitaxel (PTX MD, 4 mg/kg) that inhibited tumor growth on its own; online supplemental figure 13C). When tumor volume reached 50 mm^3 at day 15 postgraft, we treated mice with F1M1-Fc$^+$ (15 mg/kg; three times per week), PTX LD (1 mg/kg; once per week), F1M1-Fc$^+$ (15 mg/kg; three times per week)+PTX LD (1 mg/kg; once per week), or control (rituximab, three times per week+saline, once per week; all ip) for 37 days. Both F1M1-Fc$^+$ and PTX LD+F1M1-Fc$^+$ significantly delayed tumor growth compared with control (p=0.039 for F1M1-Fc$^+$, p=0.032 for PTX LD+F1M1-Fc$^+$) (figure 7A). At day 52 (treatment end), tumor volume was reduced by 37.4% (p=0.07) in the F1M1-Fc$^+$ group, by 18.7% (p=0.0005) in the PTX LD group, and by 50.5% (p=0.002) in the PTX LD+F1M1-Fc$^+$ group compared with control group (figure 7B). Tumor volume was significantly smaller in the PTX LD+F1M1-Fc$^+$ group than in the PTX LD group (p=0.0293). The overall survival rate, reflected by a tumor volume <2000 mm^3, was significantly longer in mice treated with F1M1-Fc$^+$ and with PTX LD+F1M1-Fc$^+$ than in controls (median survival of 59 and 66 days for the F1M1-Fc$^+$ and PTX LD+F1M1-Fc$^+$ groups, respectively, compared with 55 days for control animals) (figure 7C; Kaplan-Meier survival analysis, p=0.0313 for F1M1-Fc$^+$, p=0.0009 for PTX LD+F1M1-Fc$^+$). The overall survival rate was significantly longer in mice treated with PTX LD+F1M1-Fc$^+$ (66 days) than in mice treated with PTX LD (57 days) (p=0.0219). Overall, these results demonstrated that in combination therapy, F1M1-Fc$^+$ improved the therapeutic efficacy of a suboptimal dose of paclitaxel that was poorly effective in vivo (online supplemental figure 13C).

Similarly, F1M1-Fc$^+$, PTX MD, and PTX MD+F1M1-Fc$^+$ significantly delayed tumor growth compared with control (p=0.039 for F1M1-Fc$^+$, p=0.042 for PTX MD, p=0.013 for PTX MD+F1M1-Fc$^+$) (figure 7D). At day 52 (treatment end), tumor volume was reduced by 37.4% (p=0.07) in the F1M1-Fc$^+$ group, by 32.9% (p=0.0289) in the PTX MD group, and by 55.5% (p=0.0012) in the PTX MD+F1M1-Fc$^+$ group compared with control (figure 7E). The overall survival rate was significantly longer in mice treated with F1M1-Fc$^+$, PTX MD and PTX MD+F1M1-Fc$^+$ than in control (median survival of 59, 59 and 69 days for the F1M1-Fc$^+$, PTX MD, and PTX MD+F1M1-Fc$^+$ groups, respectively, compared with 55 days for control animals) (figure 7F; Kaplan-Meier survival analysis, p=0.0313 for F1M1-Fc$^+$, p=0.0312 for PTX MD, p=0.001 for PTX MD+F1M1-Fc$^+$). The overall survival rate was significantly longer in mice treated with PTX MD+F1M1-Fc$^+$ (69 days) than with PTX MD (59 days) (p=0.041). All mice treated with the combination therapy gained weight (figure 7G) and displayed normal activities, suggesting no apparent toxicity. Overall, these results demonstrated that F1M1-Fc$^+$ improved PTX therapeutic efficacy without increasing toxicity.

F1M1-Fc$^+$ improves the therapeutic efficacy of the antiandrogen enzalutamide

We previously found that coexpression of cath-D and androgen receptor (AR) in non-metastatic TNBC is an independent prognostic factor of worse overall survival, suggesting the possibility of adjuvant combination therapy with anti-androgen drugs and anti-cath-D antibodies.[16] We first showed that in the AR-expressing SUM159 TNBC cell line (online supplemental figure 14A), incubation with enzalutamide, an antiandrogen drug, did not decrease cath-D expression and secretion (online supplemental figure 14B), and incubation with F1M1-Fc$^+$ did not reduce AR expression (online supplemental figure 14C).

Then, we treated mice harboring SUM159 cell xenografts with F1M1-Fc$^+$ alone. Tumor volume increase was significantly slowed down in mice treated with F1M1-Fc$^+$ (15 mg/kg by ip three times per week) compared with control (rituximab) (p<0.001) (figure 8A). Tumor volume at day 48 (treatment end) was significantly reduced by 71.9% in the F1M1-Fc$^+$ compared with control group (p<0.0001) (figure 8B). The overall survival rate, reflected by a tumor volume <1000 mm^3, was significantly longer in mice treated with F1M1-Fc$^+$ than in the control group (median survival of 62 days and 55 days, respectively) (figure 8C; Kaplan-Meier survival analysis, p=0.0024), without any apparent toxicity (figure 8D).

We then treated nude mice bearing SUM159 cell xenografts with F1M1-Fc$^+$ (15 mg/kg, twice per week, ip) or/and enzalutamide (Enza, 30 mg/kg, five times per week, per os). F1M1-Fc$^+$ and Enza+F1M1-Fc$^+$ significantly delayed tumor growth compared with control (p=0.001 for F1M1-Fc$^+$, p=0.003 for Enza+F1M1-Fc$^+$) (figure 8E). Tumor growth was significantly more reduced in the Enza+F1M1-Fc$^+$ group than in the Enza group (p=0.008). At day 50 (treatment end), tumor volume was reduced by 55.7% (p=0.0019) in the F1M1-Fc$^+$ group, by 43.4% (p=0.02) in the Enza group, and by 71% (p=0.0002) in the Enza+F1M1-Fc$^+$ group compared with control (figure 8F). Tumor volume was significantly smaller in the Enza+F1M1-Fc$^+$ group than in the Enza group (p=0.0082). Overall survival was significantly longer in mice treated with F1M1-Fc$^+$, Enza, and Enza+F1M1-Fc$^+$ than in controls (median survival of 63, 61, 64, and 57 days, respectively) (figure 8G; Kaplan-Meier survival

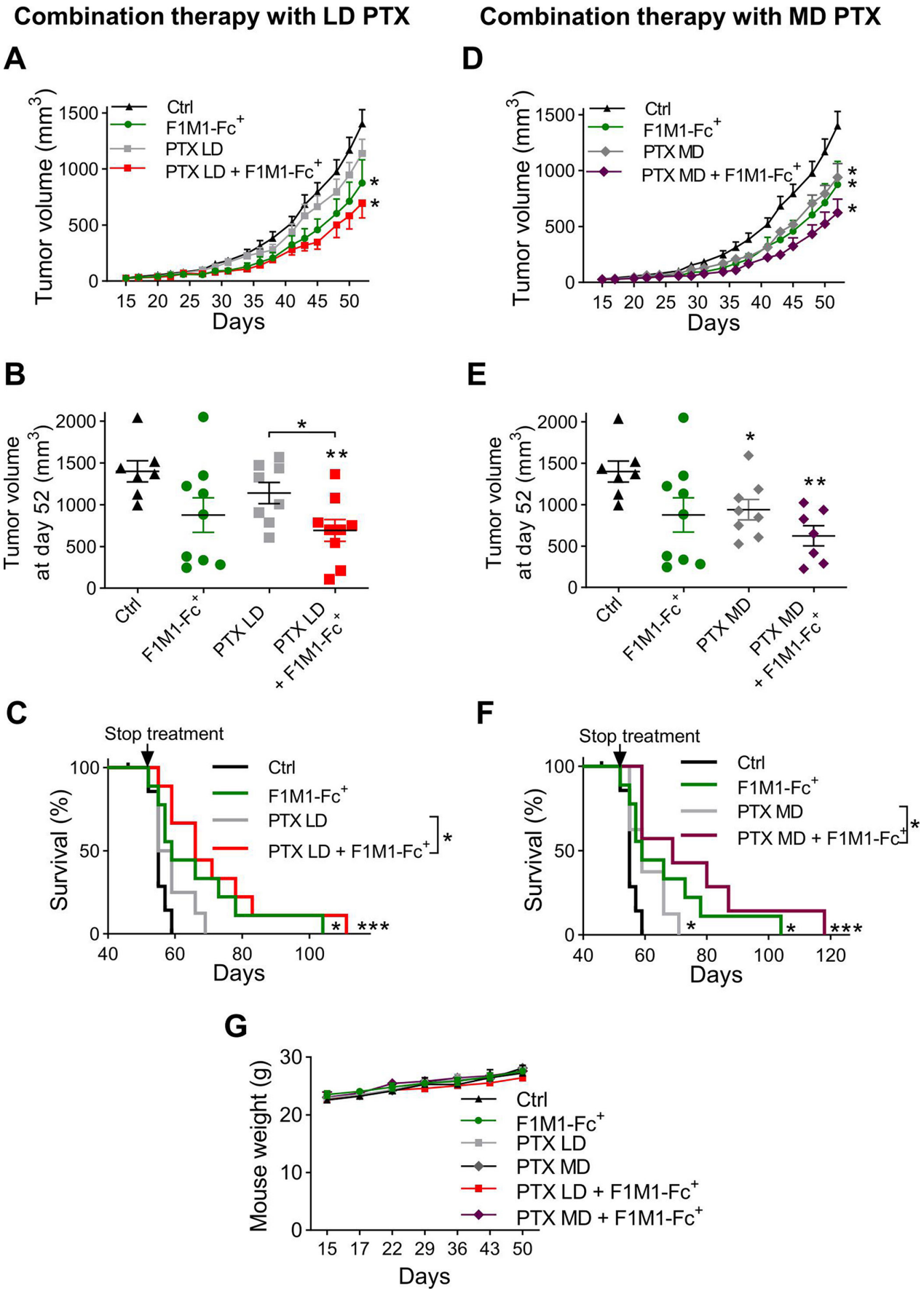

Figure 7 (Continued)

Figure 7 Therapeutic efficacy of the anti-cath-D F1M1-Fc$^+$ antibody in combination with paclitaxel in mice xenografted with MDA-MB-231 cells. (A) Tumor growth in mice treated with F1M1-Fc$^+$ and/or paclitaxel (1 mg/kg; PTX LD). MDA-MB-231 cells were subcutaneously injected in nude mice. When tumor volume reached 50 mm^3 (day 15 postgraft), mice were treated with F1M1-Fc$^+$ (15 mg/kg; three times per week) (n=9), PTX LD (1 mg/kg; once per week) (n=8), F1M1-Fc$^+$ (15 mg/kg; three times per week)+PTX LD (1 mg/kg; once per week) (n=9), or rituximab (three times per week)+saline (once per week; all ip) (Ctrl; n=7) for 37 days. Mice were sacrificed when tumor volume reached 2000 mm^3. Tumor volume (in mm^3) is shown as the mean±SEM. *p=0.039 for F1M1-Fc$^+$ vs Ctrl, p=0.689 for PTX LD vs Ctrl, *p=0.032 for PTX LD+F1M1-Fc$^+$ vs Ctrl, p=0.092 for PTX LD+F1M1-Fc$^+$ vs PTX LD, p=0.88 for PTX LD+F1M1-Fc$^+$ vs F1M1-Fc$^+$ (mixed-effects multiple linear regression test). PTX LD; low dose of paclitaxel (1 mg/kg). (B) Mean tumor volume at day 52 in mice receiving F1M1-Fc$^+$ and/or paclitaxel (1 mg/kg; PTX LD). *p=0.0189 for all groups (Kruskal-Wallis); p=0.0712 for F1M1-Fc$^+$ vs Ctrl; p=0.3211 for PTX LD vs Ctrl; **p=0.0020 for PTX LD+F1M1-Fc$^+$ vs Ctrl; *p=0.0293 for PTX LD+F1M1-Fc$^+$ vs PTX LD; p=0.5302 for PTX LD+F1M1-Fc$^+$ vs F1M1-Fc$^+$ (Mann-Whitney t-test); Data are the mean±SEM. (C) Kaplan-Meier survival analysis in mice receiving F1M1-Fc$^+$ and/or paclitaxel (1 mg/kg; PTX LD). *p=0.0313 for F1M1-Fc$^+$ vs Ctrl, p=0.0875 for PTX LD vs Ctrl, ***p=0.0009 for PTX LD+F1M1-Fc$^+$ vs Ctrl, *p=0.0216 for PTX LD+F1M1-Fc$^+$ vs PTX LD, p=0.3714 for PTX LD+F1M1-Fc$^+$ vs F1M1-Fc$^+$ (log-rank Mantel-Cox test). (D) Tumor growth in mice receiving F1M1-Fc$^+$ and/or paclitaxel (4 mg/kg; PTX MD). MDA-MB-231 cells were subcutaneously injected in nude mice. When tumor volume reached 50 mm^3 (day 15 postgraft), mice were treated with F1M1-Fc$^+$ (15 mg/kg; three times per week) (n=9), PTX MD (4 mg/kg; once per week) (n=8), F1M1-Fc$^+$ (15 mg/kg; three times per week)+PTX MD (4 mg/kg; once per week) (n=7), or rituximab (three times per week)+saline (once per week) (Ctrl; n=7) for 37 days. Mice were sacrificed when tumor volume reached 2000 mm^3. Tumor volume (in mm^3) is shown as the mean±SEM. *p=0.039 for F1M1-Fc$^+$ vs Ctrl, *p=0.042 for PTX MD vs Ctrl, *p=0.013 for PTX MD+F1M1-Fc$^+$ vs Ctrl, p=0.107 for PTX MD+F1M1-Fc$^+$ vs PTX MD, p=0.857 for PTX MD+F1M1-Fc$^+$ vs F1M1-Fc$^+$ (mixed-effects multiple linear regression test). PTX MD; medium dose of paclitaxel (4 mg/kg). (E) Mean tumor volume at day 52 in mice receiving F1M1-Fc$^+$ and/or paclitaxel (4 mg/kg; PTX MD). *p=0.0200 for all groups (Kruskal-Wallis); p=0.0712 for F1M1-Fc$^+$ vs Ctrl; *p=0.0289 for PTX MD vs Ctrl; **p=0.0012 for PTX MD+F1M1-Fc$^+$ vs Ctrl; p=0.1520 for PTX MD+F1M1-Fc$^+$ vs PTX MD; p=0.4698 for PTX MD+F1M1-Fc$^+$ vs F1M1-Fc$^+$ (Mann-Whitney t-test). Data are the mean±SEM. (F) Kaplan-Meier survival analysis in mice receiving F1M1-Fc$^+$ and/or paclitaxel (4 mg/kg; PTX MD). *p=0.0313 for F1M1-Fc$^+$ vs Ctrl, *p=0.0312 for PTX MD vs Ctrl, ***p=0.001 for PTX MD+F1M1-Fc$^+$ vs Ctrl, *p=0.0410 for PTX MD+F1M1-Fc$^+$ vs PTX MD, p=0.2010 for PTX MD+F1M1-Fc$^+$ vs F1M1-Fc$^+$ (log-rank Mantel-Cox test). (G) Weight monitoring in mice receiving F1M1-Fc$^+$ and/or paclitaxel. Mean±SEM. Ctrl (n=7); F1M1-Fc$^+$ (n=9); PTX LD (n=8); F1M1-Fc$^+$+PTX LD (n=9); PTX MD (n=8); F1M1-Fc$^+$+PTX MD (n=7).

analysis, p=0.0126 for F1M1-Fc$^+$, p=0.0196 for Enza, p<0.0001 for Enza+F1M1-Fc$^+$), without apparent toxicity (figure 8H). Overall survival was significantly longer in the Enza+F1M1-Fc$^+$ group than in the Enza group (64 vs 61 days, p=0.017) and in the F1M1-Fc$^+$ group (64 vs 63 days) (p=0.0091) (figure 8G). Overall, these results demonstrated that F1M1-Fc$^+$ improves enzalutamide therapeutic efficacy.

DISCUSSION

Here, we showed that F1M1-Fc$^+$, a novel human Fc-engineered anti-cath-D antibody, enhanced ADCC and tumor growth inhibition, and triggered NK cell recruitment, activation, and cytotoxic activity in the MDA-MB-231 cell xenograft TNBC model. In addition, NK cell depletion impaired F1M1-Fc$^+$ therapeutic efficacy in this model. Furthermore, in combination therapy, F1M1-Fc$^+$ increased the efficacy of chemotherapy (paclitaxel) and antiandrogens (enzalutamide). These data suggest that F1M1-Fc$^+$ may represent a first-in-class treatment for patients with TNBC.

Numerous afucosylated antibodies and Fc-protein engineered antibodies are in clinical trials. Two afucosylated antibodies, obinutuzumab (against CD20) and mogamulizumab (against CCR4), and two Fc-optimized antibodies, tafasitamab (against CD19) and margetuximab (against HER2) that harbor mutations (S329D, I332E and F243L, R292P, Y300L, V305I, P396L, respectively) to increase ADCC, are approved for clinical use.[6 8] Here, to improve the NK cell-mediated effector functions of F1M1, an anti-cath-D antibody that binds to both human and mouse cath-D in vitro and exhibits antitumor activity in vivo without apparent toxicity, we generated the F1M1-Fc$^+$ antibody with four mutations (S239D, H268F, S324T, I332E) in the Fc domain to increase its affinity for FcγRIIIA (CD16a) and enhance NK cell-mediated ADCC.[37] These four mutations substantially improved F1M1-Fc$^+$ binding to CD16a 158V and 158F expressed in human NK92 cells compared with F1M1. Conversely, F1M1-Fc$^-$ (L234A, L235A, and P329G substitutions) showed no detectable binding to CD16a 158V or CD16a 158F.[38] Many clinically relevant anti-cancer antibodies, such as rituximab, trastuzumab and cetuximab, induce NK cell-mediated ADCC in vitro.[6 8] However, the clinical effects of these ADCC-inducing therapeutic antibodies could be limited by the presence of the V158F polymorphism on the FcγRIIIA/CD16a receptor. Indeed, the CD16a 158F/F and CD16a 158F/V allotypes have been associated with a poorer clinical response to antibody treatment in some clinical trials,[39–41] but not in others.[41 42]

We then showed that compared with F1M1, F1M1-Fc$^+$ activated more potently the functional response of NK cells in vitro (ie, degranulation and intracellular IFNγ production) in NK92 cells expressing CD16a 158V or CD16a 158F, while F1M1-Fc$^-$ was completely ineffective. Moreover, F1M1-Fc$^+$ was the most potent antibody

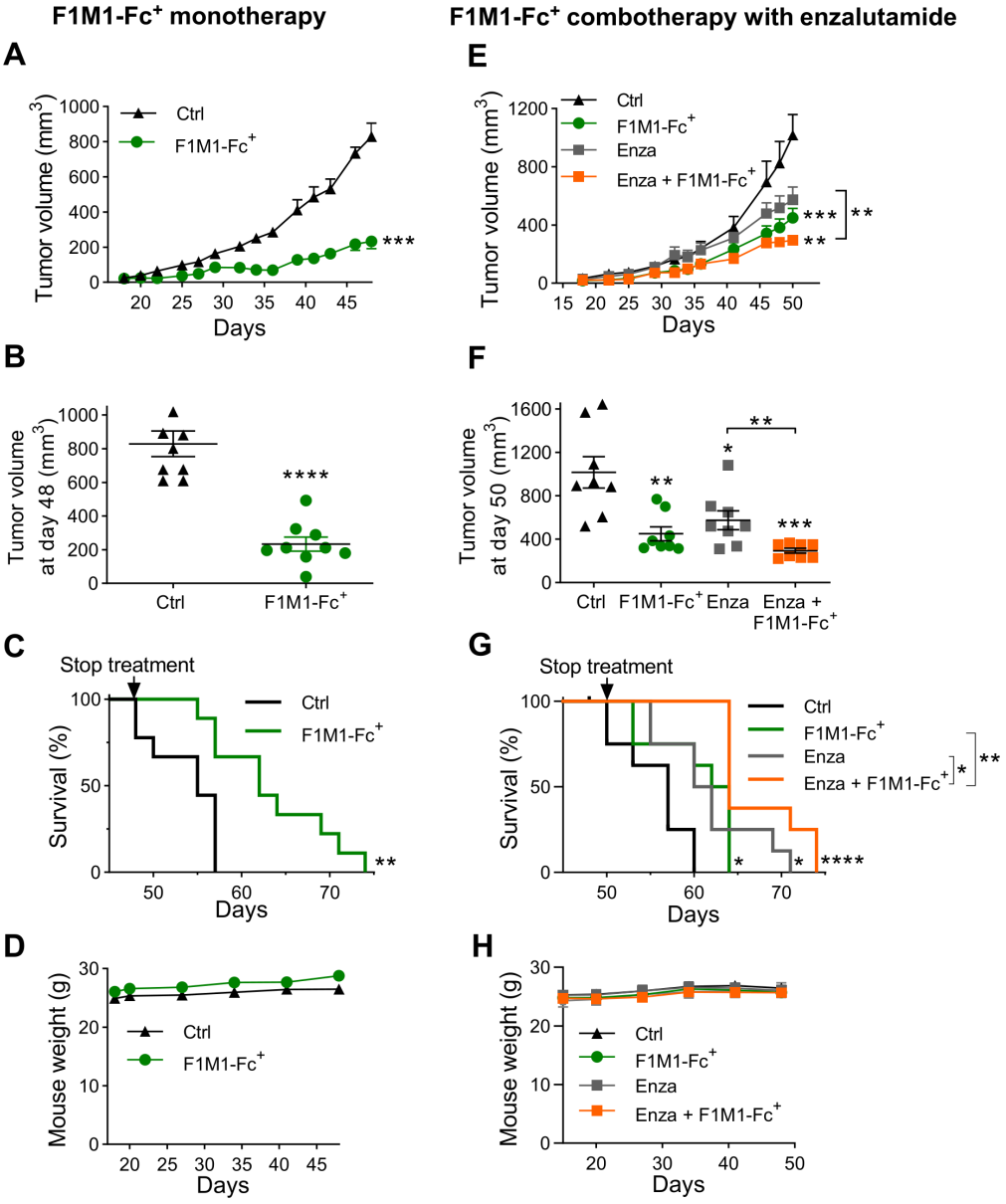

Figure 8 Therapeutic efficacy of the anti-cath-D F1M1-Fc$^+$ antibody alone and in combination with enzalutamide in mice xenografted with SUM159 cells. (A) Tumor growth in mice receiving F1M1-Fc$^+$ monotherapy. SUM159 cells were subcutaneously injected in nude mice. When tumor volume reached 50 mm^3, mice were treated with F1M1-Fc$^+$ (n=9) (15 mg/kg), or rituximab (Ctrl; n=9) (15 mg/kg), three times per week for 30 days. Mice were sacrificed when tumor volume reached 1000 mm^3. Tumor volume (in mm^3) is the mean±SEM. ***p<0.001 (mixed-effects multiple linear regression test). (B) Mean tumor volume at day 48 in mice receiving F1M1-Fc$^+$ monotherapy. Mean±SEM. ****p<0.0001 for F1M1-Fc$^+$ vs Ctrl (Mann-Whitney t-test). (C) Kaplan-Meier survival analysis in mice receiving F1M1-Fc$^+$ monotherapy.*p=0.0024 for F1M1-Fc$^+$ vs Ctrl (log-rank Mantel-Cox test). (D) Weight monitoring in mice receiving F1M1-Fc$^+$ monotherapy. Mean±SEM. Rituximab (Ctrl; n=9), F1M1-Fc$^+$ (n=9). (E) Tumor growth in mice receiving the F1M1-Fc$^+$+enzalutamide combination therapy. SUM159 cells were subcutaneously injected in nude mice. When tumor volume reached 50 mm^3, mice were treated with rituximab+corn oil (Ctrl; n=8), F1M1-Fc$^+$ (n=8) (15 mg/kg, twice per week), enzalutamide (Enza; 30 mg/kg, five times per week, per os) (n=8), or F1M1-Fc$^+$ (15 mg/kg, twice per week, ip) + enzalutamide (Enza; 30 mg/kg, five times per week, per os) (n=8) for 32 days. Mice were sacrificed when tumor volume reached 1500 mm^3. Tumor volume (in mm^3) is shown as the mean±SEM. ***p=0.001 for F1M1-Fc$^+$ vs Ctrl, p=0.5 for Enza vs Ctrl, *p=0.019 for Enza vs F1M1-Fc$^+$, **p=0.003 for Enza+F1M1-Fc$^+$ vs Ctrl, **p=0.008 for Enza+F1M1-Fc$^+$ vs Enza, p=0.887 for Enza+F1M1-Fc$^+$ vs F1M1-Fc$^+$ (mixed-effects multiple linear regression test). (F) Mean tumor volume at day 50 in mice receiving the F1M1-Fc$^+$+ enzalutamide combination. Mean±SEM. ***p=0.0005 for all groups (Kruskal-Wallis), **p=0.0019 for F1M1-Fc$^+$ vs Ctrl, *p=0.02 for Enza vs Ctrl, ***p=0.0002 for Enza+F1M1-Fc$^+$ vs Ctrl, **p=0.0092 for Enza+F1M1-Fc$^+$ vs Enza, p=0.0985 for Enza+F1M1-Fc$^+$ vs F1M1-Fc$^+$ (Mann-Whitney t-test). (G) Kaplan-Meier survival analysis in mice receiving the F1M1-Fc$^+$ + enzalutamide combination.*p=0.0126 for F1M1-Fc$^+$ vs Ctrl, *p=0.0196 for Enza vs Ctrl, ****p<0.0001 for Enza+F1M1-Fc$^+$ vs Ctrl, *p=0.017 for Enza+F1M1-Fc$^+$ vs Enza, **p=0.0091 for Enza+F1M1-Fc$^+$ vs F1M1-Fc$^+$ (log-rank Mantel-Cox test). (H) Weight monitoring in mice receiving the F1M1-Fc$^+$+ enzalutamide combination. Mean±SEM. Rituximab (Ctrl; n=8), F1M1-Fc$^+$ (n=8); Enza (n=8), Enza+F1M1-Fc$^+$ (n=8).

to trigger ADCC in vitro against MDA-MB-231 TNBC cells in the presence of NK92 cells that express CD16a 158V or CD16a 158F and also of human primary NK cells that express endogenous CD16a 158V/F. These results strongly highlighted the relevance of potentiating the NK cell-mediated Fc effector functions of F1M1 by Fc-engineering.

This is the first study showing that cell surface cath-D can be targeted by a human antibody to mediate ADCC in TNBC cells. To our knowledge, only incubation with a humanized antibody against cathepsin S, another protease, triggered ADCC mechanism in colorectal and pancreatic cancer cells.[43] Importantly, cath-D can also be associated with cell surface receptors on CAFs,[23 29] and we found that F1M1-Fc$^+$ also induced ADCC against breast CAFs. This suggests the possibility of a cytotoxic effect in the tumor stroma following its targeting, which has never been described before. We also found that the M6P/IGF2 receptor was involved in F1M1-Fc$^+$-mediated ADCC on both TNBC cells and CAFs.

Next, we showed that compared with F1M1 and F1M1-Fc$^-$, F1M1-Fc$^+$ inhibited more potently MDA-MB-231 tumor growth and prolonged survival of mice harboring TNBC cell xenografts. F1M1-Fc$^-$ was significantly less effective, reflecting the importance of Fc-dependent mechanisms also in vivo, and suggesting an important role of immune cells in mice. In addition, nude mice treated with F1M1-Fc$^+$ showed no sign of leukopenia, thrombopenia, anemia, and neutropenia, suggesting the absence of toxicity. Importantly, F1M1-Fc$^+$, our most potent antibody, inhibited tumor growth also of two TNBC PDXs (B1995 and B3977) and prolonged survival of these mice. PDX B1995 was isolated from a patient with TNBC after neo-adjuvant therapy, whereas PDX B3977 was isolated from a patient with TNBC resistant to neoadjuvant chemotherapy.[36] Therefore, our results suggest that F1M1-Fc$^+$ may represent a new therapeutic strategy for patient with chemotherapy-resistant TNBC.

Recent studies and clinical trials highlighted that NK cell-based immunotherapy can awake the innate anticancer response, particularly against tumor metastases.[4–6] Using mouse TNBC models, it was shown that NK cells are selectively increased in the dormant milieu, and that adjuvant IL15-based immunotherapy ensures an abundant pool of NK cells to sustain dormancy, thus preventing liver metastasis formation and prolonging survival.[7] By phenotyping the NK cell infiltrates in MDA-MB-231 cell xenografts, we observed that only treatment with F1M1-Fc$^+$ led to the tumor recruitment of immature CD27$^-$CD11b$^-$ NK and mature stage 1 CD27$^+$CD11b$^-$ NK cells that were undergoing activation, as indicated by the concomitant upregulation of the *Eomes* transcription factor.[35] Moreover, following F1M1-Fc$^+$ treatment, the cell surface expression of CD107a, a functional marker of NK cell degranulation, and the intracellular expression of granzyme B, a marker of NK cell cytotoxic activity, were significantly increased in NK cells that infiltrated MDA-MB-231 cell xenografts. This was corroborated by the upregulation of granzyme B and perforin in MDA-MB-231 tumor xenografts and also of the antitumor cytokine TNFα. These effects were limited when using F1M1-Fc$^-$, suggesting that F1M1-Fc$^+$ can target NK cells to tumors and possibly also to metastases, sustaining dormancy.[7] We also found that in nude mice, NK cell depletion, by treatment with the anti-asialo GM1 antibody, impaired F1M1-Fc$^+$ therapeutic efficacy in MDA-MB-231 TNBC cell xenografts, demonstrating the key role of tumor-infiltrating NK cells in F1M1-Fc$^+$ effect. Interestingly, the limited antitumor activity of F1M1-Fc$^+$ observed in mice treated with the anti-asialo GM1 antibody was very similar to that observed with F1M1-Fc$^-$, which depends solely on Fab-mediated effector functions. This strongly suggests that NK cells are the main effectors of the Fc-dependent response with F1M1-Fc$^+$. In addition, our unpublished experiments in MDA-MB-231 cells strongly suggest that F1M1-Fc$^+$ only slightly triggered ADCP in the presence of THP1 M1-polarized macrophages and did not induce CDC (data not shown). However, macrophage depletion experiments are needed to conclude on the potential role of macrophages in F1M1-Fc$^+$ antitumor effect. Taken together, these results demonstrated that the Fc-mediated effector functions of F1M1-Fc$^+$ are dependent on NK cells. The mechanism by which F1M1-Fc$^+$ induces NK cell recruitment to the tumor remains unexplained. F1M1-Fc$^+$ via its improved Fc-part might bind to immature NK cells in the bloodstream and direct them to the tumor where they become activated.

The immunomodulating effects of standard and novel chemotherapeutic approaches can also be exploited in combination with tumor-targeting antibodies.[44] In metastatic TNBC, pembrolizumab (anti-PD-L1 antibody) in association with chemotherapy, sacituzumab govitecan (anti-TROP2 antibody-drug conjugate, ADC), and trastuzumab-deruxtecan (ADC against HER2^{low} tumors) showed improved overall and progression-free survival compared with chemotherapy alone.[3 45] Paclitaxel induces cell-cycle arrest and also promotes tumor immunity,[46] guiding tumor-associated macrophages toward the M1-like antitumor phenotype.[47] As neoadjuvant chemotherapy (nanoparticle-bound paclitaxel, epirubicin, and cyclophosphamide) decreases by ~50% the frequency of NK cells,[48] combining chemotherapy with immunotherapy that recruits and/or reactivates NK cell cytotoxic activity is an attractive treatment option. Therefore, we analyzed the combination of paclitaxel and F1M1-Fc$^+$. We found that this combination significantly enhanced paclitaxel therapeutic effect in MDA-MB-231 tumor xenografts. As incubation of TNBC cells with paclitaxel in vitro did not have any

effect on cath-D expression and secretion, adding a protease-targeting agent, such as F1M1-Fc$^+$, may benefit chemotherapy-based treatment regimens for patients with TNBC. Moreover, combined cytotoxic effects of chemotherapy and NK cells, should favor priming of CD4$^+$ and CD8$^+$ T cells and increase efficacy of adaptative antitumoral response.[49]

Recently, we performed a preclinical pilot study to characterize the biological TNBC subtypes that express cath-D by IHC using a TMA of 147 TNBC to identify patients who could benefit most of anti-cath-D antibody based-therapy.[16] We found that AR/cath-D coexpression in non-metastatic TNBC is an independent prognostic factor of worse overall survival, suggesting the possibility of adjuvant anti-androgen therapy combined with anti-cath-D antibodies.[16] The AR antagonist enzalutamide has clinical activity and is well tolerated in patients with early and advanced AR$^+$ TNBC.[50 51] A recent clinical trial showed the safety and efficacy of enzalutamide in combination with the PI3K inhibitor taselisib in patients with metastatic AR$^+$ TNBC.[52] Here, we demonstrated that the combination of F1M1-Fc$^+$ with enzalutamide improved the therapeutic efficacy of enzalutamide in AR$^+$ SUM159 TNBC tumor xenografts. We also showed that in vitro cath-D secretion and AR expression in SUM159 cells were not affected by incubation with enzalutamide and with F1M1-Fc$^+$, respectively. Thus, the F1M1-Fc$^+$+ enzalutamide combination may have a therapeutic advantage for patients with AR$^+$ TNBC. In this study (mouse model), we injected 15 mg/kg F1M1-Fc$^+$ 3 times/week ip for 5 weeks. As the ip route is less efficient than the iv route in terms of PK/PD, we increased the dose to 15 mg/kg (3–4 fold more than the intravenous dose in humans). Therefore, a dose similar (4–8 mg/kg) to the one classically used for naked anti-HER2 trastuzumab, according to the FDA and EMA recommendations, could be used when the naked F1M1-Fc$^+$ is transferred to the clinic.

CONCLUSION

Overall, our data indicate that the Fc-enhanced anti-cath-D F1M1-Fc$^+$ antibody increased ADCC, triggered the recruitment, activation and cytotoxic activity of tumor-infiltrating NK cells, had higher antitumor efficacy, and prolonged survival of mice harboring TNBC cell xenografts with no associated toxicity. Our preclinical proof-of-concept study validated the feasibility and efficacy of combining an Fc-optimized anti-cath-D antibody with chemotherapy or antiandrogens for TNBC treatment.

Author affiliations
[1]IRCM, INSERM U1194, University of Montpellier, ICM, Montpellier, France
[2]Université de Tours - INRAE, UMR1282, Infectiologie et Santé Publique (ISP), équipe BioMédicaments Anti-Parasitaires (BioMAP), Tours, France
[3]RHEM, IRCM, Montpellier, France
[4]IRMB, University of Montpellier, INSERM, CNRS, CHU Montpellier, Montpellier, France
[5]Translational Research Unit, ICM, Montpellier, France
[6]Biometry Department, ICM, Montpellier, France
[7]Institut du Cancer Avignon-Provence Sainte Catherine, Avignon, France
[8]Department of Pathology, CHU Nîmes, Nimes, France
[9]Department of Medical Oncology, ICM, Montpellier, France
[10]CNRS, Centre national de la recherche Scientifique, Paris, F-75016, France

Twitter Laurie Lajoie @LAJOIE Laurie

Acknowledgements We thank Cecile Dejou (MRI, Montpellier, France) for flow cytometry support. We thank Charles Theillet for providing PDXs. We thank Béatrice Clémenceau and Henri Vié (INSERM U892, Nantes, France) for kindly providing NK92 cells. We thank Hervé Watier (University of Tours, France), Bruno Robert (IRCM, Montpellier, France) and William Jacot (ICM, Montpellier, France) for helpful discussions and support. We thank the IRCM's animal facility unit members (BioCampus RAM-PEFO, IRCM, Montpellier, France) for animal care and for in vivo studies. SPR experiments were carried out using the facilities of the Montpellier Proteomics Platform (PPM-PP2I, BioCampus Montpellier). This publication is based upon work from COST Action ProteoCure, CA20113, supported by COST (European Cooperation in Science and Technology).

Contributors PDdR, LL, TC, LG and EL-C designed the experiments and prepared the manuscript. PDdR, LL, LG, AM, GN, LR, LBA, LF, VG and EL-C performed the experiments. PDdR, LL, LG, AM, LBA, HM, LC, TD, FBM, M-CC, MJ, MV, TC, PM, VL-M, PR, SG, TC and EL-C provided material and analyzed data. PDdR, TC and EL-C analyzed data and proof-read and finalized the manuscript. EL-C acted as guarantor.

Funding This work was supported by a public grant overseen by the French National Research Agency (ANR) as part of the "Investissements d'Avenir" program (reference: LabEx MabImprove ANR-10-LABX-53- 01), University of Montpellier, Inserm Transfert, Région Occitanie, the association "Ligue Régionale du Gard CD30", "Ligue Régionale de l'Herault CD34", and "Ligue Régionale de la Charente Maritime CD17".

Competing interests None declared.

Patient consent for publication Not applicable.

Ethics approval This study involves human participants for immunohistochemistry (IHC) and TNBC cytosols. TNBC biopsy samples were provided by the biological resource center (Biobank number BB-0033-00059) after approval by the Montpellier Cancer Institute Institutional Review Board, following the French national Ethics and Legal dispositions for patients' information and consent. For TNBC cytosols, patient samples were processed according to the French Public Health Code (law no 2004-800, articles L. 1243-4 and R. 1243-61), and the biological resources center has been authorized (authorization number: AC-2008-700; Val d'Aurelle, ICM, Montpellier) to deliver human samples for scientific research. All patients were informed before surgery that their surgical specimens might be used for research purposes. For human primary NK cell isolation and expansion, this work benefited from umbilical cord blood units and John De Vos' expertise (head of the Biological Resource Center Collection of the University Hospital of Montpellier, http://www.chu-montpellier.fr/en/platforms; BIOBANQUES Identifier: BB-0033-00031).The study approval for PDXs was previously published. Participants gave informed consent to participate in the study before taking part.

Provenance and peer review Not commissioned; externally peer reviewed.

Data availability statement Data are available on reasonable request.

ORCID iDs
Pénélope Desroys du Roure http://orcid.org/0009-0000-0848-5450
Laurie Lajoie http://orcid.org/0000-0001-7299-6407
Aude Mallavialle http://orcid.org/0000-0002-9380-6788
Lindsay B Alcaraz http://orcid.org/0000-0003-1912-7186
Lise Fenou http://orcid.org/0009-0005-2888-3145
Timothée David http://orcid.org/0000-0003-0581-2406
Loïs Coenon http://orcid.org/0000-0002-9533-3320
Florence Boissière-Michot http://orcid.org/0000-0003-2431-5157
Marie-Christine Chateau http://orcid.org/0009-0002-7878-8726
Giang Ngo http://orcid.org/0000-0002-5859-8995
Marta Jarlier http://orcid.org/0000-0002-5156-7395
Martin Villalba http://orcid.org/0000-0002-4385-4888
Pierre Martineau http://orcid.org/0000-0002-7993-7183
Valérie Laurent-Matha http://orcid.org/0000-0002-3277-7397
Pascal Roger http://orcid.org/0000-0002-4040-5892
Séverine Guiu http://orcid.org/0000-0002-4901-6295
Thierry Chardès http://orcid.org/0000-0002-1836-7439
Laurent Gros http://orcid.org/0000-0001-5116-2980
Emmanuelle Liaudet-Coopman http://orcid.org/0000-0001-9313-9690

REFERENCES

1 Bianchini G, De Angelis C, Licata L, *et al*. Treatment landscape of triple-negative breast cancer - expanded options, evolving needs. *Nat Rev Clin Oncol* 2022;19:91–113.
2 Wojtukiewicz MZ, Pogorzelska M, Politynska B. Immunotherapy for triple negative breast cancer: the end of the beginning or the beginning of the end *Cancer Metastasis Rev* 2022;41:465–9.
3 Ribeiro R, Carvalho MJ, Goncalves J, *et al*. Immunotherapy in triple-negative breast cancer: insights into tumor immune landscape and therapeutic opportunities. *Front Mol Biosci* 2022;9:903065.
4 Souza-Fonseca-Guimaraes F. NK cell-based Immunotherapies: awakening the innate anti-cancer response. *Discov Med* 2016;21:197–203.
5 López-Soto A, Gonzalez S, Smyth MJ, *et al*. Control of metastasis by NK cells. *Cancer Cell* 2017;32:135–54.
6 Rugo HS, Im S-A, Cardoso F, *et al*. Efficacy of Margetuximab vs Trastuzumab in patients with pretreated Erbb2-positive advanced breast cancer: A phase 3 randomized clinical trial. *JAMA Oncol* 2021;7:573–84.
7 Correia AL, Guimaraes JC, Auf der Maur P, *et al*. Hepatic Stellate cells suppress NK cell-sustained breast cancer dormancy. *Nature* 2021;600:E7:566–71.:.
8 Liu R, Oldham RJ, Teal E, *et al*. Fc-engineering for modulated Effector functions-improving antibodies for cancer treatment. *Antibodies (Basel)* 2020;9:64.
9 Scott AM, Wolchok JD, Old LJ. Antibody therapy of cancer. *Nat Rev Cancer* 2012;12:278–87.
10 Trinchieri G, Valiante N. Receptors for the FC fragment of IgG on natural killer cells. *Nat Immun* 1993;12:218–34.
11 Voskoboinik I, Whisstock JC, Trapani JA. Perforin and Granzymes: function, dysfunction and human pathology. *Nat Rev Immunol* 2015;15:388–400.
12 Prager I, Watzl C. Mechanisms of natural killer cell-mediated cellular cytotoxicity. *J Leukoc Biol* 2019;105:1319–29.
13 Warren HS, Kinnear BF. Quantitative analysis of the effect of Cd16 ligation on human NK cell proliferation. *J Immunol* 1999;162:735–42.
14 Kang J, Yu Y, Jeong S, *et al*. Prognostic role of high cathepsin D expression in breast cancer: a systematic review and meta-analysis. *Ther Adv Med Oncol* 2020;12:1758835920927838.
15 Huang L, Liu Z, Chen S, *et al*. A Prognostic model for triple-negative breast cancer patients based on node status, cathepsin-D and Ki-67 index. *PLoS ONE* 2013;8:e8308112.
16 Mansouri H, Alcaraz LB, Mollevi C, *et al*. Co-expression of androgen receptor and cathepsin D defines a triple-negative breast cancer subgroup with poorer overall survival. *Cancers (Basel)* 2020;12:1244.
17 Vignon F, Capony F, Chambon M, *et al*. Autocrine growth stimulation of the MCF 7 breast cancer cells by the estrogen-regulated 52 K protein. *Endocrinology* 1986;118:1537–45.
18 Glondu M, Coopman P, Laurent-Matha V, *et al*. A Mutated cathepsin-D devoid of its catalytic activity stimulates the growth of cancer cells. *Oncogene* 2001;20:6920–9.
19 Glondu M, Liaudet-Coopman E, Derocq D, *et al*. Down-regulation of cathepsin-D expression by Antisense gene transfer inhibits tumor growth and experimental lung metastasis of human breast cancer cells. *Oncogene* 2002;21:5127–34.
20 Fusek M, Vetvicka V. Mitogenic function of human Procathepsin D: the role of the Propeptide. *Biochem J* 1994;303 (Pt 3)(Pt 3):775–80.
21 Berchem G, Glondu M, Gleizes M, *et al*. Cathepsin-D affects multiple tumor progression steps in vivo: proliferation, angiogenesis and apoptosis. *Oncogene* 2002;21:5951–5.
22 Hu L, Roth JM, Brooks P, *et al*. Thrombin up-regulates cathepsin D which enhances angiogenesis, growth, and metastasis. *Cancer Res* 2008;68:4666–73.
23 Beaujouin M, Prébois C, Derocq D, *et al*. Pro-cathepsin D interacts with the extracellular domain of the beta chain of Lrp1 and promotes Lrp1-dependent fibroblast outgrowth. *J Cell Sci* 2010;123(Pt 19):3336–46.
24 Derocq D, Prébois C, Beaujouin M, *et al*. Cathepsin D is partly Endocytosed by the Lrp1 receptor and inhibits Lrp1-regulated Intramembrane proteolysis. *Oncogene* 2012;31:3202–12.
25 Ketterer S, Mitschke J, Ketscher A, *et al*. Cathepsin D deficiency in Mammary epithelium transiently stalls breast cancer by interference with Mtorc1 signaling. *Nat Commun* 2020;11:5133.
26 Alcaraz LB, Mallavialle A, David T, *et al*. A 9-kDa Matricellular SPARC fragment released by cathepsin D exhibits pro-tumor activity in the triple-negative breast cancer Microenvironment. *Theranostics* 2021;11:6173–92.
27 Ashraf Y, Mansouri H, Laurent-Matha V, *et al*. Immunotherapy of triple-negative breast cancer with cathepsin D-targeting antibodies. *J Immunother Cancer* 2019;7:29.
28 Mathieu M, Rochefort H, Barenton B, *et al*. Interactions of cathepsin-D and insulin-like growth factor-II (IGF-II) on the IGF-II/Mannose-6-phosphate receptor in human breast cancer cells and possible consequences on Mitogenic activity of IGF-II. *Mol Endocrinol* 1990;4:1327–35.
29 Laurent-Matha V, Farnoud MR, Lucas A, *et al*. Endocytosis of pro-cathepsin D into breast cancer cells is mostly independent of Mannose-6-phosphate receptors. *J Cell Sci* 1998;111 (Pt 17)(Pt 17):2539–49.
30 van de Bovenkamp FS, Hafkenscheid L, Rispens T, *et al*. The emerging importance of IgG Fab Glycosylation in immunity. *J Immunol* 2016;196:1435–41.
31 Koene HR, Kleijer M, Algra J, *et al*. Fc gammaRIIIa-158V/F polymorphism influences the binding of IgG by natural killer cell FC gammaRIIIa, independently of the FC gammaRIIIa-48L/R/H phenotype. *Blood* 1997;90:1109–14.
32 Alter G, Malenfant JM, Altfeld M. Cd107A as a functional marker for the identification of natural killer cell activity. *J Immunol Methods* 2004;294:15–22.
33 Held W, Jeevan-Raj B, Charmoy M. Transcriptional regulation of murine natural killer cell development, differentiation and maturation. *Cell Mol Life Sci* 2018;75:3371–9.
34 Gordon SM, Chaix J, Rupp LJ, *et al*. The transcription factors T-bet and Eomes control key checkpoints of natural killer cell maturation. *Immunity* 2012;36:55–67.
35 Zhang J, Le Gras S, Pouxvielh K, *et al*. Sequential actions of EOMES and T-BET promote stepwise maturation of natural killer cells. *Nat Commun* 2021;12.
36 du Manoir S, Orsetti B, Bras-Gonçalves R, *et al*. Breast tumor Pdxs are genetically plastic and correspond to a subset of aggressive cancers prone to relapse. *Mol Oncol* 2014;8:431–43.
37 Moore GL, Chen H, Karki S, *et al*. Engineered FC variant antibodies with enhanced ability to recruit complement and mediate Effector functions. *MAbs* 2010;2:181–9.
38 Schlothauer T, Herter S, Koller CF, *et al*. Novel human Igg1 and Igg4 FC-engineered antibodies with completely abolished immune Effector functions. *Protein Eng Des Sel* 2016;29:457–66.
39 Musolino A, Naldi N, Bortesi B, *et al*. Immunoglobulin G fragment C receptor Polymorphisms and clinical efficacy of Trastuzumab-based therapy in patients with HER-2/neu-positive metastatic breast cancer. *J Clin Oncol* 2008;26:1789–96.
40 Bibeau F, Lopez-Crapez E, Di Fiore F, *et al*. Impact of Fcgammariia-Fcgammariiia Polymorphisms and KRAS mutations on the clinical outcome of patients with metastatic colorectal cancer treated with Cetuximab plus Irinotecan. *J Clin Oncol* 2009;27:1122–9.
41 Strefford JC, Nowicka M, Hargreaves CE, *et al*. Single-nucleotide Fcgamma receptor Polymorphisms do not impact Obinutuzumab/Rituximab outcome in patients with lymphoma. *Blood Adv* 2021;5:2935–44.
42 Musolino A, Gradishar WJ, Rugo HS, *et al*. Role of Fcgamma receptors in Her2-targeted breast cancer therapy. *J Immunother Cancer* 2022;10:e003171.

43 Kwok HF, Buick RJ, Kuehn D, *et al*. Antibody targeting of cathepsin S induces antibody-dependent cellular cytotoxicity. *Mol Cancer* 2011;10:147.
44 Toffoli EC, Sheikhi A, Höppner YD, *et al*. Natural killer cells and anti-cancer therapies: reciprocal effects on immune function and therapeutic response. *Cancers (Basel)* 2021;13:711.
45 Hurvitz SA, Hegg R, Chung W-P, *et al*. Trastuzumab Deruxtecan versus Trastuzumab Emtansine in patients with Her2-positive metastatic breast cancer: updated results from DESTINY-Breast03, a randomised, open-label, phase 3 trial. *Lancet* 2023;401:105–17.
46 Chen Y, Liu R, Li C, *et al*. Nab-paclitaxel promotes the cancer-immunity cycle as a potential Immunomodulator. *Am J Cancer Res* 2021;11:3445–60.
47 Wanderley CW, Colón DF, Luiz JPM, *et al*. Paclitaxel reduces tumor growth by Reprogramming tumor-associated Macrophages to an M1 profile in a Tlr4-dependent manner. *Cancer Res* 2018;78:5891–900.
48 Massa C, Karn T, Denkert C, *et al*. Differential effect on different immune Subsets of Neoadjuvant chemotherapy in patients with TNBC. *J Immunother Cancer* 2020;8:e001261.
49 Garofalo C, De Marco C, Cristiani CM. NK cells in the tumor Microenvironment as new potential players mediating chemotherapy effects in metastatic Melanoma. *Front Oncol* 2021;11:754541.
50 Traina TA, Miller K, Yardley DA, *et al*. Enzalutamide for the treatment of androgen receptor-expressing triple-negative breast cancer. *J Clin Oncol* 2018;36:884–90.
51 Walsh EM, Gucalp A, Patil S, *et al*. Adjuvant Enzalutamide for the treatment of early-stage androgen-receptor positive, triple-negative breast cancer: a feasibility study. *Breast Cancer Res Treat* 2022;195:341–51.
52 Lehmann BD, Abramson VG, Sanders ME, *et al*. TBCRC 032 IB/II multicenter study: molecular insights to AR antagonist and Pi3K inhibitor efficacy in patients with AR(+) metastatic triple-negative breast cancer. *Clin Cancer Res* 2020;26:2111–23.

On line supplemental file 1

Materials

The mouse monoclonal antibody against the 52-, 48-, and 34-kDa forms of human cath-D (#610801) was purchased from BD Transduction Laboratories (San Jose, CA). The anti-human, cath-D monoclonal antibody M2E8 recognizes only 52-kDa cath-D, and not 48- and 34 kDa cath-D[1, 2]. The anti-human cath-D rabbit polyclonal antibody (H-75; sc-10725) to detect 52-kDa human pro-cath-D was from Santa Cruz Biotechnology (Dallas, TX). The anti-mouse cath-D goat polyclonal antibody (clone AF1029) was from R&D Systems (Minneapolis, MN). The 11H4 hybridoma against the C-terminal part of the LRP1β chain was provided by P. van der Geer (San Diego State University, USA). The mouse monoclonal anti-human M6P/IGF2 receptor antibody (clone MEM-238) was from Origene. The mouse monoclonal anti-human cath-D antibody (clone E-7; sc-13148) to detect 52-kDa pro-cath-D, the mouse monoclonal anti-human cath-D antibody (clone C-5), and the anti- HSC70 antibody (clone B-6, sc-7298) were purchased from Santa Cruz Biotechnology (Dallas, TX). The rabbit monoclonal anti-androgen receptor (AR) antibody (clone D6F11, #5153) was from Cell Signaling Technology. The anti-β actin polyclonal antibody (#A2066) and the anti-human cath-D mouse monoclonal antibody (clone CTD19) were from Sigma-Aldrich (Saint-Louis, MO). The mouse monoclonal anti-tubulin antibody (clone 236-10501, #A11126) and Hoechst (#33342) were from Thermo Fisher Scientific (Waltham, MA). Human F1 IgG1, human F1M1 IgG1 and Fc-mutated F1M1 IgG1 (F1M1-Fc^{+} with the mutations S239D, H268F, S324T, I332E and F1M1-Fc^{-} with the mutations L234A, L235A and P329G) were constructed from the scFv (F1, F1M1) sequences using gene synthesis, expressed in the Chinese hamster ovary (CHO) cell line, and purified on protein-A HiTrap columns (GE Healthcare) by Evitria AG (Schlieren, Switzerland). The PC5-conjugated anti-CD107a (clone H4A3) IgG1, and PE-conjugated anti-IFNγ (clone B27) IgG1 were from BD Biosciences. Unconjugated and APC-conjugated anti-hCD16a (clone 3G8) IgG1 were from Beckman Coulter. Enzalutamide was purchased from Euromedex and 3(4,5-dimethyl-thiazol-2-yl)2,5-diphenol tetrazolium bromide (MTT) from Sigma-Aldrich. The anti-human CD20 chimeric IgG1 antibody rituximab (Truxima®) was from Healthcare Celltrion. Paclitaxel (Taxol®) was from Fresenius Kabi. Cetuximab (anti-human EGFR chimeric IgG1 antibody) was from Merck. Matrigel (10 mg/ml,

#354234) was purchased from Corning. Collagenase IV (#C5138) and DNase I (#11284932001) were from Sigma-Aldrich (St Louis, MO). Mouse Fc Block (#130-097-575) and the fluorescent-conjugated antibody against CD27 (clone REA499, #130-114-163 were from Miltenyi Biotec (Bergisch Gladbach, Germany). Viakrome IR 808 (#C36628) was from Beckman Coulter (Brea, CA). The fluorescent-conjugated antibodies against CD45 (clone 30-F11, #103149), CD19 (clone 6D5, #115507), F4/80 (clone BM8, #123109), NKp46 (clone 29A1.4, #137606), CD11b (clone M1/70, #101237), and granzyme B (clone QA16A02, #372215) were from Biolegend (San Diego, CA). The antibodies against CD3 (clone 17A2, #555275), CD11c (clone HL3, #553802) and CD107a (clone 1D4B, #565533) were from BD Biosciences (Franklin Lakes, NJ). The fixation/permeabilization kit (#00-5523-00) was from Invitrogen. The anti-human Fc goat polyclonal antibody conjugated to HRP (A0170) and 3(4,5-dimethyl-thiazol-2-yl)2,5-diphenol tetrazolium bromide (MTT) were from Sigma Aldrich (Saint-Louis, MO). The HRP-conjugated anti-mouse F(ab)2 (#115-036-072) was from Jackson ImmunoResearch (West Grove, PA). The substrate reagent for HRP was purchased from Bio-Techne (R&D Systems, #DY999). The APC-Vio770-labeled anti-CD19, VioGreen-labeled anti-CD45, PE-Vio770-labeled anti-CD56, PE-labeled anti-CD69 antibodies and 7AAD were from Miltenyi Biotec. (Germany). Calcein (sc-203865) was from Santa Cruz Biotechnology (Dallas, TX). The anti-asialo GM1 antibody (clone Poly21460, #146002) was from BioLegend (San Diego, CA). The fluorescent-conjugated antibodies against Ly6G (clone 1A8, #127621), B220 (clone RA3-6B2, #103241), CD11c (clone N418, #117329) and F4/80 (clone QA17A29, #157307) were from BioLegend (San Diego, CA). The fluorescent-conjugated antibody against I-A/I-E (clone 2G9, #743876) was from BD Biosciences (Franklin Lakes, NJ). The ACK (Ammonium-Chloride-Potassium) lysis buffer (#A1049201) was from Gibco. Precision count beads (#424902) were from BioLegend (San Diego, CA).

Cell lines, conditioned medium, and western blotting, ELISA, and immunoprecipitation

The MDA-MB-231 (TNBC) cell line was previously described[3]. The SUM159 cell line was from Asterand (Bioscience, UK). MDA-MB-231 cells were cultured in DMEM with 10% fetal calf serum (FCS, Eurobio), and SUM159 cells in RPMI with 10% FCS. NK92 hCD16a 158V and NK92 hCD16a 158F cells were kindly provided by Beatrice Clémenceau and Henri Vié (INSERM U892, Nantes,

France)[4]. These two NK cell lines were cultured in RPMI1640/GlutaMAX with 10% decomplemented FCS, 1% penicillin-streptomycin supplemented with 100 IU/mL IL-2 (Peprotech, #200-02). The human CAF1 (hCAF1)[5] cell line (breast cancer-associated fibroblasts, CAF) was kindly provided by Olivier de Wever (Ghent University, Ghent, Belgium).The E0771Luc mouse cell line, transformed to constitutively express luciferase as reporter, was kindly provided by Dr. C-L. Tomasetto (IGBMC, Strasbourg, France). E0771Luc cells were cultured in RPMI1640 with 10% FCS and 10 mM Hepes, pH=7.5. To produce conditioned medium, cells grown to 90% confluence were incubated in the absence of FCS for 24 h or in the presence of FCS for 48 h. Then, conditioned medium was centrifuged at 800 x g for 5 min. Cell lysates were prepared in lysis buffer (50 mM Hepes pH 7.5, 150 mM NaCl, 10% glycerol, 1% Triton X-100, 1.5 mM MgCl2, 1 mM EGTA) containing cOmplete™ Protease Inhibitor Cocktail (Roche, Switzerland) and centrifuged at 13,000 x g for 15 min. For western blotting experiments, proteins (10-30 µg) from cell lysates and conditioned media (40 µl) were separated on 13.5% SDS-PAGE and analyzed by immunoblotting using standard techniques. For the sandwich ELISA against human cath-D, 96-well plates were coated with the M2E8 antibody in PBS (250 ng/well) at 4°C overnight. After blocking non-specific sites with PBS/0.1% Tween-20/1% BSA, cath-D-containing conditioned medium with FCS from MDA-MB-231 cells was added at 4°C for 2h. After washes in PBS/0.1% Tween 20, serial dilutions of F1, the F1M1, F1M1-Fc^-, or F1M1-Fc^+ antibodies were added at 4°C for 2h, and interaction revealed with an anti-human Fc antibody conjugated to HRP for 1h at 37°C (1/2000; 355ng/well). For the sandwich ELISA against mouse cath-D, 96-well plates were coated with the anti-cath-D antibody (#AF1029, Bio-Techne) in PBS (100 ng/well) at 4°C overnight. After blocking non-specific sites with PBS/0.1% Tween-20/1% BSA, cath-D-containing supernatants from E0771Luc cells in the presence of serum were added at 37°C for 2h. After washes in PBS/0.1% Tween 20, serial dilutions of F1 or F1M1 in PBS were added at 37°C for 2h, followed by washes in PBS/0.1% Tween 20, and incubation with a HRP-conjugated anti-mouse F(ab')2 (1/2000) at 37°C for 2h. For immunoprecipitation, conditioned medium without FCS from MDA-MB-231 cells was adjusted to different pH and incubated with 2.5 µg of F1M1, F1M1-Fc^-, or F1M1-Fc^+ at 4°C overnight, and subsequently with 50 µl of 10% protein A-Sepharose, at 4°C on a shaker for 2h. Sepharose beads

were washed four times with PBS, boiled in SDS sample buffer for 5min (95°C), and analyzed by SDS-PAGE and immunoblotting.

Fluorescence microscopy

Paraffin-embedded PDX1995, PDX3977 or MDA-MB-231 tumor sections were deparaffined, rehydrated, rinsed, and saturated in PBS with 5% FCS at 4°C overnight. Sections were incubated with 0.4 µg/ml anti-cath-D mouse monoclonal antibody (clone C-5) followed by incubation with a Cy3-conjugated anti-mouse IgG (1/500). Nuclei were stained with 0.5 µg/ml Hoechst 33342. Sections were then imaged with a 63X Plan-Apochromat objective on z stacks with a Zeiss Axio Imager light microscope.

Immunohistochemistry

For cath-D immunostaining in TNBC samples from patients, tumor tissue sections were incubated with 0.4 µg/ml anti-human cath-D mouse monoclonal antibody (clone C-5) for 20 min after heat-induced antigen retrieval with the PTLink pre-treatment (Dako) and the High pH Buffer (Dako) and endogenous peroxidase quenching with Flex Peroxidase Block (Dako). After two rinses in EnVision™ Flex Wash buffer (Dako), sections were incubated with an HRP-labeled polymer coupled to a secondary anti-mouse antibody (Flex® system, Dako) for 20 min, followed by incubation with 3,3'-diaminobenzidine as chromogen. Sections were counterstained with Flex Hematoxylin (Dako) and mounted after dehydration. For human cath-D immunostaining in MDA-MB-231 tumor xenografts, tumor sections were incubated with 6.5 ng/ml anti-human cath-D mouse monoclonal antibody (clone CT19, SIGMA) after heat-induced antigen retrieval with the PT-Link pre-treatment device (Dako) and the High pH Buffer (Dako). Endogenous peroxidase was quenched with Flex Peroxidase Block (Dako). After two rinses in EnVisionTM Flex Wash buffer (Dako), the primary antibody was bridged to the anti-rabbit HRP-labeled polymer (Envision® system, Dako) using a rabbit anti-mouse antibody (ab133469, abcam). Sections were analyzed independently by two experienced pathologists, both blind. Cath-D signal was scored in cancer cells according to the staining intensity (0: none, 1: low, 2: moderate, 3: high).

Surface plasmon resonance

Surface plasmon resonance experiments were performed at 25°C using a Biacore T200 apparatus (Cytiva) in PBS supplemented with 0.05% P20 surfactant (ThermoFisher). The anti-His antibody (R&D Systems) was immobilized on a CM5S dextran sensor chip (Cytiva) by amine coupling according to the manufacturer's instructions. The human receptor proteins FcγRIIIA/hCD16a 158V and FcγRIIIA/hCD16a 158F (R&D Systems) were captured at 170 RU. All kinetic measurements were performed by single-cycle kinetic titration. Five increasing concentrations of these analytes (3.7, 11, 33, 100, 300 nM) were injected onto the captured hCD16a 158V and hCD16a 158F at a flow rate of 100 µl/min (injection time of 60ms), followed by a dissociation phase of 600ms after the final injection. Regeneration was done using 10mM glycine-HCl buffer, pH 1.5. All curves were analyzed with the Biacore T200 BiaEvaluation software 3.2 (Cytiva) after double-referencing subtraction. Because of the binding kinetics complexity, the two-state fitting model was chosen to allow comparing the KD values of the different antibodies with the two receptors[6].

Study approvals

Mouse experiments were performed in compliance with the French regulations and ethical guidelines for experimental animal studies in an accredited establishment (Agreement No. #31135-2021042212479661). The study approval for PDXs was previously published[7]. For immunohistochemistry (IHC), TNBC biopsy samples were provided by the biological resource center (Biobank number BB-0033-00059) after approval by the Montpellier Cancer Institute Institutional Review Board, following the French national Ethics and Legal dispositions for patients' information and consent. For TNBC cytosols, patient samples were processed according to the French Public Health Code (law n°2004-800, articles L. 1243-4 and R. 1243-61), and the biological resources center has been authorized (authorization number: AC-2008-700; Val d'Aurelle, ICM, Montpellier) to deliver human samples for scientific research. All patients were informed before surgery that their surgical specimens might be used for research purposes. For human primary NK cell isolation and expansion, this work benefited from umbilical cord blood units and John De Vos' expertise (head of the Biological Resource

Center Collection of the University Hospital of Montpellier, http://www.chu-montpellier.fr/en/platforms; BIOBANQUES Identifier: BB-0033-00031).

***In vivo* experiments**

In monotherapy experiments, MDA-MB-231 cells (2×10^6; mixed 1:1 with Matrigel) or SUM159 cells ($5x10^6$; mixed 1:1 with Matrigel) were injected subcutaneously in 6-week-old female athymic mice (NU(NCr)-Foxn1^{nu}) (Charles River Laboratory, France). For PDX models, approximately 5x5x5 mm of B1995 and B3977 tumor fragments were transplanted subcutaneously in 5-week-old female Swiss nude mice (NU(Ico)-Foxn1^{nu}) (Charles River Laboratory, France). When xenografts reached a volume of ~50 mm^3 (MDA-MB-231 and SUM159 cell xenografts) and ~100mm^3 (PDXs), tumor-bearing mice were randomized and treated with F1M1, F1M1-Fc$^-$, F1M1-Fc$^+$, or rituximab (15 mg/kg for all) by intraperitoneal injection (ip) three times per week. In other experiments, when tumors reached a volume of about 50 mm^3, tumor-bearing mice were randomized and treated with paclitaxel (1, 4, or 7 mg/kg), or saline by intraperitoneal injection once a week. In combined treatments, when MDA-MB-231 cell xenografts reached a volume of ~50 mm^3, tumor-bearing mice were randomized and treated with paclitaxel (1 or 4 mg/kg) or saline by ip once per week or/and F1M1-Fc$^+$ (15 mg/kg), or rituximab (15 mg/kg) by ip three times per week. When SUM159 cell xenografts reached a volume of ~50 mm^3, tumor-bearing mice were randomized and were treated with enzalutamide (30mg/kg) or DMSO in corn oil (per os, five times per week) or/and with F1M1-Fc$^+$ (15 mg/kg), or with rituximab (15 mg/kg) by ip twice per week. For the oral treatment, 5 µl of enzalutamide in DMSO (120 µg/µl) or DMSO alone was added to 145 µl of corn oil and given by oral gavage. Tumors were measured using a caliper and volume was calculated with the formula $V = (\text{tumor length} \times \text{tumor width}^2)/2$, until the tumor volume reached 1000-2000 mm^3, depending on the experiment. In the NK cell depletion experiments, athymic mice were treated with anti-asialo GM1 antibodies (50µL) by ip two times per week. When tumor volume reached 50 mm^3, tumor-bearing mice were randomized and treated with F1M1-Fc$^+$ or rituximab (15 mg/kg for both) by ip three times per week.

***In vivo* immunophenotyping of NK cell depletion in spleen and blood**

Spleens were crushed. Both spleens and blood samples were lysed with ACK lysis buffer for 10 min at room temperature. Cells were washed and resuspended in FACS buffer (PBS pH 7.2, 1% decomplemented FCS, 2mM EDTA, and 0.02% sodium azide). Cells were blocked with FACS Buffer containing 1% (v/v) mouse Fc block for 30 min and stained with fluorescent-conjugated antibodies against the cell surface markers CD45, CD3, B220, Ly6G, NKp46, CD11c, I-A/I-E (MHC-II), CD11b and F4/80 for 1h. After fixation with 1% paraformaldehyde in PBS, cell samples were analyzed by flow cytometry using a Beckman and Coulter Cytoflex flow cytometer and FlowJo 10.8.1. Living immune cells were defined as Viakrome IR808$^-$ CD45$^+$ cells. Neutrophils were defined as CD45$^+$CD3$^-$Ly6G$^+$ cells. B cells were defined as CD45$^+$CD3$^-$Ly6G$^-$B220$^+$ cells. NK cells were defined as NKp46$^+$ cells within the gate excluding CD3$^+$ T and NK T cells, B220$^+$ B cells and Ly6G$^+$ neutrophils. Dendritic cells were defined as CD45$^+$CD3$^-$Ly6G$^-$B220$^-$NKp46$^-$CD11c$^+$MHC-II$^+$ cells. Macrophages were defined as CD11b$^+$ F4/80$^+$ cells in the gate excluding all other immune cells.

Blood counts

20µL of blood was collected from the tail vein of mice in EDTA tubes (EDTA K3E, 200µL, Kabe Labortechnik). Blood samples were analyzed with the scil Vet abc Plus+ system (scil Animal Care Co).

Quantitative RT-PCR

Reverse transcription of total RNA was performed at 37°C using the Moloney murine leukemia virus reverse transcriptase (Invitrogen, Carlsbad, CA) and random hexanucleotide primers (Promega, Madison, WI). Real-time quantitative PCR analyses were performed on a Light Cycler 480 SYBR Green I master and a Light Cycler 480 apparatus (both from Roche Diagnostics, Indianapolis, IN). The PCR product integrity was verified by melting curve analysis. Quantification data were normalized to the amplification data for the reference gene encoding ribosomal protein S9 (*Rps9*). The sequences of the primers for *Eomes*, *Tnfa, Gzmb, Prf1* and *Rps9* are in the online supplemental table 1.

Cell viability assay

8 x10^3 MDA-MB-231 cells were seeded in 96-well plates in DMEM/10% FCS. When cells reached 60-70% of confluence, they were serum-deprived for 24h to induce synchronization, and then were incubated or not with paclitaxel in DMEM/2% FCS for 48h. Cell survival was evaluated with the mitochondrial dehydrogenase enzymatic assay, using MTT (Sigma) and determination of OD_{540nm}.

Human primary NK cell isolation, expansion, and characterization

Umbilical cord blood mononuclear cells were isolated through density gradient centrifugation using Histopaque-1077 (Sigma). Briefly, blood samples were diluted (1:1 ratio) with RPMI, then layered above 10mL of Histopaque in a 50mL conical tube. After centrifugation at 400xg for 30min, the white layers of mononuclear cells were collected and washed. Using the EasySep Human CD3 Positive Isolation kit (StemCell Technologies), the $CD3^+$ cell fraction (T and NK T cells) from the mononuclear cell samples was depleted to better culture NK cells. After depletion verification by flow cytometry, NK cells were cultured with γ-irradiated PLH feeder cells at 1:4 (NK cell: feeder cell) ratio, IL-2 (100 IU/mL) and IL-15 (5 ng/mL) for 20 days. Feeder cells and cytokines were refreshed every 3-4 days. To monitor expansion, NK cells were immunophenotyped. Briefly, 2.10^5 cells were stained with APC-labeled anti-CD3, VioBlue-labeled anti-CD16, APC-Vio770-labeled anti-CD19, VioGreen-labeled anti-CD45, PE-Vio770-labeled anti-CD56, PE-labeled anti-CD69 antibodies and with 7AAD at 4°C in the dark for 20min. After two washes, cells were analyzed using a Gallios flow cytometer (Beckman Coulter) and the FlowJo V10 software.

ADCC by live cell imaging

MDA-MB-231 cells (5 x 10^3; target) were labeled with calcein 2µM for 30 min and then seeded on Ultra Low Attachment 96-well plates (#7007, Corning). After 72h, MDA-MB-231 cell spheroids were first incubated with F1M1-Fc^+, F1M1-Fc^-, or cetuximab at 37 °C for 30min and then with NK92 $hCD16a^+$ 158V cells (effector) at an effector:target ratio of 20:1 for 24 h. Cells were scanned every hour for 24h and green fluorescence intensity was measured using the Sartorius IncuCyte® device by live imaging using user-informed algorithms that are part of the IncuCyte™ software package.

Desroys du Roure P, *et al. J Immunother Cancer* 2024; 12:e007135. doi: 10.1136/jitc-2023-007135

On line supplemental legends to figures

Online supplemental figure 1. Representative images of TNBC tissue sections showing cath-D expression

Cath-D was monitored in a TNBC biopsy by IHC using an anti-cath-D (C-5) antibody. Scale bar, 50 µm (left panel). Higher magnifications of the boxed region showing extracellular cath-D expression (right panel). Arrows show cath-D localization at the cancer cell surface.

Online supplemental figure 2. Generation of the VH- and VL-aglycosylated anti-cath-D F1M1 antibody that binds to secreted cath-D and inhibits TNBC MDA-MB-231 cell xenograft growth

(A) Coomassie blue staining of F1 and F1M1 in denaturing and non-denaturing conditions. The IgG1 F1 and F1M1 (2.5 µg) were separated on 13.5% SDS-PAGE followed by Coomassie blue staining.

(B) Binding of F1M1 to human cath-D secreted from MDA-MB-231 cells. Sandwich ELISA in which human cath-D from conditioned medium of MDA-MB-231 cells was added to wells pre-coated with the anti-human cath-D M2E8 mouse monoclonal antibody in the presence of increasing concentrations of the IgG1 F1M1. F1M1 binding to secreted human cath-D was revealed with an anti-human Fc HRP-conjugated antibody. The EC_{50} values are shown.

(C) Binding of F1 and F1M1 to mouse cath-D secreted from E0771Luc cells. Sandwich ELISA in which mouse cath-D from conditioned medium of E0771Luc cells was added to wells pre-coated with the anti-mouse cath-D AF1029 antibody in the presence of increasing concentrations of the IgG1 F1 or F1M1. Binding of F1 and F1M1 to secreted mouse cath-D was revealed with an anti-mouse F(ab')2 HRP-conjugated antibody. The EC_{50} values are shown.

(D) Tumor growth. MDA-MB-231 cells were subcutaneously injected in nude mice. When tumor volume reached 50 mm^3, mice were treated with F1 (n=7), F1M1 (n=7), or rituximab (Ctrl; n=7) (15 mg/kg) three times per week for 36 days. Tumor volume (in mm^3) is shown as the mean ± SEM. ***P <0.001 for F1 versus Ctr; **P=0.003 for F1M1 versus Ctrl, P= 0.378 F1 versus F1M1 (mixed-effects ML regression test).

Online supplemental figure 3. Characterization of the anti-cath-D F1M1, F1M1-Fc$^-$, and F1M1-Fc$^+$ antibodies

(A) Coomassie staining of the F1M1, F1M1-Fc$^-$, and F1M1-Fc$^+$ antibodies in denaturing conditions. F1M1, F1M1-Fc$^-$, and F1M1-Fc$^+$ (3.5µg) were analyzed on 15% SDS PAGE followed by Coomassie staining.

(B) Immunoprecipitation of pro-cath-D by F1M1, F1M1-Fc$^-$ and F1M1-Fc$^+$ at acidic pH. Conditioned medium of MDA-MB-231 cells was immunoprecipitated with F1M1, F1M1-Fc$^-$, or F1M1-Fc$^+$ (2.5µg) at different pH values (7.5, 6.5, 6.0 and 5.5). Cath-D was detected by immunoblotting using an anti-cath-D (H-75) antibody. *Mr*, relative molecular mass (kDa).

Online supplemental figure 4. ADCC induction with the anti-cath-D F1M1-Fc$^+$, F1M1 and F1M1-Fc$^-$ antibodies in the presence of primary human NK cells

(A) Characterization of primary human NK 4928 V/F cells. Primary human NK cells from the 4928 V/F donor were immunophenotyped at day 17 of expansion. Shown are the percentages of CD3$^-$ CD19$^-$ negative cells (left panel) and of CD3$^-$ CD19$^-$ CD56$^+$ cells (middle panel), and also CD16a$^+$ expression in CD3$^-$ CD19$^-$ CD56$^+$ cells (right panel).

(B) ADCC activity against MDA-MB-231 cells in the presence of human primary NK cells in response to F1M1-Fc$^-$, F1M1 or F1M1-Fc$^+$. MDA-MB-231 cells (target) were pre-incubated with F1M1-Fc$^-$, F1M1, F1M1-Fc$^+$, or with cetuximab (Cetux; positive control) at 100 µg/ml (666 nM) at 37°C for 30 min, followed by incubation with primary human NK cells (human NK V/F; hCD16a V/F allotype; effector) at an effector:target ratio of 3:1 for 24h. ADCC of MDA-MB-231 cells was measured as described in Figure **2C.** ****P <0.0001 for F1M1-Fc$^+$ versus F1M1, ****P <0.0001 for F1M1-Fc$^+$ versus F1M1-Fc$^-$, *P=0.046 for F1M1 versus F1M1-Fc$^-$ (one-way ANOVA).

(C) Characterization of primary human NK 4924 V/V cells. Primary human NK cells from the 4924 V/V donor were immunophenotyped at day 17 of expansion as described in **(A).**

(D) Blocking cath-D binding to M6P receptors in MDA-MB-231 cells affects F1M1-Fc$^+$-induced ADCC in the presence of human primary NK cells. MDA-MB-231 cells (target) were pre-incubated with M6P (10 mM) or G6P (10 mM) for 24h. Then, ADCC was evaluated in the presence of primary

human NK cells (human NK V/V; hCD16a V/V allotype; effector) at an effector:target ratio of 3:1 after incubation with F1M1-Fc$^+$ at 100µg/ml (666 nM) and M6P (10 mM) or G6P (10 mM), as described in **figure 2F**. Cetuximab (Cetux), positive control (100µg/ml). F1M1-Fc$^-$, negative control (100µg/ml). ****P <0.0001 for F1M1-Fc$^+$ versus F1M1-Fc$^+$ + M6P, ****P <0.0001 for F1M1-Fc$^+$ + G6P versus F1M1-Fc$^+$ + M6P (one-way ANOVA).

Online supplemental figure 5. Fc-mediated cytotoxicity of F1M1-Fc$^+$ in spheroids by live imaging.

(A) Representative images of calcein-labeled MDA-MB-231 cell spheroids. MDA-MB-231 cells were labeled with calcein (2µM) and co-cultured or not with hCD16 158V-expressing NK92 cells. Representative images obtained using IncuCyte® after 20h of co-culture. Bars, 800 µm.

(B) Green fluorescence intensity measurement by live imaging. Green fluorescence intensity of calcein-labeled MDA-MB-231 cells was measured using IncuCyte® by live imaging at different time points of incubation with F1M1-Fc$^-$, F1M1-Fc$^+$, or cetuximab (Cetux, positive control) at 100µg/ml or buffer (Ctrl-, negative control) in the presence of hCD16V-expressing NK92 cells at a ratio of 20:1. Values are the mean ± SD (n=3 spheroids/group).

(C) Green fluorescence intensity at 24h. Values are the mean ± SD (n=3 spheroids/group). ***P=0.001 for F1M1-Fc$^+$ versus Ctrl-, ***P=0.0004 for F1M1-Fc$^+$ versus F1M1-Fc$^-$, P=0.7962 for F1M1-Fc$^-$ versus Ctrl$^-$.

Online supplemental figure 6. Cath-D expression in MDA-MB-231 cell xenografts of mice treated with F1M1-Fc$^-$, F1M1, or F1M1-Fc$^+$

(A) Representative images of MDA-MB-231 cell xenograft sections showing cath-D expression

Cath-D was monitored in MDA-MB-231 cell xenografts from mice treated with F1M1-Fc$^-$, F1M1, or F1M1-Fc$^+$ **(**from **figure 4B**) (n=9 for F1M1-Fc$^-$; n=8 for F1M1; n=5 for F1M1-Fc$^+$; n=9 for Ctrl) by IHC using an anti-cath-D (clone CTD19) antibody. Scale bar, 50 µm.

(B) Quantification of cath-D expression in MDA-MB-231 cell xenograft sections. (n=9 for F1M1-Fc$^-$; n=8 for F1M1; n=5 for F1M1-Fc$^+$; n=9 for Ctrl). P=0.8815, Kruskal-Wallis test.

(C) Cath-D expression in MDA-MB-231 cell xenografts. Cath-D expression was determined in MDA-MB-231 cell xenografts from mice treated with F1M1-Fc$^-$, F1M1, or F1M1-Fc$^+$ **(**from **figure 4B**) (n=3 for F1M1-Fc$^-$; n=3 for F1M1; n=3 for F1M1-Fc$^+$; n=3 for Ctrl). Whole cytosols (10 µg proteins) were immunoblotted with the mouse monoclonal (#610801) (to detect mature cath-D) and rabbit polyclonal (H-75) (to detect pro-cath-D) anti-cath-D antibodies. HSC70 (clone B-6) was used as loading control. *Mr*, relative molecular mass (kDa).

Online supplemental figure 7. Percentage of living cells in MDA-MB-231 cell xenografts from mice treated with F1M1-Fc$^-$, F1M1, or F1M1-Fc$^+$ at day 48. The percentage of living cells from MDA-MB-231 cell xenografts from mice treated with F1M1-Fc$^-$, F1M1, or F1M1-Fc$^+$ at day 48 **(**from figure **4B**) was quantified by FACS (n=7 for F1M1-Fc$^-$; n=7 for F1M1; n=9 for F1M1-Fc$^+$; n=8 for Ctrl). *P*=0.6280 for all groups (Kruskal-Wallis), *P*= 0.4088 for F1M1-Fc$^+$ versus Ctrl, *P*= 0.3969 for F1M1 versus Ctrl, *P*= 0.2810 for F1M1-Fc$^-$ versus Ctrl, *P*=0.5859 for F1M1-Fc$^+$ versus F1M1-Fc$^-$, *P*=0.7365 for F1M1-Fc$^+$ versus F1M1, *P*>0.9999 for F1M1-Fc$^-$ versus F1M1 (Mann-Whitney t-test). Data are the mean ± SEM.

Online supplemental figure 8. Linear regression analysis of CD107a$^+$ NK cells or granzyme B$^+$ NK cells and volumes of MDA-MB-231 cell xenografts from mice treated with F1M1-Fc$^-$, F1M1, or F1M1-Fc$^+$.

(A) Linear regression analysis of CD107a$^+$ NK cells and tumor volumes. The percentage of CD107a$^+$ degranulating NK cells was quantified by FACS and expressed relative to all NKp46$^+$ NK cells. Tumor volumes are those from **figure 4B** (n=7 for F1M1-Fc$^-$; n=7 for F1M1; n=9 for F1M1-Fc$^+$; n=8 for Ctrl). R^2 =0.1703; **P*=0.0211; n=31 mice (all treatment groups).

(B) Linear regression analysis of granzyme B$^+$ NK cells and tumor volumes. The percentage of GZMB$^+$ activated NK cells was quantified by FACS and expressed relative to all NKp46$^+$ NK cells. Tumor volumes are those from **figure 4B**. GZMB, granzyme B. (n=7 for F1M1-Fc$^-$; n=7 for F1M1; n=9 for F1M1-Fc$^+$; n=8 for Ctrl). R^2 =0.3085; ***P*=0.0012; n=31 mice (all treatment groups).

Online supplemental figure 9. Quantification of granzyme B, perforin, and TNFα mRNA expression in MDA-MB-231 cell xenografts of mice treated with F1M1-Fc$^-$, F1M1, or F1M1-Fc$^+$.

(A) Quantification of granzyme B *(Gzmb)* mRNA expression. Total RNA was extracted from MDA-MB-231 cell xenografts from figure **4B** at treatment end and granzyme B expression level was analyzed by RT-qPCR. Relative fold change was normalized to *Rps9* expression and expressed as fold change relative to control. Data are the mean ± SEM (n=8 for F1M1-Fc$^-$; n=8 for F1M1; n=8 for F1M1-Fc$^+$; n=7 for Ctrl). *P*=0.1975 for all groups (Kruskal-Wallis). *P*= 0.3969 for F1M1-Fc$^+$ versus Ctrl, **P*=0.0207 for F1M1-Fc$^+$ versus F1M1-Fc$^-$, *P*=0.2345 for F1M1-Fc$^+$ versus F1M1, *P*=0.3823 for F1M1 versus F1M1-Fc$^-$ (Mann-Whitney t-test).

(B) Quantification of perforin (*Prf1*) mRNA expression, done as described in panel (**A**). *P*=0.0638 for all groups (Kruskal-Wallis). *P*= 0.2319 for F1M1-Fc$^+$ versus Ctrl, **P*= 0.0379 for F1M1-Fc$^+$ versus F1M1-Fc$^-$, **P*=0.0148 for F1M1-Fc$^+$ versus F1M1, *P*=0.7984 for F1M1 versus F1M1-Fc$^-$ (Mann-Whitney t-test).

(C) Quantification of TNFα (*Tnf)* mRNA expression, done as described in (**A**). ***P*=0.0038 for all groups (Kruskal-Wallis). ***P*= 0.0059 for F1M1-Fc$^+$ versus Ctrl, *P*= 0.0541 for F1M1 versus Ctrl, ***P*=0.0030 for F1M1-Fc$^+$ versus F1M1-Fc$^-$, **P*=0.0214 for F1M1 versus F1M1-Fc$^-$, *P*=0.7984 for F1M1 versus F1M1-Fc$^+$ (Mann-Whitney t-test).

Online supplemental figure 10. Depletion of NK cells with the anti- αGM1 antibody in nude mice.

(A) Treatment schedule. Mice were treated by ip injection of saline (control) or anti-asialo GM1 antibody (αGM1) (50µl) (n=4 by group) at day 0 and day 3. Peripheral blood was collected 6 days before the first injection, and 1 day after the second injection (day 4). Mice were sacrificed at day 7 after the first injection and blood samples and spleens were collected.

(B) Percentage of NK cells in peripheral blood before and after αGM1 treatment. The percentage of NK cells in peripheral blood samples of nude mice treated with αGM1 was quantified by FACS at day 1 and 4. NK cells were defined as CD45$^+$ CD3$^-$ Ly6G$^-$ B220$^-$ NKp46$^+$ cells (n=4).

(C) NK cell gating. NK cells were defined as described in **(B).** A representative gate from the same mouse before (day 6 before the first injection) (left panel) and at day 4 (right panel) after αGM1 treatment is shown.

(D) Immune cell populations in blood. The percentage of B cells, neutrophils and NK cells in blood samples of nude mice treated or not with αGM1 was quantified by FACS at day 4 (n=4 for both groups). Neutrophils were defined as $CD45^+$ $CD3^-$ $Ly6G^+$ cells. B cells were defined as $CD45^+$ $CD3^-$ $Ly6G^-$ $B220^+$ cells. NK cells were defined as $CD45^+$ $CD3^-$ $Ly6G^-$ $B220^-$ $NKp46^+$ cells.

(E) Immune cell populations in spleen. The percentage of B cells, neutrophils, NK cells, dendritic cells and macrophages from spleens of nude mice treated or not with αGM1 was quantified by FACS at day 7 (n=4 for both groups). B cells, neutrophils and NK cells are defined as described in **(D).** Dendritic cells were defined as $CD45^+$ $CD3^-$ $Ly6G^-$ $B220^-$ $NKp46^-$ $MHC\text{-}II^+$ $CD11c^+$ cells. Macrophages were defined as $CD45^+$ $CD3^-$ $Ly6G^-$ $B220^-$ $NKp46^-$ $MHC\text{-}II^-$ $CD11c^-CD11b^+$ $F4/80^+$ cells.

Online supplemental figure 11. Efficacy of NK cell depletion with the αGM1 antibody in MDA-MB-231 cell xenografted nude mice treated with F1M1-Fc^+.

(A) Depletion of NK cells in peripheral blood. The percentage of NK cells from peripheral blood of nude mice treated with F1M1-Fc^+ or rituximab in the presence or absence of αGM1 was quantified by FACS at day 45 (n=7 for F1M1-Fc^+; n=6 for F1M-Fc^+ + αGM1; n=8 for Ctrl; n=7 for Ctrl + αGM1). NK cells were defined as $CD45^+$ $CD3^-$ $Ly6G^-$ $B220^-$ $NKp46^+$ cells.

(B) Depletion of NK cells in spleen. The percentage of NK cells in the spleen of nude mice treated with F1M1-Fc^+ or rituximab in the presence or absence of αGM1 was quantified by FACS at day 48 (n=8 for F1M1-Fc^+; n=8 for F1M-Fc^+ + αGM1; n=7 for Ctrl; n=8 for Ctrl + αGM1). NK cells were defined as $CD45^+$ $CD3^-$ $Ly6G^-$ $B220^-$ $NKp46^+$ cells.

Online supplemental figure 12. Analysis of neutrophils and blood counts in MDA-MB-231 cell xenografted nude mice treated with F1M1-Fc^+.

(A) Neutrophils in peripheral blood. The percentage of neutrophils in peripheral blood samples of nude mice treated with F1M1-Fc$^+$ or rituximab (control, Ctrl) was quantified by FACS at day 45 (n=7 for F1M1-Fc$^+$; n=8 for Ctrl). Neutrophils were defined as CD45$^+$ CD3$^-$ Ly6G$^+$ cells.

(B) Blood counts. Blood samples from mice treated with F1M1-Fc$^+$ or rituximab (Ctrl) were analyzed using the scil Vet abc Plus+ system at day 48 (scil Animal Care Co) (n=8 for F1M1-Fc$^+$; n=8 for Ctrl). White blood cells (top left panel), platelets (top right panel), red blood cells (bottom left panel) and hemoglobin (bottom right panel) were quantified.

Online supplemental figure 13. Effect of paclitaxel on *in vitro* and *in vivo* cancer cell growth and on cath-D expression in MDA-MB-231 cells.

(A) Concentration-response curve of paclitaxel in MDA-MB-231 cells. MDA-MB-231 cells were incubated or not with increasing concentrations of paclitaxel for 2 days and then, cell viability was evaluated with the MTT assay. Results are expressed as the percentage of cell viability inhibition relative to control (cells without treatment). Values are the mean ± SD (n=6). The IC_{50} value is shown. PTX, paclitaxel.

(B) Effect of paclitaxel on cath-D expression level. MDA-MB-231 cells in DMEM/2% FCS were incubated or not with 5 nM PTX for 48h. Conditioned medium (40 µl) and cell lysates (20µg) were analyzed by 13.5% SDS-PAGE and immunoblotting with anti-cath-D (#610801) (to detect cellular cath-D) and anti-cath-D (H-75) (to detect secreted pro-cath-D) antibodies. β-actin, loading control. *Mr*, relative molecular mass (kDa). PTX, paclitaxel.

(C) Dose-dependent effect of paclitaxel on the growth of MDA-MB-231 cell xenografts. MDA-MB-231 cells were subcutaneously injected in nude mice. When tumor volume reached 50 mm^3, mice were treated with PTX at different concentrations (1 mg/kg: n=3; 4 mg/kg: n=3; and 7 mg/kg: n=3), or NaCl (Ctrl; n=4) once per week for 55 days. Tumor volume (in mm^3) is shown as the mean ± SEM. P=0.209 for PTX (1 mg/kg) versus Ctrl, **P=0.007 for PTX (4 mg/kg) versus Ctrl, and ***P<0.001 for PTX (7mg/kg) versus Ctrl (mixed-effects multiple linear regression test). PTX, paclitaxel.

Online supplemental figure 14. Expression of androgen receptor (AR) and cath-D in SUM159 cells.

(A) Expression of AR and cath-D in SUM159 cells. Conditioned medium (40 µl) and cell lysates (20µg) from SUM159 cells were analyzed by 13.5% SDS-PAGE and immunoblotting with anti-AR (D6F11) (left panel), anti-cath-D (#610801) (to detect cellular cath-D), and anti-cath-D (H-75) (to detect secreted pro-cath-D) (right panel) antibodies. Tubulin, loading control. β-actin, loading control. *Mr*, relative molecular mass (kDa). AR, androgen receptor.

(B) Effect of enzalutamide on cath-D expression and secretion in SUM159 cells. SUM 159 cells were incubated with DMSO (Ctrl) or enzalutamide (20 µM; Enza) in the absence of FCS for 24h. Cell extracts (25µg proteins) and conditioned media (40 µl) were immunoblotted for cellular cath-D (#610801) and secreted cath-D (H-75) detection, respectively. β-actin, loading control. *Mr*, relative molecular mass (kDa).

(C) Effect of F1M1-Fc$^+$ on AR expression. SUM 159 cells were incubated with DMSO (Ctrl) or F1M1-Fc$^+$ (50 µg/ml=333 nM) in the absence of FCS for 24h. Cell extracts (25 µg proteins) were immunoblotted with an anti-AR antibody (D6F11). β-actin, loading control. 110K, 110-kDa. *Mr*, relative molecular mass (kDa).

References

1. Beaujouin M, Prebois C, Derocq D, et al. Pro-cathepsin D interacts with the extracellular domain of the beta chain of LRP1 and promotes LRP1-dependent fibroblast outgrowth. J Cell Sci. 2010;123(Pt 19):3336-46. doi: jcs.070938 [pii]

10.1242/jcs.070938.

2. Freiss G, Vignon F, Rochefort H. Characterization and properties of two monoclonal antibodies specific for the Mr 52,000 precursor of cathepsin D in human breast cancer cells. Cancer Res. 1988;48(13):3709-15.

3. Glondu M, Liaudet-Coopman E, Derocq D, et al. Down-regulation of cathepsin-D expression by antisense gene transfer inhibits tumor growth and experimental lung metastasis of human breast cancer cells. Oncogene. 2002;21(33):5127-34.

4. Clemenceau B, Vivien R, Pellat C, et al. The human natural killer cytotoxic cell line NK-92, once armed with a murine CD16 receptor, represents a convenient cellular tool for the screening of mouse mAbs according to their ADCC potential. MAbs. 2013;5(4):587-94. doi: 10.4161/mabs.25077.

5. Primac I, Maquoi E, Blacher S, et al. Stromal integrin alpha11 regulates PDGFR-beta signaling and promotes breast cancer progression. J Clin Invest. 2019;129(11):4609-4628. doi: 10.1172/JCI125890.

6. Hayes JM, Frostell A, Cosgrave EF, et al. Fc gamma receptor glycosylation modulates the binding of IgG glycoforms: a requirement for stable antibody interactions. J Proteome Res. 2014;13(12):5471-85. doi: 10.1021/pr500414q.

7. du Manoir S, Orsetti B, Bras-Goncalves R, et al. Breast tumor PDXs are genetically plastic and correspond to a subset of aggressive cancers prone to relapse. Mol Oncol. 2014;8(2):431-43. doi: 10.1016/j.molonc.2013.11.010.

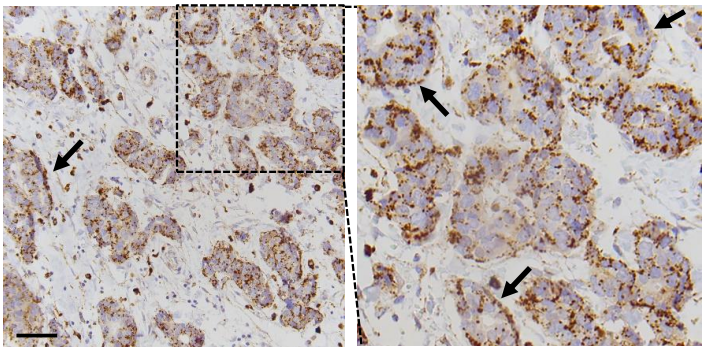

Online supplemental figure 1. Representative images of TNBC tissue sections showing cath-D expression

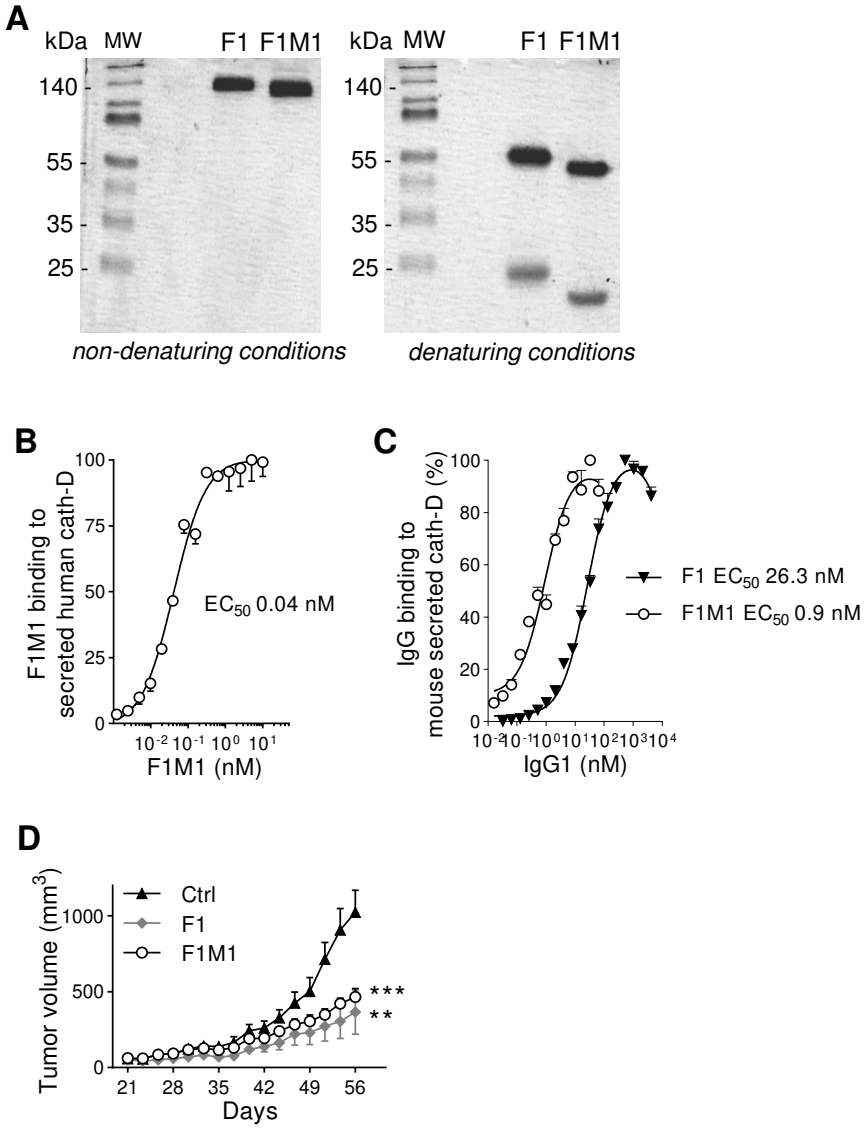

Online supplemental figure 2. Generation of the VH- and VL-aglycosylated anti-cath-D F1M1 antibody that binds to secreted cath-D and inhibits TNBC MDA-MB-231 cell tumor growth

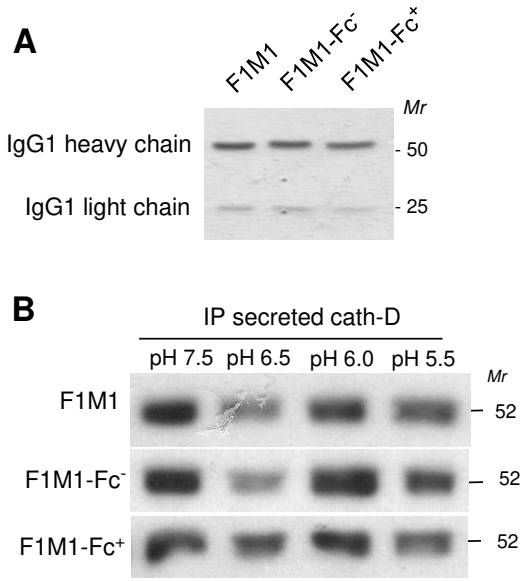

Online supplemental figure 3. Characterization of anti-cath-D F1M1, F1M1-Fc⁻ and F1M1-Fc⁺ antibodies

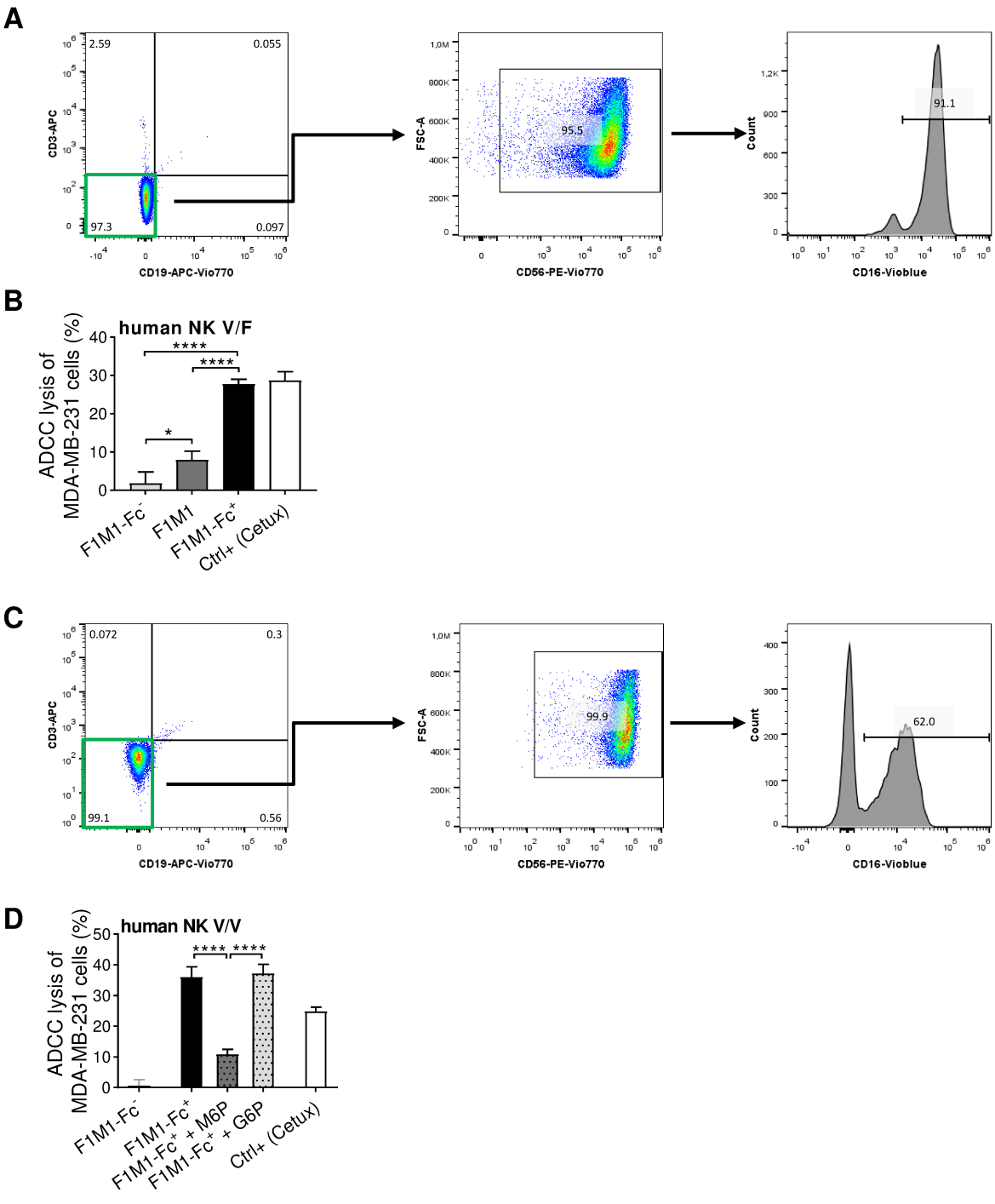

Online supplemental figure 4. ADCC induction with the anti-cath-D F1M1-Fc⁺, F1M1 and F1M1-Fc⁻ antibodies in the presence of primary human NK cells

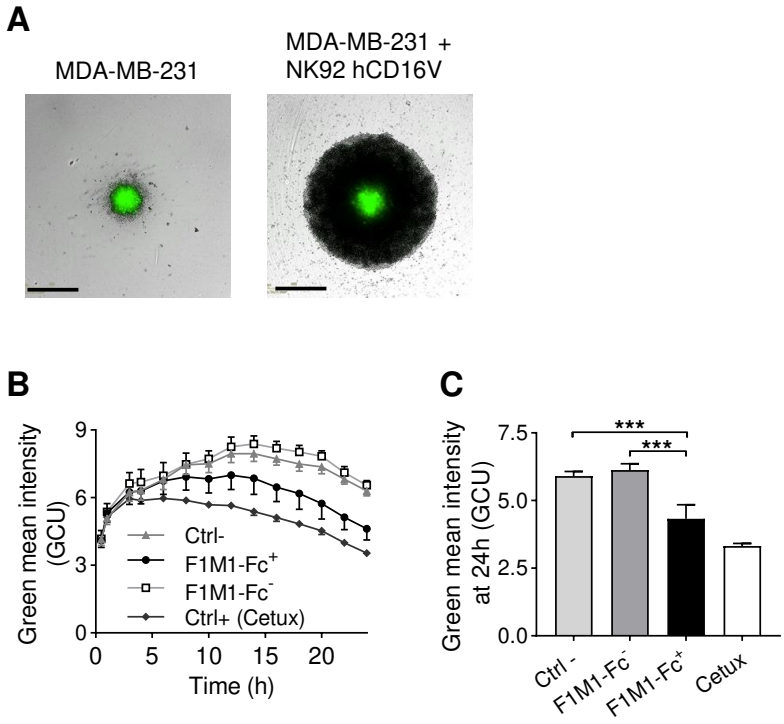

Online supplemental figure 5. Fc-mediated cytotoxicity of F1M1-Fc+ in spheroids by live imaging

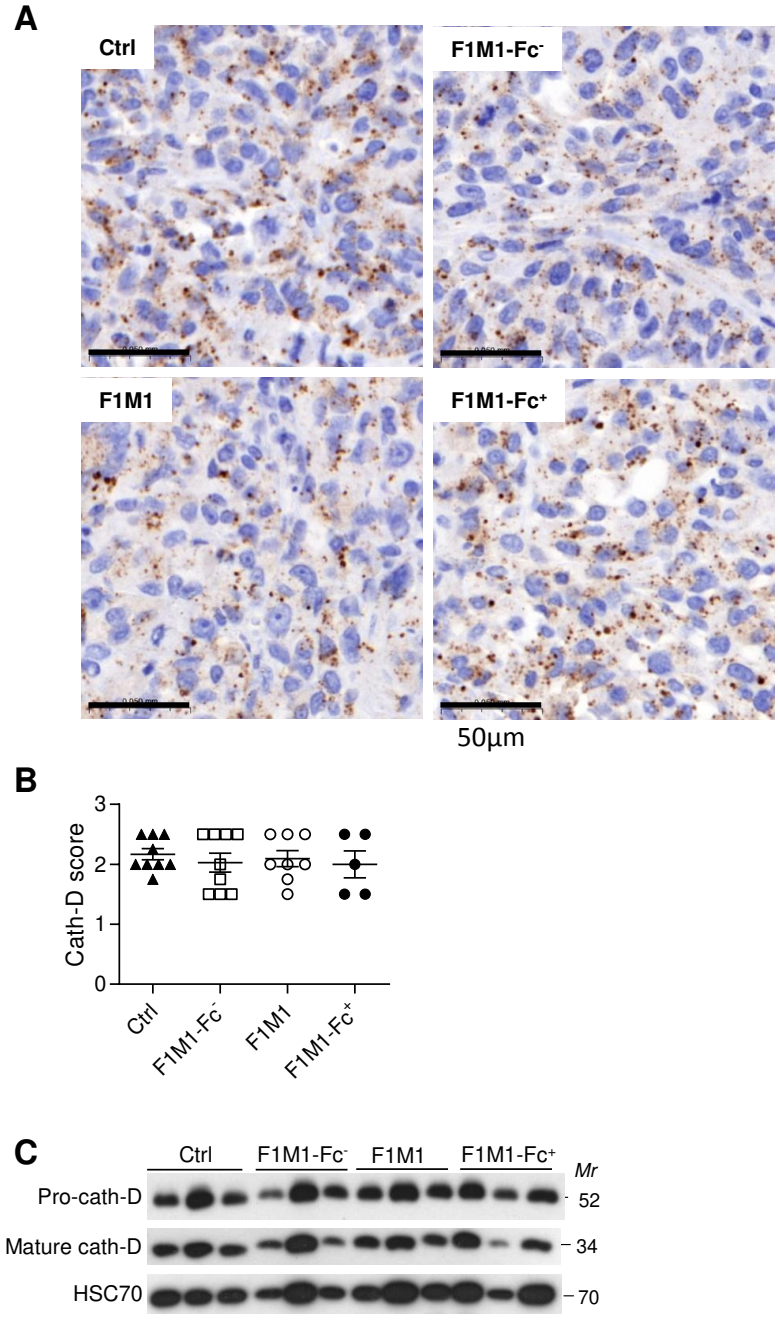

Online supplemental figure 6: Cath-D expression in MDA-MB-231 cell xenografts of mice treated with F1M1-Fc⁻, F1M1, or F1M1-Fc⁺

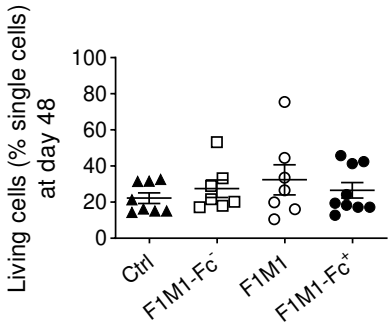

Online supplemental figure 7. Percentage of living cells in MDA-MB-231 cell xenografts from mice treated with F1M1-Fc$^-$, F1M1, or F1M1-Fc$^+$ at day 48

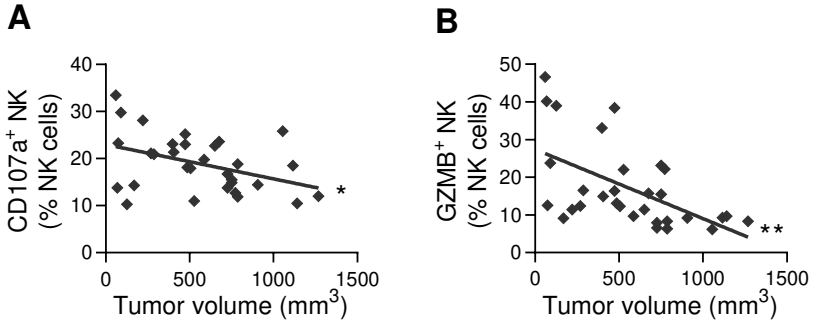

Online supplemental figure 8. Linear regression analysis of CD107a+ NK cells or granzyme B+ NK cells and tumor volumes of MDA-MB-231 cell xenografts from mice treated with F1M1-Fc-, F1M1, or F1M1-Fc+ .

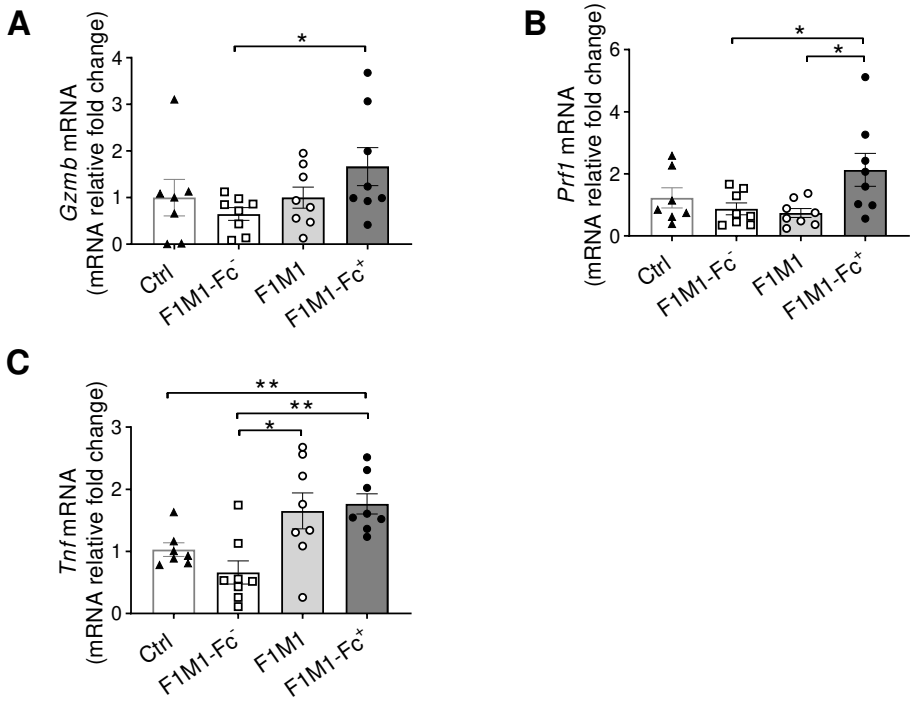

Online supplemental figure 9. Quantification of granzyme B, perforin and TNFα mRNA expression in MDA-MB-231 cell xenografts of mice treated with F1M1-Fc$^-$, F1M1, or F1M1-Fc$^+$

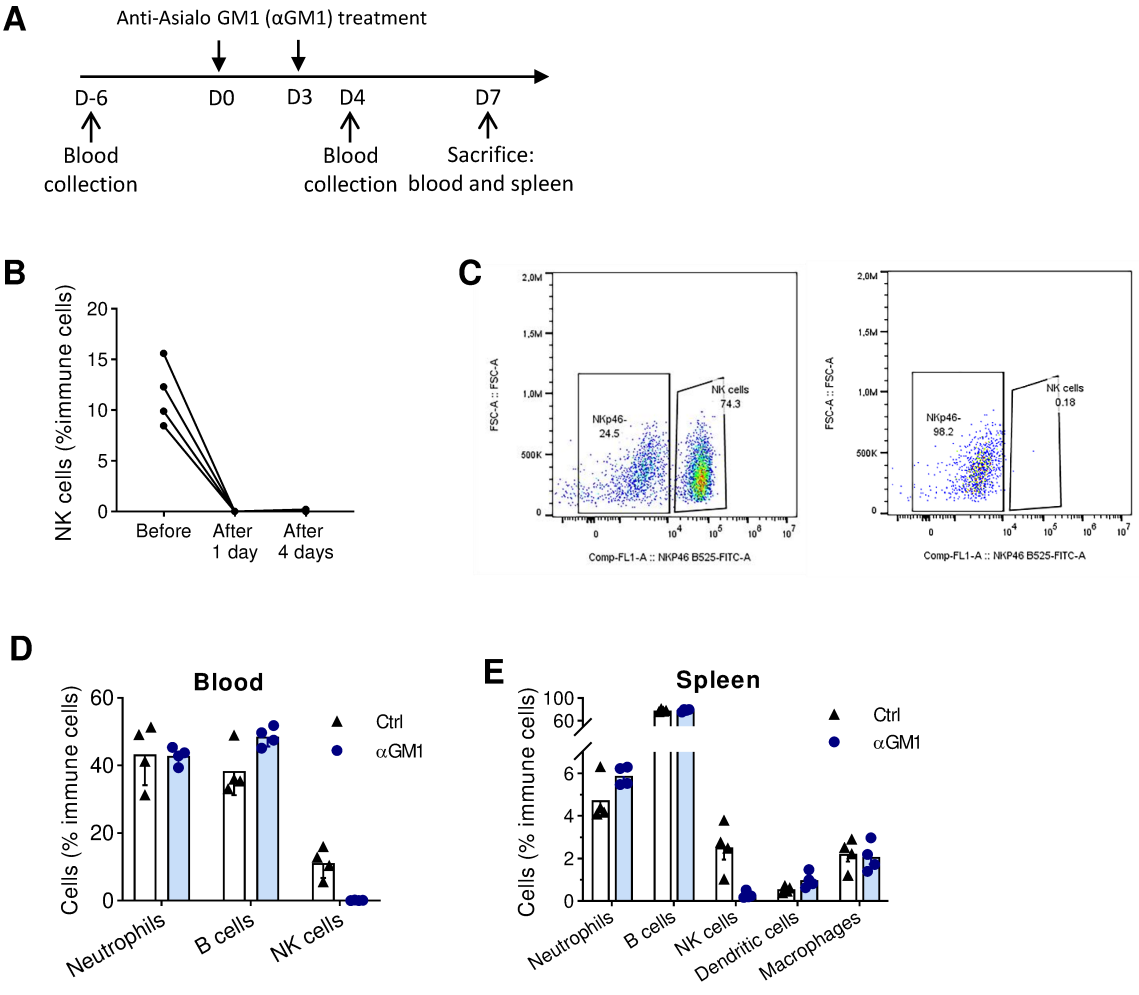

Online supplemental figure 10. Depletion of NK cells with the anti-αGM1 antibody in nude mice.

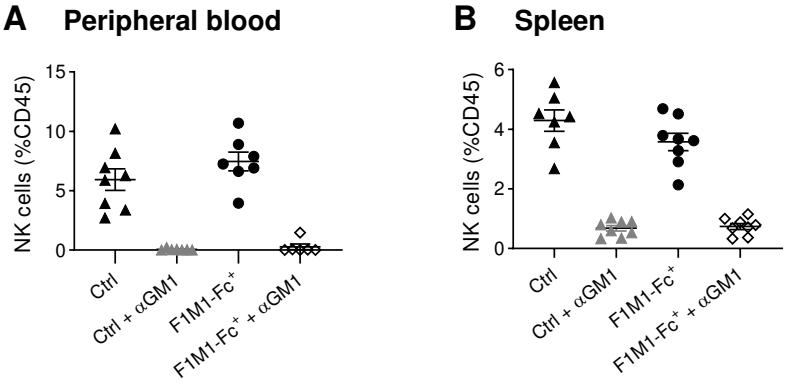

Online supplemental figure 11. Efficacy of NK cell depletion with the aGM1 antibody in MDA-MB-231 cell xenografted nude mice treated with F1M1-Fc+.

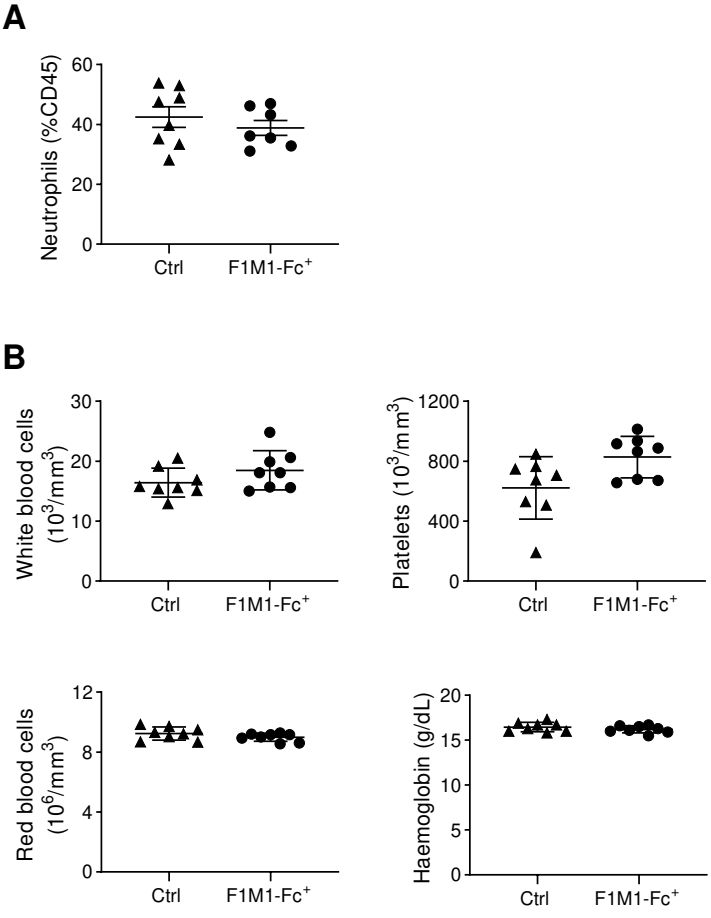

Online supplemental figure 12. Analysis of neutrophils and blood counts in MDA-MB-231 cell xenografted nude mice treated with F1M1-Fc⁺.

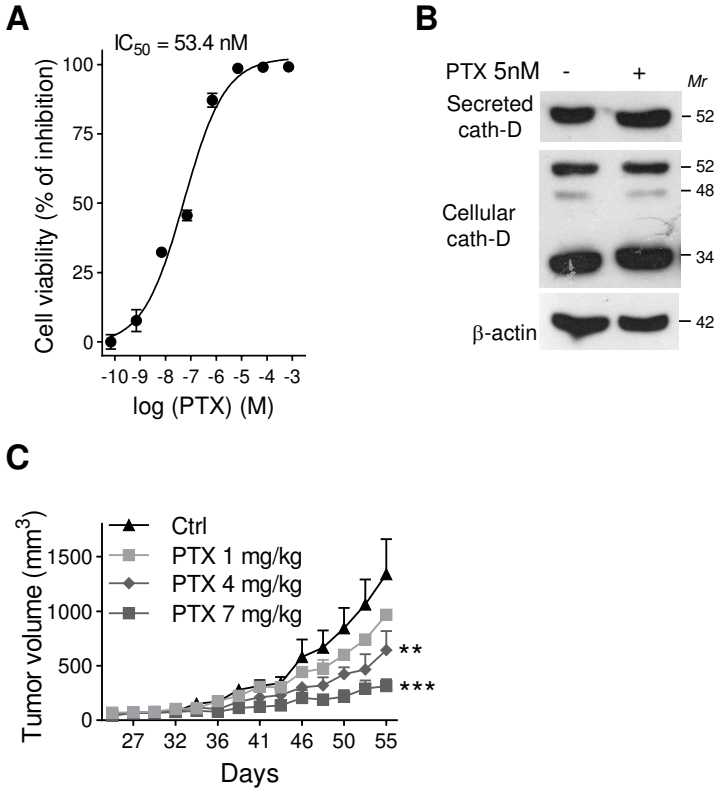

Online supplemental figure 13. Effect of paclitaxel on *in vitro* and *in vivo* growth and on cath-D expression by MDA-MB-231 cells

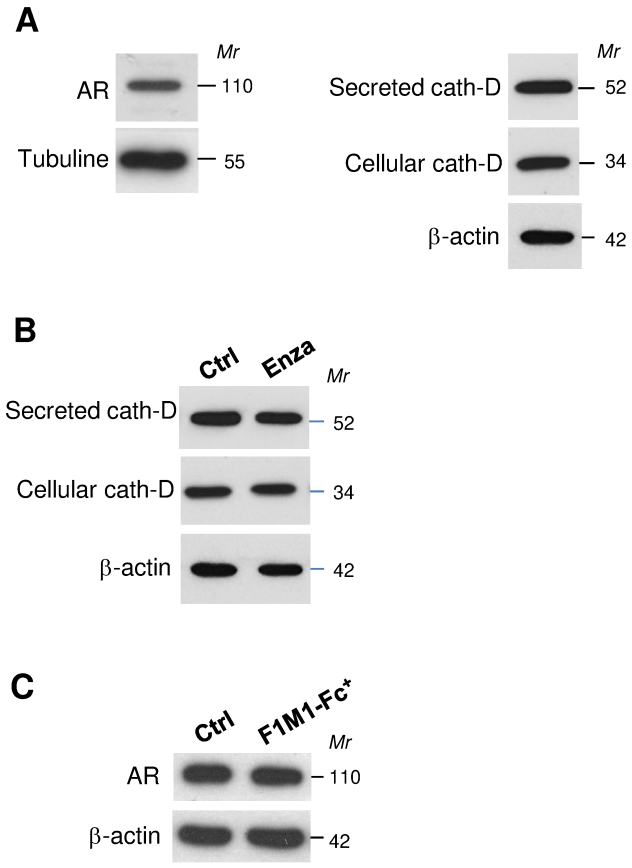

Online supplemental figure 14. Expression of androgen receptor (AR) and cath-D in SUM159 cells

Name	Forward (5' → 3')	Reverse (5' → 3')
GZMB	CCACTCTCGACCCTACATGG	GGCCCCCAAAGTGACATTTATT
PRF1	AGCACAAGTTCGTGCCAGG	GCGTCTCTCATTAGGGAGTTTTT
TNFA	CTGAACTTCGGGGTGATCGG	GGCTTGTCACTCGAATTTTGAG
EOMES	CCAGGAATTAAGCAAGACATC	TGCCCTTACTTTCTAGTTCTC

Online supplemental Table 1. Nucleotide sequences of the primers used for qPCR experiments.